INSIGHT INTO THE INTERACTIONS BETWEEN KIR CHANNELS AND LIPIDS

A Dissertation

by

PEI QIAO

Submitted to the Graduate and Professional School of
Texas A&M University
in partial fulfillment of the requirements for the degree of

DOCTOR OF PHILOSOPHY

Chair of Committee,	Thomas Meek
Co-Chair of Committee,	Pingwei Li
Committee Members,	Arthur Laganowsky
	David Russell
Head of Department,	Joshua Wand

May 2022

Major Subject: Biochemistry

ABSTRACT

The structure and function of membrane proteins are often under the regulation of cofactors such as lipids and other small molecules in the biological membrane bilayer. The characterization of most membrane proteins with lipids, however, remains challenging due to the inherent complicacy of membrane protein complexes and the lack of methods. The emergence of native mass spectrometry (MS) has largely facilitated the study of the interaction between membrane proteins and lipids, as native MS offers direct measurements on individual ligand binding events, protein stabilization, allosteric coupling, and thermodynamics. This thesis will be focused on the study of the interaction between inwardly rectifying potassium channels (Kirs) and phospholipids by employing native MS. Specifically, the work will include the following topics: the correlation between Kir channels activity and their binding affinity towards key regulators phosphorylated phosphotidylinositdes (PIPs), the intervention of copurified contaminants on membrane proteins towards the interaction between lipids and membrane proteins, the specific roles of conserved amino acid residues in the binding pocket of Kir channel, the corroboration of the lipid-binding measurements made by native MS and a soluble binding assay using Förster resonance energy transfer (FRET), and the thermodynamic binding signatures of Kir3.2 with PIPs.

ACKNOWLEDGEMENTS

I would like to thank my advisor, Dr. Arthur Laganowsky, and my committee members, Dr. Thomas Meek, Dr. Pingwei Li, and Dr. David Russell for their support and guidance on the course of research. Dr. Yang Liu, a former graduate student of our group and a close colleague, offered great help to my preliminary work. Special thanks to Dr. Mary Bryk, Dr. Justine deGruyter, and Ms. Megan Teel for their support and assistance on administrative affairs.

Thanks to my family, friends, colleagues, faculty, and staff of the department for providing a temperate environment for my study at Texas A&M University.

CONTRIBUTORS AND FUNDING SOURCES

Contributors

This work was supervised by a thesis (or) dissertation committee consisting of Professor Arthur Laganowsky (advisor) and David Russell of the Department of Chemistry, Professors Thomas Meek and Pingwei Li of the Department of Biophysics, and Biochemistry.

A part of the cloning and protein expression work in Chapter II was conducted By Dr. Yang Liu of the Department of Chemistry. All other work conducted for the thesis (or) dissertation was completed by the student independently.

Funding Sources

Graduate study was supported by Professor Arthur Laganowsky's funds.

This work was also made possible in part by the National Institutes of Health (NIH) under Grant Number DP2GM123486, R01GM121751, P41GM128577, and R01GM138863.

NOMENCLATURE

MS	Mass Spectrometry
FRET	Förster resonance energy transfer
Kir3.2	G-protein Activated Inwardly Rectifying Potassium Channel 3.2
Kir3.4	G-protein Activated Inwardly Rectifying Potassium Channel 3.4
DDM	n-Dodecyl-β-D-Maltopyranoside
$C_{10}E_5$	Pentaethylene glycol monodecyl ether
DHPC	1,2-dihepanoyl-sn-glycero-3-phosphocholine
PIP	Phosphorylated Phosphatidylinositides

TABLE OF CONTENTS

Page

ABSTRACT ii

ACKNOWLEDGEMENTS iii

CONTRIBUTORS AND FUNDING SOURCES iv

NOMENCLATURE v

TABLE OF CONTENTS vi

LIST OF FIGURES viii

LIST OF TABLES x

CHAPTER I INTRODUCTION TO THE APPLICATION OF NATIVE MASS SPECTROMETRY ON MEMBRANE PROTEIN-LIPID INTERACTION 1

CHAPTER II INSIGHT INTO THE SELECTIVITY OF KIR3.2 TOWARD PHOSPHATIDYLINOSITIDES 6

- Introduction of Kir channels 6
- Materials and Methods 9
  - Protein Expression 9
  - Protein purification 11
  - Preparation of Phospholipids 13
  - Native Mass Spectrometry 13
  - Fluorescence Resonance Energy Transfer (FRET) Lipid Binding Assay 14
  - Data Analysis 15
- Results 16
  - Modification of Kir3.2 Expression Construct for Lipid Binding Studies 16
  - Characterizing Kir3.2-Lipid Interactions 17
  - Kir3.2 mutants to probe PIP binding selectivity 20
  - Impact of A Group1 Mutant on Lipid Binding 21
  - Impact of A Group2 Mutant on Lipid Binding 22
  - Impact of A Group3 Mutant on Lipid Binding 23
- Discussion and Conclusion 24

CHAPTER III INSIGHT INTO THE PHOSPHOLIPID BINDING PREFERENCES OF KIR3.4 29

Introduction of Kir3.4 29
Materials and Methods 31
Protein Expression 31
Protein Purification and Delipidation 33
Native Mass Spectrometry 34
Fluorescent Lipid Competition Assay 34
Results 35
Preparation of full-length human Kir3.4 and Kir3.2 for nMS studies 35
Characterization of Kir3.4-lipid interactions 36
Characterization of Kir3.2-lipid interactions 37
Probing Kir-lipid interacitons using fluorescent lipid competition assay 38
Characterization of mutant Kir3.4 channels with lipids 39
Discussion and Conclusion 40

CHAPTER IV ENTROPY CONFORMATIONAL ENTROPY IN THE MOLECULAR RECOGNITION OF MEMBRANE PROTEIN-LIPID INTERACTIONS 43

Introduction 43
Method and Materials 45
Plasmid construction and protein expression 45
Protein purification 46
Preparation and titration of phospholipids 47
Native mass spectrometry (MS) 47
Native MS data analysis 48
Results and Discussion 50
Conclusion 55

CHAPTER V SUMMARY AND CONCLUSION 56

REFERENCES 59

APPENDIX A FIGURES 79

APPENDIX B TABLES 116

LIST OF FIGURES

Page

Figure 1 High-throughput expression screen of *Pichia* transformants. 79

Figure 2 Identification and scale-up of well expressing Pichia transformants. 80

Figure 3 Native mass spectra of purified Kir3.2 mutants after delipidation with DHPC.....81

Figure 4 Biophysical characterization of mouse Kir3.2-lipid interactions using native mass spectrometry (MS). 82

Figure 5 Kir3.2-lipid interactions characterized by solution FRET-based lipid binding assays. 83

Figure 6 Details of the molecular interaction of PI(4,5)P2-d8 with Kir2.2 and Kir3.2. ..84

Figure 7 Kir3.2^{K64Q} characterized by native MS and FRET-based lipid binding assays uncover a preference toward acyl chains. 85

Figure 8 Native MS and FRET assay reveal Kir3.2^{R92P} non-selective binding to PIPs...86

Figure 9 Native MS and FRET-based lipid binding assays of Kir3.2^{K194A}-lipid interactions. 87

Figure 10 Biophysical characterization of Kir3.4-lipid interactions. 88

Figure 11 Native MS of human Kir3.2 in complex with phospholipids. 89

Figure 12 Kir3.4 and Kir3.2 fluorescent lipid binding and competition assays. 90

Figure 13 Kir3.4^{S143T} lipid interactions characterized by native MS. 91

Figure 14 Native MS reveals Kir3.4^{D223N} enhanced binding to PIPs. 92

Figure 15 Biophysical characterization of full-length human Kir3.4 channels before and after delipidation. 93

Figure 16 Biophysical characterization of full-length human Kir3.2 channels before and after delipidation. 94

Figure 17 Native mass spectra for Kir3.4 with lipids. 95

Figure 18 Native mass spectra for Kir3.2 with lipids. 96

Figure 19 Native mass spectra for Kir3.4^{S143T} with lipids. 97

Figure 20 Native mass spectra for Kir3.4^{D223N} with lipids.....98

Figure 21 Determination of binding thermodynamics for Kir3.2-lipid interactions.....99

Figure 22 Thermodynamic signatures of specific phosphoinositides binding to different states of Kir3.2. 100

Figure 23 Alterations in thermodynamic signatures for a stepwise transition from DOPI to DOPI(3,4,5)P_3 and acyl chain chemistry of PI(4,5)P_2. 101

Figure 24 Native mass spectra of Kir3.2 with DOPI from one of the titration series....102

Figure 25 Deconvoluted native mass spectra of Kir3.2 with DOPI. 103

Figure 26 Representative native mass spectra of Kir3.2 with DOPI(4)P.....104

Figure 27 Deconvoluted native mass spectra of Kir3.2 with DOPI(4)P. 105

Figure 28 Representative native mass spectra of Kir3.2 with DOPI(4,5)P_2. 106

Figure 29 Deconvoluted native mass spectra of Kir3.2 with DOPI(4,5)P_2.....107

Figure 30 Representative native mass spectra of Kir3.2 with DOPI(3,4,5)P_3. 108

Figure 31 Deconvoluted native mass spectra of Kir3.2 with DOPI(3,4,5)P_3.....109

Figure 32 Representative native mass spectra of Kir3.2 with SAPI(4,5)P_2. 110

Figure 33 Deconvoluted native mass spectra of Kir3.2 with SAPI(4,5)P_2. The panels match the concentrations reported in figure 24. 111

Figure 34 The plot of the mole fraction of Kir3.2 and Kir3.2•DOPI$_1$ as a function of free DOPI concentration. 112

Figure 35 Plots of the mole fraction of apo and lipid-bound protein as a function of free lipid concentration. 113

Figure 36 Equilibrium-coupled-binding model for the docked and extended states of Kir3.2 binding lipids. 114

Figure 37 van't Hoff plots for Kir3.2-lipid interactions.....115

LIST OF TABLES

Page

Table 1 Full name and abbreviations for synthetic and BODIPY-modified lipids used in Chapter 2.....116

Table 2 Apparent binding parameters determined for WT and mutant Kir channels binding BODIPY-modified lipids in Chapter 2.....117

Table 3. Summary of expression and purification of mutant Kir3.2 channels in Chapter 2.....118

Table 4 Representative average number of lipids bound to WT and mutant Kir3.2 channels in Chapter2.....119

Table 5 Phospholipids and their abbreviations used in Chapter 3. 120

Table 6 Theoretical and measured mass of protein complexes in Chapter 3. 121

Table 7 Equilibrium binding constants for Kir3.2-lipid interactions in chapter 4. 122

Table 8 Thermodynamic parameters for Kir3.2-lipid binding in chapter 4. 123

Table 9 Differences in thermodynamic parameters for Kir3.2-lipid interactions in chapter 4.....124

CHAPTER I

INTRODUCTION TO THE APPLICATION OF NATIVE MASS SPECTROMETRY ON MEMBRANE PROTEIN-LIPID INTERACTION

As one of the major components of biological membranes, membrane proteins are vital in sustaining the membrane function[1-3]. Membrane proteins can be categorized into two groups based on their interactions with membranes: peripheral and integral membrane proteins[2, 4]. Peripheral membrane proteins transiently associate with the cell membrane and can easily be removed by changing the environment in the solution, such as pH value. Integral membrane proteins, on the other hand, are embedded in the cell membrane and can only be isolated with the disruption of lipid bilayer using chemical reagents, like detergents[5, 6]. Membrane proteins are involved in vital physiological functions, including molecular trafficking through the cell membrane, cell-to-cell signal transduction, and chemical reaction catalysis[7, 8]. Due to their unique roles in the human body, misfunction of membrane proteins can cause serious diseases, such as Bartter and Andersen syndromes and Alzheimer's disease [9-11]. Therefore, membrane proteins have drawn great attention from the pharmaceutical industry. Nearly half of all drugs on the market target membrane proteins[12].

The structure and function of membrane proteins are under the regulation of many factors in the surrounding environment, including lipids[13, 14]. The regulatory impacts lipids can have on membrane proteins includes matter transport [15], enzymatic activity [16], protein oligomerization[17], and structure stabilization[18]. The lipids in the biological membrane bilayer can be categorized into three groups: bulk lipids, annual

lipids, and non-annular, based on their relationship with membrane proteins[19]. As the major component in the membrane, bulk lipids regulate membrane proteins by randomly constituting the lipid bilayer plane. Annual lipids associate with membrane proteins more tightly by forming a 'belt' around the membrane protein. Thus, annual lipids are also referred to as boundary lipids. Non-annular lipids bind to membrane protein at specific sites and directly regulate the function of membrane proteins[19, 20]. Lipids that play direct roles in membrane protein regulation are often non-annular, they are also known as lipid cofactors[21].

Non-annular lipids are prone to bind membrane proteins avidly. Take phosphorylated phosphotidylinositdes (PIPs) as an example. Over two decades, many studies have been conducted to demonstrate the regulation of PIPs on most ion channels, such as inwardly rectifying potassium channels (Kirs), voltage-gated calcium channels (Ca_V), and two-pore domain potassium channels (K_{2P})[22-26]. As lipid regulation and lipid binding are often correlated, the binding between lipids and membrane proteins have become a shared interest in the field. Tightly bound lipids are often identified during the isolation of membrane proteins[5, 27]. For example, a tightly bound lipid analog was observed on the crystal structure of KcsA, a pH-regulated potassium channel from the gram-positive bacterium *Streptomyces lividans* [28]. Thin-layer chromatography (TLC) was used to separate and identify this lipid that copurified with KcsA. The ligand turned out to be an anionic lipid phosphatidylglycerol (PG) that stabilizes the tetrameric structure of KcsA[28]. As most purified membrane proteins are extracted from the biological membrane using detergents, the type of bound lipids can be

altered by the detergents used for extraction[29, 30]. This hypothesis was verified in a systematic study where three model membrane proteins AdiC (amino acid transporter), UT (urea transporter), and LacY (lactose permease) were over-expressed and extracted from *E. coli* with nine different detergents. The amount and type of the extracted lipids were characterized with size-exclusive chromatography (SEC) and mass spectrometry (MS). The results showed significantly different lipid ingredients that were copurified with membrane protein across the tested detergents [29].

Although these works have provided insight into the interactions between membrane proteins and lipids, the direct protein-lipid binding study was not included. To address this gap in knowledge, membrane protein-lipid interactions are being studied by methods including cryo-EM, solid state NMR (Nuclear Magnetic Resonance), X-ray crystallography, differential scanning calorimetry, surface plasmon resonance, and Förster resonance energy transfer (FRET)[19]. The methods that are commonly used in structural studies, X-ray crystallography, NMR and Cryo-EM give direct insight into the ligand binding information on the protein structure[19, 31, 32]. These methods, however, are often limited by the high sample heterogeneity and the low lipid integration efficiency of membrane protein-lipid complex[33, 34]. Besides, these methods are suitable for proteins with specific sizes. For example, NMR are appropriate only for small proteins. Cryo-EM, on the other hand, can only observe large protein particles. X-ray crystallography is restricted by the crystallization efficiency that depends on the protein quality. Recently, a fluorescent lipid-binding assay based on FRET has been introduced to obtain the binding constant between lipid and membrane proteins [35].

This study observed a high binding affinity between a fluorophore-labeled $PI(4,5)P_2$ ($FL\text{-}PIP_2$) and a two-pore domain potassium channel (TREK-1). However, almost no binding was observed between Kir3.2 and $FL\text{-}PIP_2$, which is in contrast to the physiological effect of PIPs [15, 26, 35-38].

With the emergence of native mass spectrometry (MS), researchers have been granted a new method in membrane protein studies. Different from the conventional mass spectrometry techniques that are largely used in the detection of molecules for lipidomics, proteomics, and metabolomics[39], native mass spectrometry analyzes the intact protein complex. The term 'native' describes the protein preserved in an environment that is close to its natural conditions prior to the ionization process[40, 41].

Native MS is also known as 'non-covalent MS' because it emphasizes maintaining both the covalent and non-covalent interaction within the complex, including the interaction within the protein or between protein and the ligands[40, 42]. One advantage of native MS is the ability to distinguish individual lipid binding events instead of the ensemble of interactions reported by other methods. Native MS has been utilized in many studies with membrane proteins, such as the identifying lipids that stabilize membrane protein complexes [17, 18]. It has also been used to determine the binding thermodynamics of protein-lipid interactions, and the allosteric coupling for protein-lipid interactions [43-45]. For example, the binding preference of Kir3.2 for the $PI(4,5)P_2$ headgroup was observed in native MS [45]. Although great insights have been given into the membrane protein lipid interactions, the study upon this topic is still limited. This dissertation will be focused on the interactions between inwardly rectifying

potassium channels (Kirs) and phosphorylated phosphotidylinositdes (PIPs) using native MS. Native MS, together with soluble lipid binding assay will be used to show the importance of pure membrane proteins devoid of copurified contaminants. This work will also look into the thermodynamic signatures of Kir3.2 with PIPs, and also investigate the impacts of phosphate groups and acyl chains.

CHAPTER II

INSIGHT INTO THE SELECTIVITY OF KIR3.2 TOWARD PHOSPHATIDYLINOSITIDES

Introduction to Kir channels

[1]Inwardly rectifying potassium (Kir) channels are integral membrane proteins that facilitate directional transport of potassium ions across the cell membrane[6, 46]. Kir channels participate in numerous physiological functions, such as renal potassium transport, regulation of heartbeat rate, pancreatic insulin secretion and neuronal signaling[47-50]. Kir channels are expressed in tissues throughout the body and genetic alterations in these channels have been linked to a number of diseases[51-54]. Importantly, Phosphatidylinositol 4,5-bisphosphate ($PI(4,5)P_2$), a minor component of the cytoplasmic leaflet [55], is required for activation of all Kir channels[20, 56-58]. Most interestingly, mutations in residues important for binding PIP_2 are associated with Bartter and Andersen syndromes, and other diseases[48, 59]. Kir channels are also regulated by a number of other molecules including phosphorylation by protein kinases A and C, sodium, pore blockers (polyamine, Mg^{2+}), and ethanol[47, 60, 61]. Kir3.x channels (GIRKs) are unique in that they require G proteins in addition to $PI(4,5)P_2$ for function with some of these channels modulated by sodium ions[47, 62]

---

*Reprinted with permission from "Insight into the selectivity of Kir3.2 toward Phosphatidylinositides" by Qiao *et al.,* 2020, Biochemistry 59, 2089-2099, Copyright 2020 by American Chemical Society

Kir channels appear to have varied specificity towards phosphoinositides (PIPs) [57, 63-66]. The constitutively open Kir channels (*e.g.*, Kir2.x) are maximally activated by $PI(4,5)P_2$ and marginally activated by $PI(3,4)P_2$ and $PI(3,4,5)P_3$. The G-protein-gated K^+ channels Kir3.4 and Kir3.1/Kir3.4 complexes are activated to the greatest extent by $PI(3,4,5)P_3$ and $PI(4,5)P_2$ and to a lesser extent by other PIPs, such as $PI(3,4)P_2$ and $PI(3,5)P_2$ [47, 56, 57]. More specifically, almost all Kir channels are not activated by $PI(3,4)P_2$ demonstrating that PIPs can also have inhibitory roles[57]. Some Kir channels, such as Kir6.2, are promiscuously activated by PIP isoforms[57]. Moreover, phosphoinositides have variable lipid tails with $PI(4,5)P_2$ primarily comprised of polyunsaturated fatty acyl chains, whereas PIP_3 contains either saturated or monounsaturated acyl chains[67, 68]. The hetero oligomeric Kir3.1/Kir3.4 channel has a distinct preference for $PI(4,5)P_2$ with 18:0-20:4 tails[63], which is the most physiologically abundant form in mammalian cells[69], whereas Kir2.1 displays no preference for the acyl chains[70]. The marked differences in Kir channel activation by signaling lipids suggest Kir channel subtypes may exhibit unique selectivity toward PIP isoforms.

Crystal structures of Kir2.2 and Kir3.2 in complex with a short chain (di-octanoyl, 8:0-8:0) derivative of $PI(4,5)P_2$ have revealed detailed chemical properties of the molecular interaction and provide clues to the observed selectivity towards PIPs [20, 71]. The signaling lipid binds a distinct site on an individual Kir channel subunit located at the interface of transmembrane domain (TMD) and N-terminal cytoplasmic domain (NTD)[37, 71, 72], where a number of residues are precisely positioned to interact with

the negatively charged head group of $PI(4,5)P_2$. More specifically, the outer helix forms several interactions with the phosphoglycerol backbone of the lipid and inositol headgroup. A network of conserved lysine, glutamine, and arginine residues located on the C-linker (or "tether helix") primarily interact with the 5' phosphorylation of $PI(4,5)P_2$[38]. Lys64 of Kir3.2 interacts with the 4' phosphorylation position of $PI(4,5)P_2$ whereas this electrostatic interaction is absent for Kir2.2. Although these structures illuminate key molecular interactions, the molecular mechanism for the selectivity of Kir channels toward $PI(4,5)P_2$ over other isoforms remains poorly understood.

A number of studies have been directed at understanding the residues involved in the interaction of PIPs with Kir channels by means of functional assays [38, 59, 73, 74]. The use of $PI(4,5)P_2$ antibodies has suggested that Kir1.1 binds PIPs more strongly than Kir3.2 and Kir3.1/3.4 [56]. Studies of mutant and chimeric channels indicate the specific residues, located within the PIP binding site, contribute to the different preferences for PIPs [59, 73, 74]. Mutation of lysine residues within the "tether helix" of the Kir3.2 channel showed that Lys200 can enhance the interaction of $PI(4,5)P_2$ with the channel [38]. Functional assays have implicated residues responsible for Kir channel activation by PIPs, however the consequence of mutant and chimeric channels on individual PIP binding events is not known.

Native mass spectrometry (MS) is an emerging biophysical technique that can provide invaluable insight into biomolecular interactions. Unlike other approaches that typically report on the ensemble, native MS can resolve individual ligand binding

events. Native MS has also revealed that specific protein-lipid interactions can stabilize protein complexes [17, 75] and allosterically modulate other interactions with protein[76, 77], lipids[78], and drugs[79, 80]. Moreover, the technique has also been applied to determine thermodynamic binding signatures for individual phospholipid binding to an integral membrane protein, demonstrating both the head-group and acyl chain length of the lipid contribute to binding [43, 44]. More recently, we reported lipid-binding profiles of Kir3.2 using native MS, revealing a defined selectivity toward PIP isoforms whereby weakly activating PIP isoforms have reduced affinity towards the channel [45]. This finding agrees with earlier electrophysiology studies on similar Kir channels[56].

To gain insight into the selectivity of Kir3.2 toward PIP isoforms, mutations were generated for the conserved residues within the PIP binding pocket of Kir3.2. Lipid binding to mutant channels that could be successfully expressed and purified were characterized by native MS and fluorescence resonance energy transfer (FRET) based lipid binding assays. Our results demonstrate the necessity of pure samples, devoid of co-purified contaminants, to properly characterize membrane protein-lipid interactions. We also find that a single point mutation in the PIP binding site of Kir3.2 can alter phospholipid binding profiles and consequently tune the selectivity for PIPs.

Materials and Methods

Protein Expression

The plasmid for expression of mouse Kir3.2 (KCNJ6, residues 52-380, Uniprot P48542) in *Pichia pastoris* reported in our previous study [45] (AddGene 124277) was

modified as follows. The C-terminal green fluorescent protein was replaced by the monomeric red fluorescent protein (mCherry), which was codon-optimized for *Pichia pastoris* using the Codon Optimization Tool available on the Integrated DNA Technologies (IDT) website, synthesized as a gBlock gene fragment (IDT) with a C-terminal Strep-tag II, and cloned into the expression vector using HiFi DNA Assembly (New England Biolabs, NEB) following manufacturer protocol. The three-residue linker located between the Kir3.2 and the Tobacco Etch Virus (TEV) protease sequence was modified to Gly-Pro-Gly using a Q5 Site Directed Mutagenesis kit (NEB). Strep-tag II sequence was fused to the C terminus of mCherry for affinity purification. Point mutants were introduced using a Q5 Site Directed Mutagenesis kit (NEB) following manufacturer's protocol. Sequence-verified expression plasmids were amplified by polymerase chain reaction with Q5 High-Fidelity PCR (NEB) with primers flanking the PmeI restriction site (pIC_LINEAR_F: 5'-GCTGTCTTGGAACCTA-ATATG-3'; pIC_LINEAR_R: 5'-TGTCAGTTTTGGGCCATTTG-3'). The linearized vectors were purified by agarose gel electrophoresis and extracted from gel slices using gel extraction kit (Omega BioTek). The linearized plasmid (~2 μg) was then transformed into *P. pastoris* KM71 (Invitrogen) by electroporation (ECM 630 from BTX) following manufacturer's protocol. Transformants were selected on 1.5% agar plates containing 500 μM and 1000 μM Zeocin at 30 ^{o}C. A high-throughput expression screen [81] was adapted for selection of high-level expressing transformants. In brief, individual colonies were inoculated into 500 μl of YPD media with 100 μM Zeocin in 96 deep well blocks, then grown overnight in an incubating microplate shaker (30 ^{o}C, 900 rpm, VWR). 50 μl

of culture was transferred into 900 µl BMGY (1% yeast, 2% peptone, 1% glycerol, 1% yeast nitrogen base and 0.1 M potassium phosphate, pH 6.1) on the following day into a new 96-well block and grown at 30 °C while shaking at 900 rpm. After 24 hours, cells were pelleted by centrifugation (2500 *xg* for 5 minutes) and the supernatant was carefully discarded. The cell pellets were resuspended in 900 µL of BMMY media (1% yeast, 2% peptone, 1% methanol, 1% yeast nitrogen base and 0.1 M potassium phosphate, pH 6.1) and incubated at 30 °C, 900 rpm. After 36 to 48 hours, cells were pelleted by centrifugation as described above. Cells that appeared red in color corresponding to the mCherry expression reporter were selected for scale-up expression (typically 4L). For scale-up expression, the selected clone was grown in 25 mL of YPD (30 °C, 130 rpm) in a small Erlenmeyer flask overnight prior to transferring into 300 ml of BMGY (30 °C, 130 rpm). After 24 hours, cells were pelleted in a sterile container and resuspended into 600 ml BMMY, with the flask opening covered with gauze or foam plugs. After 48 hr incubation, cells were harvested with centrifugation (3,000 *xg*, 10 min) and resuspended with lysis buffer (50 mM Tris, 300 mM KCl, pH 7.5). Cells were either used immediately or stored at -80 °C.

Protein purification

Cell pellets were resuspended in lysis buffer (40 mL per 600 mL of culture) and passed through a microfluidizer (M-110PS, Microfluidics Inc.) set to 30,000 psi four times in total. Cell lysate was centrifuged at 25,000 x*g* for 20 min to remove cell debris. Membrane fraction was collected from the supernatant by centrifugation at 100,000 x*g* for 2 hr at 4 °C. The membrane pellets were resuspended in membrane resuspending

buffer (50 mM Tris, 300 mM KCl, 10% glycerol, pH7.5 at 24 °C) using a glass tissue homogenizer (Wheaton). Membrane proteins were extracted with 1.5% (w/v) n-Dodecyl-β-D-Maltopyranoside (DDM, Anatrace) overnight while stirring at 4 ^{o}C. The mixture was clarified by centrifugation (25,000 x*g*, 20 min), filtered through a 0.45 μm syringe filter (Pall corp.) prior to loading onto a 5mL StrepTrapHP column (GE healthcare) equilibrated in SPKHA buffer (50 mM Tris, 150 mM KCl, 10% glycerol and 0.025% DDM, pH 7.4 at RT). After loading, the column was washed with 5 column volumes (CV) and protein was eluted with SPKHB buffer (50 mM Tris, 150 mM KCl, 10% glycerol, 0.025% DDM and 3 mM D-desthiobiotin, pH7.4 at RT). Peak fractions were pooled and injected onto a HiPrep 26/10 desalting column (GE Healthcare) pre-equilibrated in SPKHA to remove D-desthiobiotin. Protein can be stored at -80 ^{o}C at this point.

To obtain pure Kir3.2 samples devoid of contaminants, an aliquot of protein was loaded onto a drip column packed with 0.5 ml of Strep-tactin Sepharose (IBA Biosciences) equilibrated in SPKHA at room temperature. After loading, five CVs of delipidation buffer SPKHC (50 mM Tris, 150 mM KCl, 10% glycerol and 6 mM DHPC [1,2-dihepanoyl-sn-glycero-3-phosphocholine], pH7.4) was passed through the column. The column was capped and incubated at room temperature for 10 min. Afterwards, an additional 5 CV of SPKHC was applied followed by washing with 10 CVs of SPKHD (50 mM Tris, 150 mM KCl, 10% glycerol and 0.065% $C_{10}E_5$ [Pentaethylene Glycol Monodecyl Ether], pH7.4). The protein was eluted with 0.5 mL of SPKHE (50 mM Tris, 150 mM KCl, 10% glycerol, 0.065% $C_{10}E_5$ and 3 mM D-desthiobiotin, pH7.4 at RT).

The sample at this stage was used for FRET-based lipid binding assays. For native MS studies, the sample was mixed with TEV protease produced in-house[82] and 10 mM 2-Mercaptoethanol. The molar ratio between membrane protein and TEV was roughly 70:1, respectively, and the reaction mixture was incubated at room temperature for 3-4 hours or overnight at 4 ^{o}C. After incubation, sample solution was filtered through a 0.45 μm centrifugal device (Milipore spin-filter) prior to loading onto a Superdex 200GL 10/300 column (GE) pre-equilibrated with SPKHD buffer. Peak fractions were pooled and concentrated using a 100,000 MWCO centrifugal concentrator (MilliporeSigma). The concentration of fusion protein was determined by absorbance at 587 nm using an extinction coefficient of 0.27 $\mu M^{-1}cm^{-1}$, which was obtained using a *DC* Protein Assay Kit (Bio-Rad Laboratories). The concentration of protein after TEV treatment was determined by absorbance at 280 nm using an extinction coefficient of 6.4 $\mu M^{-1}cm^{-1}$. The concentrated protein (~ 2 μM) was exchanged into an aqueous ammonium acetate solution AA (200 mM ammonium acetate, 0.065% $C_{10}E_5$, pH 7.4) for native mass spectrometry studies.

Preparation of Phospholipids

Phospholipids were purchased from Avanti Polar Lipids. Lipids and their abbreviations used in this study can be found in Table 1. Lipids were prepared as previously described. [44] In brief, lipids in chloroform solution were dried and lipid films solubilized in AA. Diluted lipid stocks were prepared one day in advance of native mass spectrometry measurements.

Native Mass Spectrometry

WT and mutant Kir3.2 channels in AA were analyzed on a Synapt G1 HDMS mass spectrometer (Waters Corporation). For lipid binding studies, Kir3.2 samples were mixed with lipids at a molar ratio of 1:3.3, respectively. Samples were loaded into gold-coated capillaries prepared in-house and infused into the mass spectrometer using nanoelectrospray ionization with instrument settings as previously described [45]. Briefly, the source was tuned to 1.75 kV capillary voltage, 150 V sampling cone voltage, 10 V extraction cone voltage, and 80 ^{o}C source temperature. The trap collision energy and transfer collision energy were set to 130 V and 60 V, respectively. Data acquisition per replicate was on the order of two minutes. Data collected from the mass spectrometer was deconvoluted using UniDec [83] to determine the mole fraction of different species.

Fluorescence Resonance Energy Transfer (FRET) Lipid Binding Assay

BODIPY PE (1-palmitoyl-2-(dipyrrometheneboron difluoride) undecanoyl-sn-glycero-3-phosphoethanolamine, cat no. 810282 from Avanti Polar Lipids) and BODIPY PI(4,5)P_2 (BODIPY FL Phosphatidylinositol 4,5-bisphosphate, cat no. C-45F6 from Echelon Biosciences) served as donors to excite the Kir3.2-mCherry fusion (acceptor). FRET measurements and correction factors were performed in a similar fashion as described by Hieb *et al*. [84]. In detail, spectral overlap for donor crosstalk with acceptor emission (χ_D) was calculated from the ratio of the FRET (**F**; 477 nm excitation, 620 nm emission) and Donor (**D**; 477 nm excitation, 525 nm emission) signals for donor only sample:

$$\chi_D = \left(\frac{F}{D}\right)_{Donor\ Only}$$

Correction for direct excitation (χ_D) of acceptor (**A**; 570 nm excitation, 620 nm emission) for acceptor only sample:

$$\chi_A = \left(\frac{F}{A}\right)_{Acceptor\ Only}$$

The FRET signal for samples containing acceptor and donor can be corrected (Fcorr) by subtracting overlap values using the following equation:

$$F_{corr} = F - (\chi_D \cdot D) - (\chi_A \cdot A)$$

FRET signals were normalized according to the detergent class. Fluorescent lipids were titrated into a solution containing 0.5 μM final concentration of protein in SPKHE buffer supplemented with 2x CMC of detergent. A total volume of 50 μl of the protein-lipid mixture was measured in a 384-well plate with black walls and clear bottom (NUNC, cat no. 142761) with a CLARIOstar microplate reader (BMG LABTECH) at room temperature. For competition assay, BODIPY lipids at 4 μM final concentration and phospholipids were added to a final concentration of 8 μM in SPKHE buffer supplemented with 2x CMC of detergent and measurements recorded at room temperature.

Data Analysis

Multiple-sequencing alignment was conducted on the online Clustal Omega server [85]. Structural images were prepared with Pymol version 2.3.

Results

Modification of Kir3.2 Expression Construct for Lipid Binding Studies

In our previous study[45] we observed a number of phosphorylation events of the intact Kir3.2 complex by native MS, which we subsequently mapped to several sites using traditional bottom-up proteomics. Two serine residues that are part of the linker region between Kir3.2 and the TEV protease cleavage site of the expression construct were unexpectedly both found to be singly phosphorylated. This result prompted us to modify the linker to remove these post-translational modifications (see methods). At the same time, we replaced the C-terminal green fluorescent protein (GFP) fusion protein with a *Pichia* codon optimized monomeric red fluorescent protein (mCherry)[86]. The mCherry fusion protein was selected in our study for FRET-based lipid binding studies (discussed below) but we also find this protein to be a better reporter for identifying *Pichia* transformants that display high-level of protein expression (Figure 1 and 2).

To compare our modified construct to our previous version, we expressed and purified Kir3.2 for native MS analysis. The native mass spectrum of the fusion protein purified following methods for structural studies [20, 37, 71] using dodecyl-β-D-maltopyranoside (DDM), a commonly used detergent in membrane protein research, yielded broad mass spectral peaks that could be assigned to the mass of the tetrameric complex but with additional mass (Figure 4A). The broad peaks stem from co-purified contaminants bound to the Kir3.2 complex that are heterogenous in nature, convoluting MS analysis [45]. Notably, the broadness observed for the mCherry fusion is reduced compared to our previous construct *i.e.,* less heterogenous. The nature of the

contaminants is unknown, but we speculate that the impurities are co-purified lipids and/or other small hydrophobic molecules. In our previous work,[45] pure samples of the Kir3.2 complex could readily be obtained by washing with a short chain phospholipid, DHPC (1,2-diheptanoyl-sn-glycero-3-phosphocholine) followed by exchange into pentaethylene glycol monodecyl ether ($C_{10}E_5$), a charge-reducing detergent with ideal properties for native MS studies [45, 87, 88]. Here, we employed a detergent screening approach[89] whereby the fusion protein is washed with DHPC while bound to affinity resin. The eluted material resulted in a well-resolved native mass spectrum consistent in mass with the tetrameric Kir3.2 channel (Figure 4B). This result is in contrast to our previous expression construct where an on-column wash was ineffective at completely removing the contaminants. Taken together, native MS analysis of membrane protein complexes provides modern means to ascertain sample quality and, in this case, revealed the necessity to improve methods to obtain pure Kir3.2 samples devoid of contaminants.

Characterizing Kir3.2-Lipid Interactions

As a step towards characterizing Kir3.2-lipid interactions, we conducted native MS studies to obtain lipid binding profiles for the pure wild type (WT) channel. In a similar fashion to our previous study, [45] we mixed Kir3.2 samples with phosphatidylinositol-4-phosphate (PI(4)P), phosphatidylinositol-3,4-bisphosphate ($PI(3,4)P_2$), and $PI(4,5)P_2$ with dioleoyl acyl chains (18:1–18:1, do), dioctanoyl (8:0–8:0, d8) $PI(4,5)P_2$, 1-stearoyl-2-arachidonoyl (18:0–20:4, sa) $PI(4,5)P_2$-sa, phosphatidylinositol-3,4,5-triphosphate ($PI(3,4,5)P_3$-sa), do-type acyl chains (DOPI),

and phosphatidylethanolamine (PE) with 1-palmitoyl-2-oleoyl (16:0–18:1, PO) acyl chains at a protein to lipid molar ratio of 1:3.3, respectively (Table 1). The native MS measurements obtained for all protein-lipid mixtures show up to four lipids bound per channel including peaks corresponding to the apo channel (Figure 4C). For comparative analyses, the native mass spectra are deconvoluted[83] allowing the intensities of different lipid bound species to be extracted followed by conversion to mole fraction. The binding profiles for Kir3.2-lipid interactions are similar to our previous study where a slightly higher molar ratio of lipid to protein was used (Figure 4D). More specifically, Kir3.2 binds avidly to PI(3,4,5)P_3-sa and PI(4,5)P_2 independent of acyl chain. In contrast, PI(4)P-do has a lower binding affinity as evident by the increased abundance of the apo state, indicating that the 5' phosphate is important for selective binding. The high binding affinity for PIPs becomes evident when comparing the binding profile for PI-do and POPE, a bulk phospholipid, where the mole fraction for the apo state predominates. In short, Kir3.2 binds PI(3,4,5)P_3 and PI(4,5)P_2 more avidly over other PIP isoforms that appears to be insensitive toward acyl chain length.

To corroborate our native MS findings, we employed a solution FRET-based lipid binding assay[35] to monitor binding of fluorophore-modified lipids to the Kir3.2-mCherry fusion protein. For these studies, we selected PE and PI(4,5)P_2 modified with a BODIPY (B-PE and B-PI(4,5)P_2) moiety covalently attached to the short acyl chain either at the sn2 or sn1 position, respectively (Figure 5A). We first tested binding of B-PE to pure Kir3.2-mCherry exchanged into different detergents: decyl-ß-D-maltopyranoside (DM), DDM, undecyl-ß-D-maltopyranoside(UDM), $C_{10}E_5$ and

octaethylene glycol monododecyl ether ($C_{12}E_8$). FRET measurements at different concentrations of B-PE were performed to generate B-PE binding curves (Figure 5B). As native MS measurements indicate that a distribution of lipids is bound to Kir3.2 under these conditions, the equilibrium dissociation constant (K_D) for individual lipid binding events is not easily extracted from these solution binding curves. Nevertheless, a Hill binding model was fit to the data to obtain a K_D and Hill coefficient to serve as proxies for comparing different samples. Pure Kir3.2-mCherry samples solubilized in the three different detergents bind B-PE with a binding affinity (Table 2) that is statistically indistinguishable. No FRET signal was observed in shorter chain detergents, DM and $C_{10}E_5$, indicating that these detergents effectively compete with B-PE binding to Kir3.2.

We next performed similar experiments for B-PI(4,5)P_2 binding to Kir3.2-mCherry in DDM or $C_{10}E_5$ (Figure 5C). The binding curve obtained in $C_{10}E_5$ revealed cooperative binding (Hill coefficient of 2.7) for B-PI(4,5)P_2 and with a higher affinity than B-PE (K_D = 0.9 μM). The cooperativity in binding B-PI(4,5)P_2 is consistent with the binding profiles obtained for unmodified PIPs using native MS. B-PI(4,5)P_2 binding to Kir3.2-mCherry in DDM had a similar binding affinity (K_D = 1.1 μM) but lacked cooperativity in binding with a Hill coefficient of 1.2. As these results are in contrast to a previous report [35], where no B-PI(4,5)P_2 binding was observed, we repeated these measurements but with the Kir3.2-mCherry fusion purified following commonly used methods where DDM is used throughout the purification. Unlike the contaminated sample, the B-PI(4,5)P_2 binding curve for the Kir3.2-mCherry sample in DDM had a shallow

binding curve, indicating a reduction in cooperativity (Figure 5C). Regression of a Hill model to the data resulted in ambiguous values. Taken together, the data clearly demonstrate that the binding curves for contaminated Kir3.2-mCherry samples, either in DDM or $C_{10}E_5$, are negatively impacted or hindered by the co-purified contaminants and highlight the importance of pure samples.

To compare the binding profiles obtained using native MS, we performed competition assays between the fluorophore-modified lipid in the presence of other lipids at a fixed molar ratio of 1:2, respectively (Figure 5D). To avoid issues associated with contaminated samples, pure Kir3.2-mCherry sample in $C_{10}E_5$ was used in these assays. All of the PIPs were able to compete with B-PI(4,5)P_2, among which PI(3,4,5)P_3-sa showed the largest decrease in FRET signal consistent with native MS studies. PI(4)P was the least competitive of the PIPs studied. In general, the PO-type lipids resulted in a marginally drop in FRET signal. Similar FRET signal was observed for PO-type lipids with the exception of POPA and POPS. Interestingly, POPA competed with B-PI(4,5)P_2 binding to Kir3.2-mCherry at the same level as PI(4)P-do. The results from the competition assay for B-PI(4,5)P_2 corroborates our native MS findings and show that POPA can compete to similar levels as PI(4)P.

Kir3.2 mutants to probe PIP binding selectivity

To glean insight into the residues responsible for the selectivity of Kir3.2 toward PIP isoforms, we inspected atomic structures of Kir channels in complex with PI(4,5)P_2-d8 and sequence alignments of Kir protein sequences (Figure 6). Although the PIP binding domain is conserved among the family of Kir channels, there are variabilities in

sequence that may account for the differences in binding and activation of the different Kir channels[64, 65]. We assigned residues responsible for the molecular interaction between PI(4,5)P_2 and Kir3.2 into three groups. The first group (Group1) contains one residue located on the N-terminal domain (NTD) where Lys64 of Kir3.2 forms a hydrogen bond to the 4' phosphate (Figure 6B). The equivalent position in Kir2.2 is Gln51, and it does not form a hydrogen bond (Cδ of Gln51 is ~8 Å from the oxygen of 4' phosphate). The second group (Group2) contains residues located at the end of the first transmembrane helix (TM1) that primarily interact with the phosphoglycerol bridge and inositol headgroup of the lipid, such as Arg78 and Arg80 in Kir2.2 (Lys90 and Arg92 in Kir3.2) (Figure 6C). This group also includes a conserved Trp79 in Kir2.2 (Trp91 in Kir3.2) that pi stacks with a conserved Lys183 in Kir2.2 (Lys194 in Kir3.2). The final group (Group3) contains a set of conserved residues located on the "C-linker" that hydrogen bond to the phosphates of PIPs. In Kir3.2, this includes Lys194, Gln197, Lys199 and Lys200 that collectively interact with the 4' and 5' phosphate groups. The three groups were targeted for mutagenesis studies with the goal of either abolishing the interaction from this residue or mimicking another Kir channel subtype.

Impact of A Group1 Mutant on Lipid Binding

To understand the impact of Group1 on lipid binding, we generated the K64Q mutant of Kir3.2 and subjected it to lipid binding studies. Native MS results for $Kir3.2^{K64Q}$ reveal an appreciable impact not only on binding affinity to PIP isoforms but also a new preference for acyl chains (Figure 7A-B). The majority of PIPs exhibited decreased binding affinity as evident from the increased abundance of the apo mutant

channel. PI(3,4,5)P_3-sa and PI(4,5)P_2-sa were among the PIPs with highest amount of binding. However, PI(4,5)P_2 with do- type tails had reduced binding nearly comparable to that of PI(3,4)P_2. A slight reduction in binding affinity was also observed for PI-do compared to the WT channel. In contrast, POPE binding was indistinguishable between the mutant and parent protein. Consistent with binding profiles from native MS, the B-PI(4,5)P_2 binding curve in $C_{10}E_5$ displayed no cooperativity and the K_D increased 6-fold (Figure 7C, Table 2). Moreover, PI(3,4,5)P_3-sa and PI(4,5)P_2-sa, lipids that bound with the highest avidity to Kir3.2^{K64Q}, competed the most with B-PI(4,5)P_2. The PO-type lipids did not strongly compete and POPA displayed no competition unlike the WT channel (Figure 7D). These results implicate a direct role of Lys64 in PIP binding affinity to Kir3.2.

Impact of A Group2 Mutant on Lipid Binding

In context of the Kir family, Group2 residues can be one of three conserved amino acids: Lys, Arg or Pro. The first mutant we generated was K90R of Kir3.2, a residue found in an equivalent position in Kir2.2. Unlike the WT channel, no transformant harboring the integrated Kir3.2^{K90R} expression cassette with suitable protein expression level was identified (Figure 1, Table 3). The second mutant Kir3.2^{R92P} - Pro being the residue in Kir6.2 - not only expressed well but could be purified for lipid binding studies. Lipid binding profiles Kir3.2^{R92P} obtained using native MS showed an overall increase in binding with lipids in comparison to Kir3.2^{K64Q} (Figure 8). In comparison to the WT channel, similar or decreased fractional abundance for apo are observed for PIPs with do tails and PI(4,5)P_2-sa. In some cases, an increase in the mole

fraction for the fourth lipid binding event, such as PI(3,4,5)P_3, suggesting an increase in binding cooperativity. Perhaps the most intriguing observation is the enhanced binding of Kir3.2^{R92P} to PI(4)P at levels nearly comparable to the other PIP isoforms studied. Consistent with the other mutants, PIP-B binding curves for Kir3.2^{R92P} displayed a reduction in binding affinity compared to the WT channel (Figure 8C). Moreover, competition experiments are consistent with the binding profiles obtained by native MS (Figure 8D). Taken together, Kir3.2^{R92P} lacks the selectivity for PIP isoforms observed for the WT protein.

Impact of A Group3 Mutant on Lipid Binding

Group3 contains four conserved residues involved in coordinating the phosphate groups of PI(4,5)P_2 that we targeted for mutagenesis in Kir3.2: K194A; Q197 to A, K or R; K199 to A or H; and K200 to N, A or R. Either no expression or purified material was unstable for Kir3.2$^{Q197A/R}$, Kir3.2$^{K199A/H}$, and Kir3.2$^{K200A/R}$ (Figure 1, Table 3). Although Kir3.2^{Q197K} and Kir3.2^{K200N} could be expressed and purified, the mass spectra of these mutants were of insufficient quality for further characterization (Figure 3). Kir3.2^{Q197K} exhibited broad mass spectral peaks whereas Kir3.2^{K200N} had unresolved peaks for the tetramer along with a resolved charge state distribution for an octamer (Figure 6E). Out of the mutants screened, high-quality mass spectra could be obtained for Kir3.2^{K194A} (Figure 9A, Figure 3C). Binding profiles for this mutant obtained by native MS show a reduction in binding affinity toward PIPs but to a lesser of extent compared to Kir3.2^{K64Q} (Figure 9B). In comparison to other mutants, a similar trend is observed for PI(4,5)P_2-sa/do and PI(3,4,5)P_3-sa, which exhibit a higher abundance of

lipid bound relative to the other PIP isoforms. Although the overall binding profile for Kir3.2^{K194A} is similar to the WT channel with poor binding of PI(4)P, the B-PI(4,5)P_2 binding curve indicates a loss in cooperativity and lower affinity (K_D = 12.9 μM) (Figure 9C). Moreover, the competition assays have similar trends as the WT channel with the exception that POPA does not compete (Figure 9D). In summary, Kir3.2^{K194A} shows an overall similar binding profile to that of the WT channel. The representative average number of lipids bound to WT and mutant Kir3.2 channels are listed in Table 4.

Discussion and Conclusion

An important discovery that emerges from this study is the importance of membrane protein sample quality for protein-ligand binding studies. Native MS reveals methods commonly employed for purifying Kir3.2 are contaminated. Furthermore, native MS can guide purification of membrane proteins by providing invaluable insight into sample quality, which we have done to obtain pure Kir3.2 samples devoid of co-purified contaminants. It is also important to note that the presence of contaminants would not be identified using traditional approaches to ascertain protein quality, such as gel-based electrophoresis[90] and denaturing mass spectrometry methods[91], including bottom-up proteomics [92]. Moreover, B-PE and B-PI(4,5)P_2 binding studies to different preparations of Kir3.2 bring to light the importance of pure samples and appropriate choice of buffer conditions. For example, B-PE binding to pure samples in different detergents are similar whereas absence of binding is observed for contaminated samples. A recent study has reported no binding of PI(4,5)P_2 modified with Bodipy-TMR to Kir3.2 in DDM even at high lipid concentrations [35]. We suspect this to be the result of

Kir3.2 samples containing co-purified contaminants since we observe significant decreases in B-PI(4,5)P_2 binding to non-DHPC treated Kir3.2 samples. However, it remains unclear if the contaminants result in a conformation change that changes binding affinity (*i.e.*, allostery) or directly compete with B-PI(4,5)P_2 binding. Taken together, native MS provides means to navigate expression and purification strategies to obtain samples conforming to more rigorous specifications needed for characterizing protein-ligand interactions.

Native MS and FRET-based lipid binding assays demonstrate that Kir3.2 cooperatively binds PI(4,5)P_2. In a study by MacKinnon and co-workers, the concentration dependence of Kir3.2 activation by PI(4,5)P_2 was quantified and Hill coefficient of 2.5 for Brain PIP_2 in lipid bilayers was determined. [93] In agreement with this study, a Hill coefficient of 2.7 was determined for B-PI(4,5)P_2 binding to pure Kir3.2 in $C_{10}E_5$. We suspect the lack of cooperativity observed for B-PI(4,5)P_2 binding in DDM to arise from a non-competitive detergent environment that supports indiscriminate lipid binding. Along these lines, cooperativity and affinity of B-PI(4,5)P_2 binding to contaminated Kir3.2 is negatively impacted. In contrast, the more competing environment of $C_{10}E_5$ suggests lipid binding is minimized to specific binding site(s). In support of this hypothesis is the fact that B-PE, a lipid not expected to bind with high affinity, binds Kir3.2 in DDM but to a lesser extent in $C_{10}E_5$. Taken together, we speculate that solution binding assays conducted in certain detergents, in some form, may emulate the competing environment of the lipid bilayer wherein protein-lipid

interactions are under constant assault by the large excess of lipids found in the biological membrane.

Mutation of residues that coordinate the headgroup of $PI(4,5)P_2$ can alter not only binding affinities but also selectivity to PIP isoforms, sometimes in unexpected ways. $Kir3.2^{K64Q}$, a mutant that mimics Gln51 in Kir2.2, largely shows a reduction in binding affinity toward PIPs compared to the wild-type channel. Although this observation is anticipated from the crystal structure where Lys64 forms a hydrogen bond to the 4' phosphate, the mutant channel exhibits an unexpected preference for sa-type lipid tails; an observation that has been reported for other Kir channels [69]. A plausible explanation for the retention of $Kir3.2^{K64Q}$ binding affinity for both $PI(4,5)P_2$-sa and $PI(3,4,5)P_3$-sa is a dynamic binding site that rearranges the orientation of the bound lipid such that the acyl tails nestle in a hydrophobic groove on the channel. In support of this idea is the observation that $PI(4,5)P_2$-d8 binds to a lesser extent than the wild-type channel. Arginine at position 92 in Kir3.2 is conserved throughout the Kir subfamily with the exception of Kir6.2, which is a proline. As prolines are known alpha helix breakers or benders [94], its introduction to the second transmembrane helix at position 92 of Kir3.2 is predicted to disturb interactions with the phosphoglycerol backbone and headgroup of PIPs. Interestingly, $Kir3.2^{R92P}$ bound avidly to the different PIP isoforms that was unlike the WT channel where a defined preference for PIP isoforms is observed. The most striking observation for $Kir3.2^{R92P}$ is the increase in affinity for PI(4)P. The promiscuous PIP binding of R92P is reminiscent of the indiscriminate channel activation

of Kir6.2 by PIPs[63]. This result suggests a single residue change in Kir3.2 may result in a channel with non-selective activation by PIPs. Lys at position 194 in Kir3.2 is highly conserved among Kir channels, and it forms a hydrogen bond to the 5' phosphate on PIPs. Although K194A was anticipated to negatively impact PIP binding, Kir3.2^{K194A} displayed similar or slightly reduced binding affinities for PIPs as the WT channel. More specifically, PIPs containing a 5' phosphate had reduced binding and implicate Lys194 in the selectivity of Kir3.2 toward PIP isoforms.

Detailed information on the residues that contribute to protein-ligand interactions is essential for understanding protein structure and function. Previous studies [57, 63-66] have established that Kir channels are activated by PIP isoforms to varying degrees, suggesting they may exhibit distinct binding to the PIP isoforms. Taken together with our previous study [45], our results demonstrate that Kir3.2 selectively binds PIPs, and lipid binding profiles can be altered by a single mutation in distinct ways. Native mass spectrometry enables individual lipid binding events to be resolved providing additional insight into binding profiles over traditional approaches, including the FRET-based lipid binding assay. Interestingly, binding profiles show PI(4,5)P_2 and PI(3,4,5)P_3 avidly bind Kir3.2 and these lipids have recently been shown to activate the channel to nearly the same degree[95]. Solution FRET-based lipid binding and competition assays are in direct agreement with lipid binding profiles obtained by native MS. Notably, our study is in the absence of sodium and $G_{\beta\gamma}$-protein, molecules known to activate Kir3.2[93], and addition of these molecules may alter PIP binding affinity and/or selectivity. In

summary, this work provides insights into how Kir channels attain PIP binding affinity and clues to the selective gating profiles observed for different Kir channels.

CHAPTER III

INSIGHT INTO THE PHOSPHOLIPID BINDING PREFERENCES OF KIR3.4

Introduction to Kir3.4

Inward rectifying potassium (Kir) channels are found in cells throughout the human body, such as neuronal cells,[96] cardiac myocytes,[97] skeletal muscle cells,[47] blood cells,[98] and endothelial cells.[99] Kir channels have roles in numerous physiological functions, such as regulating the resting membrane potential of excitable cells,[46, 100, 101] parasympathetic slowing of the heart,[102] and pancreatic insulin secretion.[103] Dysfunction of Kir from genetic defects is associated with diseases, such as Bartter and Andersen syndromes.[51-54] The Kir channel family can be categorized into four groups based on their functional mechanism: K^+ transport channels (Kir1.x, Kir4.x, Kir5.x, and Kir7.x), constitutively active channels (Kir2.x), ATP-sensitive K^+ channels (Kir6.x), and G-protein-coupled Kir channels (Kir3.x).[47]

Despite their functional diversity, all of the Kir channels adopt a similar tetrameric structure with identical or different subunits.[104, 105] Each subunit consists of two cytoplasmic domains located on the N- and C-termini, and two transmembrane domains that are connected by a pore-forming P loop.[106] The function of Kir channels is regulated by many factors, such as ethanol, polyamines, magnesium, sodium, protein kinases, guanine nucleotide-binding proteins (G proteins), and phosphorylated phosphoinositides, such as $PI(4,5)P_2$.[15, 56, 57, 60, 107-110] The structures of Kir2.2 and Kir3.2 in complex with $PI(4,5)P_2$ have revealed $PI(4,5)P_2$ with 8:0 acyl chains binds to a specific site on each subunit.[20, 71] The binding site is located at the interface of

the transmembrane domain and the cytoplasmic N-terminus, a highly conserved region that primarily consists of lysine and arginine residues. These positively charged amino acid residues interact with the phosphoglycerol backbone and the 4' and 5' phosphates of $PI(4,5)P_2$.[37, 72]

Besides $PI(4,5)P_2$, other PIPs can also activate Kir channels to different degrees.[63-65] In general, Kir2.x shows no stimulation by $PI(3,4)P_2$ and $PI(3,4,5)P_3$. Kir3.4 and Kir3.1/Kir3.4 have shown weak activation by $PI(3,4,5)P_3$ and $PI(3,4)P_2$. Kir6.2 is promiscuously activated by all PIPs.[57] In addition to the headgroups, different acyl chains of phosphoinositides also contribute to the regulation of Kir channel activity. The hetero-tetrameric Kir3.1/Kir3.4 channel shows specific selectivity for $PI(4,5)P_2$ with 18:0-20:4 acyl chains.[63, 67, 68] In contrast, Kir2.1 displays no preference for the lipid acyl chains.[70] Moreover, previous studies have shown that the activation of both Kir3.2 and Kir3.4 by $PI(4,5)P_2$ can be enhanced in the presence of sodium.[73, 111, 112] Anionic phospholipids, such as phosphatidic acid (PA), phosphatidylserine (PS), phosphatidylglycerol (PG), and phosphatidylinositol (PI) can also increase Kir2.1's sensitivity to $PI(4,5)P_2$.[113, 114]

Native mass spectrometry (MS) is a powerful technique to interrogate membrane proteins and their interactions with ligands, such as lipids.[83, 115-118] For example, native MS has identified lipids that stabilize membrane protein complexes.[17, 18, 119, 120] It has also been used to determine the binding thermodynamics of protein-lipid interactions, as well as the allosteric coupling for protein-protein and protein-lipid interactions.[43, 44, 78] Native MS has also shown for a truncated form of Kir3.2

different affinities for PIPs with a preference for $PI(4,5)P_2$ headgroup.[45, 121] The headgroup binding preference determined by native MS is consistent with those obtained using a solution-based fluorescent lipid-binding assay in which binding of a fluorophore-modified $PI(4,5)P_2$ to Kir3.2 fused to a fluorescent protein is monitored by Forster or Bioluminescent resonance energy transfer (FRET) measurements.[35, 121]

To better understand Kir-lipid interactions, we used native MS to characterize the binding of Kir3.4 and Kir3.2 to lipids varying in headgroup and acyl chain composition. Previous studies have determined lipid binding profiles for a truncated form of Kir3.2 from mouse.[121, 122] Here, lipid binding to full-length, human Kir3.4 and Kir3.2 is characterized. The results show Kir3.4 exhibits different lipid binding preferences. Interestingly, PIP binding of Kir3.4 is much weaker than that of Kir3.2. The S143T mutant that enhances Kir3.4 sensitivity to $G_{\beta\gamma}$[123] displayed an overall decrease in binding lipids. Kir3.4 containing the D223N mutation that mimics the sodium bound state[73] resulted in enhanced binding of PIPs with a preference for 18:0-20:4 acyl chains. These studies are also complemented with a competition soluble fluorescent lipid binding assay with results in line with those determined using native MS.

Materials and Methods

Protein Expression

Human Kir3.4 (KCNJ5, Uniprot 48544) and Kir3.2 (KCNJ6, Uniprot P48051) cDNA was obtained from Horizon with catalog numbers of MHS6278-202856496 and MHS6278-202857476, respectively. For native MS studies, the DNA corresponding to the full-length proteins was cloned into a modified pACEBac1 (Geneva Biotech) insect

cell expression vector as a C-terminal fusion to a StrepTag II affinity tag. For fluorescent lipid binding assays, the full-length genes were cloned into a modified insect cell expression construct to express proteins with a tobacco etch virus (TEV) protease cleavable C-terminal fusion to mCherry and StrepTag II. The expression constructs were made by first amplifying genes by polymerase chain reaction using Q5 High-Fidelity DNA polymerase (New England Biolabs, NEB) and cloned into the modified insect cell expression vectors using HiFi DNA assembly kit (NEB) according to the manufacturer's protocol. The expression plasmids of this work have been deposited at Addgene plasmid #172425 to 172428. Mutants were introduced using the Q5 site-directed mutagenesis kit (NEB) according to the manufacturer's protocol. All expression plasmids were confirmed by DNA sequencing. The Kir3.2 and Kir3.4 expression constructs were transformed into *E. coli* DH10EMBacY (Geneva Biotech) following the manufacturer's protocol. Blue/White colony screening was used to identify clones that successfully incorporated the expression cassette into the baculoviral genome. A single, white colony was grown overnight and used for purification of bacmid DNA using a HiPure Plasmid Midiprep kit (Invitrogen). A single-step protocol was used for rapid baculovirus production.[124] In detail, the purified baculoviral DNA (30 μg) was incubated with PEI Max (Polysciences) transfection reagent (60 μl, 1 mg/ml) and 2ml PBS (NaCl 137 mM, KCl 2.7 mM, Na_2HPO_4 10 mM, KH_2PO_4 1.8 mM, pH 7.4) for 20 min. After 20 minutes of incubation at room temperature, the mixture was added directly to *Spodoptera frugiperda* (Sf9) cells (30 ml, 0.8 x 10^6 cell/ml) grown in suspension and incubated at 27 ^oC with shaking for seven days. The baculovirus was amplified in Sf9 following

standard protocols. *Trichoplusia ni* (Tni) cells were used for protein expression for 2-3 days post-infection. Insect cell lines and ESF 921 insect cell culture media were obtained from Expression Systems.

Protein Purification and Delipidation

The Tni cells post-infection were harvested by centrifugation (4,000 g, 10 min). All purification steps were carried out at 4 ^{o}C unless otherwise stated. The cell pellets were resuspended in lysis buffer (50 mM TRIS, 300 mM potassium chloride, pH 7.4 at room temperature) and lysed by three passages through a microfluidizer (M-110PS, Microfluidics Inc.) operating at 25,000 psi. The cell lysate was clarified by centrifugation at 25,000 g for 20 min. Membranes were pelleted from the supernatant by ultra-centrifugation (100,000 g, 2 hours, 4 ^{o}C). The membrane pellets were resuspended in membrane resuspension buffer (30 mM TRIS, 150 mM potassium chloride, 10% Glycerol, pH 7.4 at room temperature) and homogenized using a glass homogenizer (Wheaton). Membrane proteins were extracted with 1.5% (w/v) n-Dodecyl-β-D-Maltopyranoside (DDM, Glycon Biochemicals) for two hours with gently stirring at 4 ^{o}C. The extracted membrane resuspension was clarified by centrifugation (40,000 g, 20min) and filtered through a 0.45 μm syringe filter. The protein sample was then loaded onto a drip column packed with 0.5 ml of Streptactin Sepharose (IBA Biosciences) pre-equilibrated with buffer SPKHA (50 mM Tris, 150 mM potassium chloride, 10% glycerol, and 0.025% DDM, pH 7.4 at room temperature). After loading, the column was washed with 5 column volumes (CV) of SPKHA, 10 CV of SPKHB buffer (50 mM Tris, 150 mM potassium chloride, 10% glycerol and 6 mM DHPC [1,2-dihepanoyl-sn-

glycero-3-phosphocholine], pH7.4 at room temperature) to remove the co-purified contaminants, and 10 CVs of SPKHC buffer (50 mM Tris, 150 mM potassium chloride, 10% glycerol and 0.065% $C_{10}E_5$ [Pentaethylene Glycol Monodecyl Ether], pH 7.4). The protein was eluted with SPKHD buffer (SPKHC with 3 mM D-desthiobiotin). The concentration of protein was determined by using a DC protein assay (Bio-Rad).

Native Mass Spectrometry

Protein samples were buffer exchanged into aqueous ammonium acetate (200 mM, pH 7.4 adjusted with ammonium hydroxide) supplemented with 0.065 % $C_{10}E_5$ using a centrifugal desalting column (Micro Bio-Spin 6, Bio-Rad). Lipid films were dissolved in the same buffer. Membrane protein samples were mixed with lipids at a molar ratio of 1:10 and analyzed on a Q Exactive UHMR Hybrid Quadrupole-Orbitrap mass spectrometer (Thermo). Gold-coated nanoelectrospray ionization emitters were prepared in-house as previously described.[89] Instrument settings were tuned to preserve non-covalent interactions as follows: the capillary voltage was 1.20 kV; the capillary temperature was 250 ^{o}C; collision-induced dissociation (CID) and collision energy (CE) was 60 V and 35 V, respectively; and detector mode and ion transfer target was set on high *m/z*. The in-source trapping mode was on with a desolvation voltage of -300 V. The trapping gas pressure was set at 7. Native MS was deconvoluted using UniDec[83] with the peak FWHM at 20.

Fluorescent Lipid Competition Assay

The fluorescent lipid BODIPY FL Phosphatidylinositol 4,5-bisphosphate (B-PIP, cat no. C-45F6) was purchased from Echelon Biosciences. The BODIPY fluorophore is

affixed on the short acyl chain at the *sn*1 position. BODIPY is the donor that can excite the mCherry fusion proteins through Förster resonance energy transfer (FRET) when the fluorescent lipid is bound to the protein. FRET measurements and correction factors were performed as previously described.[121] The experiments were conducted in SPKHC buffer. A total volume of 50 μl sample containing the protein and lipids was mixed at room temperature in a black 384-well plate (NUNC, cat no. 42761), and FRET measurements were made using a CLARIOstar microplate reader (BMG LABTECH).

Results

Preparation of full-length human Kir3.4 and Kir3.2 for nMS studies

Human, full-length Kir3.4 and Kir3.2 with a C-terminal affinity tag were expressed and purified from insect cells for native MS characterization. The proteins were initially extracted and purified using n-Dodecyl-β-D-Maltopyranoside (DDM), a commonly used detergent. The native mass spectra of Kir channels displayed a broad hump and, in some cases, decorated with some sharp mass spectral peaks (Figure 15A, 16A). The underlying hump in the mass spectrum indicates the purified protein is heterogenous, which we speculate is the result of co-purified lipids. Nevertheless, the broad hump hinders the ability to resolve individual lipid binding events to the channel. In our previous studies[45, 121], we discovered that washing a truncated form of Kir3.2 immobilized on affinity resin with 1,2-dihepanoyl-sn-glycero-3-phosphocholine (DHPC), a short-chain lipid that forms micelles, removes co-purified contaminants resulting in pure samples. In a similar fashion, Kir3.4 and Kir3.2 were subjected to a DHPC wash to remove the contaminants. After this procedure, the native mass spectra

of Kir channels in the pentaethylene glycol monodecyl ether ($C_{10}E_5$) detergent displayed a well-resolved mass spectrum with a measured mass in agreement with the theoretical mass of the tetrameric complex (Figure 15B, 16B; Table 6). Notably, the optimized samples provide means to resolve individual lipid binding events to the full-length channels.

Characterization of Kir3.4-lipid interactions

The Kir3.4 samples devoid of co-purified contaminants were used to characterize lipid binding using native MS. The first set of lipids we investigated included phosphatidylinositol-3-phosphate (PI(3)P), PI(4)P, PI(5)P, PI(3,4)P_2, PI(4,5)P_2, and PI(3,4,5)P_3 with dioleoyl acyl chains (18:1-18:1, DO) and, for a subset, with 1-stearoyl-2-arachidonoyl (18:0–20:4, SA) acyl chains (Figure 10 and 17). Kir3.4 at a fixed concentration (0.5 μM) was mixed with 10 equivalents of lipid. For example, up to two lipid binding events were observed in the mass spectrum of the Kir3.4 in the presence of DOPI(4,5)P_2 (Figure 10B). Although the lipid bound mass spectral peaks are not base-line resolved, the small shifts in *m/z* for DOPI(4,5)P_2 (~1 kDa) binding to the intact Kir3.4 complex (~196 kDa) are readily discernable and these shifts are consistent with the mass of the lipid (Table 5, Figure 15). To compare the binding among lipids, the measured intensities from the deconvoluted mass spectra were used to determine the mole fraction of apo and lipid bound states (Figure 10C). For the mono phosphorylated PIPs, the total fraction of DOPI(3)P and DOPI(4)P bound Kir3.4 was similar, *i.e.*, similar abundance of apo, but the abundance of one and two lipids varied. Interestingly, PI(4)P with SA acyl chains resulted in a significant reduction in binding compared to

this lipid with DO acyl chains. The total bound for $PI(3,4)P_2$ and $PI(4,5)P_2$ lipids was similar and, like the PIPs with one phosphate, showed different abundances. For example, $DOPI(4,5)P_2$ had the highest abundance for one lipid bound whereas up to three $SAPI(4,5)P_2$ were bound to Kir3.4. $PI(3,4,5)P_3$ with SA acyl chains bound more to Kir3.4 in comparison to this lipid with DO acyl chains.

The second set of lipids characterized in this study focused on those with 1-palmitoyl-2-oleoyl (16:0-18:1, PO) acyl chains. This includes phosphatidylethanolamine (PE), phosphocholine (PC), phosphatidic acid (PA), phosphatidylserine (PS), phosphatidylglycerol (PG), and PI headgroups (Figure 10D, Table 5). Of the PO lipids, Kir3.4 bound up to two POPI molecules whereas only one binding event was observed for the other lipids. More POPE was bound to Kir3.4 followed by POPC and the least to POPA, POPS, and POPG. Interestingly, DOPI binds more avidly to Kir3.4 and at comparable levels to some PIPs. Moreover, the binding pattern of DOPI is suggestive of positive cooperativity.

Characterization of Kir3.2-lipid interactions

To compare the Kir3.4-lipid interactions to other Kirs, we performed similar lipid binding studies for human Kir3.2 (Figure 11 and 18). In stark contrast to Kir3.4, native mass spectra reveal Kir3.2 binds avidly to PIPs and, in some cases, up to five lipid binding events were observed (Figure 11B). Kir3.2 robustly engages $PI(4,5)P_2$ with enhanced preference for the lipid with SA acyl chains (Figure 11C). Most interestingly, the binding pattern for $DOPI(4,5)P_2$, $SAPI(4,5)P_2$, and $DOPI(3,4,5)P_3$ suggests these lipids bind with positive cooperativity. The cooperative binding of $DOPI(3,4,5)P_2$ to Kir3.2 was

diminished when the lipid contained SA acyl chain. Of the mono-phosphorylated PIPs, more PI(5)P was bound to the channel whereas binding for PI(3)P and PI(4)P are indistinguishable.

Next, the interactions of Kir3.2 with other phospholipids was characterized (Figure 11D). Unlike Kir3.4, the binding of POPI and DOPI was similar. Up to two POPE and POPS lipids were bound to Kir3.2. POPA while only one binding event was observed POPC and POPS. No binding between Kir3.2 and POPG was observed at the molar ratio tested.

Probing Kir-lipid interacitons using fluorescent lipid competition assay

A fluorescent lipid binding assay[35, 121] was employed to corroborate the findings from native MS measurements. To this end, samples of Kir3.4 and Kir3.2 with a monomeric red fluorescent protein (mCherry) fused to the C-terminus were prepared as done for native MS studies. Importantly, the optimized protein samples did not contain any co-purified contaminants (Figure 15, 16), which we have recently shown can impede specific lipid binding to truncated Kir3.2.[121] We then performed competition assays in which PI(4,5)P_2 containing a BODIPY fluorophore affixed to the acyl at the *sn*1 position (B-PIP) is competed off with natural lipids to compare with lipid binding profiles measured for the channels using native MS (Figure 12). The fluorescent lipid binding assay was performed with a fixed concentration of B-PIP and the addition of two equivalents of the phospholipid followed by recording the Förster resonance energy transfer (FRET) signal (Figure 12A, 12B). Of the PIPs tested, DOPI(3,4)P_2 and DOPI displayed a marginal reduction in FRET signal for Kir3.4. In general, the lipids weakly

competed with the binding of B-PIP to Kir3.4, a result that agrees with the overall poor binding of lipids observed by native MS. For Kir3.2, nearly half the FRET signal was lost in the presence of SAPI(4,5)P_2 followed by the same lipid with DO acyl chains. No competition was observed for Kir3.2 in the presence of DOPI, DOPI(4)P, DOPI(3,4)P_2 and SAPI(3,4,5)P_3, indicating relatively weak binding. Interestingly, some of the PO-type lipids, particularly PC, PA, PS and PG, enhanced the FRET signal indicating an enhancement in the interaction between Kir3.2 and B-PIP.

Characterization of mutant Kir3.4 channels with lipids

We first prepared the Kir3.4 channel with the S143T mutation (Kir3.4^{S143T}) that has been shown to produce large inwardly rectifying, G-protein-modulated currents.[123] In a similar fashion as the wild-type channel, we performed native MS measurements of the mutant channel in the presence of different lipids (Figure 13 and 19). In general, the binding was largely weakened by this point mutation with a significant increase in abundance of the apo state (Figure 13C-D). SAPI(4,5)P_2 was the only lipid in which two lipid binding events to Kir3.4^{S143T} were observed. The binding profile of DOPI(3,4,5)P_3 was statistically indistinguishable from the wild-type protein (Figure 13C). A reduction of the binding of Kir3.4^{S143T} was observed for lipids with PO acyl chains (Figure 13D). More specifically, the binding of POPI and DOPI was considerably reduced compared to the avid binding of the wild-type protein.

The D223N mutant of Kir3.4 has been shown to mimic the sodium-bound state and strengthen the interaction with PI(4,5)P_2.[73] Native MS results for Kir3.4^{D223N} showed significant enhancement in PIPs binding (Figure 14 and 20). Interestingly, the

PIPs with SA acyl chains bound more avidly compared to wild-type Kir3.4 (Figure 14C). For the DO type lipids, Kir3.4^{D223N} binding to DOPI(4,5)P_2 and DOPI(3,4,5)P_3 was similar to the wild-type protein. Compared to the wild-type channel, the binding of DOPI(4)P and DOPI(5)P was enhanced, and a reduction in binding DOPI(3)P and DOPI(3,4)P_2 was measured. A significant reduction was also observed for POPI and DOPI, lipids that bound avidly to Kir3.4. The binding of POPA and POPS was enhanced whereas a reduction in the binding of POPE, POPC, and POPG to Kir^{D223N}.

Discussion and Conclusion

An important observation in this work is the rather weaker binding of Kir3.4 for PIPs in comparison to Kir3.2. The weak interaction between Kir3.4 and PIPs observed by native MS is in direct agreement with previous reports.[73, 123] Given Kirs are directly under PI(4,5)P_2 regulation, it is reasonable to speculate that the low activity is due to the channels' weak binding for PI(4,5)P_2. Interestingly, POPI and DOPI bind Kir3.4 with comparable or stronger binding than some PIPs. Kir3.2 binds PIPs more avidly and selectively compared to Kir3.4. The binding profiles for the Kir3.2 are reminiscent of our previous native MS studies using truncated mouse Kir3.2 conducted at a lower molar ratio of lipid to protein.[45, 121] The most notable difference is Kir3.2 is more selective toward PIPs with a strong preference for the PI(4,5)P_2 head group and SA acyl chains. The enhanced selectivity toward PIPs along with acyl chain dependence suggests additional N- and C-terminal components of Kir3.2 influence specific lipid binding. Another interesting observation is the pronounced abundance of the fourth PI(4,5)P_2 bound to Kir3.2, indicating strong positive cooperativity in binding this lipid.

The abundance of the fourth lipid bound state of Kir3.2 was also observed for DOPI(3,4,5)P_3.

Fluorescent lipid competition assays agree with native MS studies. Kir3.4 has shown an overall weaker binding profile for not only PIPs, but also almost all the lipids tested when compared to Kir3.2. For Kir3.2, DOPI(4,5)P_2 and SAPI(4,5)P_2 lipids show the strongest competition with B-PIP binding to Kir3.2. It is also interesting that POPA, POPC, POPS, and POPG enhances or allosterically modulates the interaction between B-PIP and Kir3.2 (p<0.05, students t-test). This observation is consistent with reports of anionic lipids significantly enhancing the sensitivity of Kir2.1 and Kir2.2 to PI(4,5)P_2.[64] However, a notable difference is the increase in B-PIP binding to Kir3.2 in the presence of POPC, a non-anionic lipid. Moreover, the enhancement in B-PIP binding to Kir3.2 in the presence of other lipids was not observed for the truncated, mouse Kir3.2.[121]

Kir3.4 can form functional homo-tetramers and its activity can be enhanced by the introduction of point mutations.[73, 123] The S143T mutation in Kir3.4 results in enhanced sensitivity to $G_{\beta\gamma}$ activation[125] and we find the mutant channel has reduced the binding for PIPs. The binding of $G_{\beta\gamma}$ to Kir1/4 hetero-tetramers has been shown to stabilize PIP_2 binding, suggesting the binding of these molecules to the channel is allosterically coupled.[56] Native MS studies were performed in the absence of $G_{\beta\gamma}$ and tight PIP binding may require the presence of $G_{\beta\gamma}$. It has been established that elevated levels of sodium (EC_{50} of 30-40 mM) activate Kir channels containing Kir3.2 or Kir3.4 subunits.[73, 111, 112, 126-128] Native MS studies cannot tolerate the high

concentration of sodium needed to activate Kir3.2 or Kir3.4, which would result in significant adduction of sodium and mass spectral peak broadening. However, the D223N mutant of Kir3.4 mimics the effects of sodium on channel activity.[73] We find Kir3.4^{D223N} shows increased PIP binding consistent with an earlier report.[73] A new finding is Kir3.4^{D223N} displays enhanced the binding for PIPs with SA over DO acyl chains. In addition, the protein is more selective for PIPs as the binding to POPI and DOPI lipid was reduced compared to Kir3.4. In summary, native MS and fluorescent lipid binding studies show that the selectivity of Kir3.2 and Kir3.4 (WT and mutants) toward PIPs depends not only on the headgroup but also the type of acyl chains.

CHAPTER IV

ENTROPY CONFORMATIONAL ENTROPY IN THE MOLECULAR RECOGNITION OF MEMBRANE PROTEIN-LIPID INTERACTIONS

Introduction

Inward rectifier potassium (Kir) channels are expressed in tissues throughout the body where they play central roles in many physiological processes, such as parasympathetic slowing of the heart[102], pain perception[129], and pancreatic insulin secretion.[48, 50, 62, 103, 130-132] Some mutations in these channels result in improper trafficking that is associated with Andersen syndrome.[47] In particular, phosphatidylinositol 4,5-bisphosphate ($PI(4,5)P_2$), a minor component of the cytoplasmic leaflet,[55] is required for activation of all Kir channels.[20, 56-58] Kir channels are also regulated by many other molecules including phosphorylation by kinases, sodium, pore blockers (polyamine, Mg^{2+}), and ethanol.[47, 60, 61] There are seven subfamilies of Kir channels: classical Kir channels (Kir2.x) are strong rectifiers that have central roles in cardiac inward rectifier current; Kir3.x channels are unique in that they require $G_{\beta\gamma}$ in addition to PIP_2 for function with some of these channels modulated by sodium ions; ATP-sensitive potassium channels (Kir6.x); and transport potassium channels (Kir1.x, Kir4.x, Kir5.x, and Kir7.x).[47, 62, 64, 73, 111, 113]

All Kir channels form tetrameric complexes composed of similar or different subunits.[20, 71, 133] Each subunit encodes two transmembrane domains (TMD), in which the K^+ selectivity filter resides, that is tethered by a short linker to the cytoplasmic domain (CTD).[71, 133] Structures have also revealed a $PI(4,5)P_2$ binding pocket

located at the interface of the TMD and CTD.[20, 71] The binding pocket is a highly conserved region that is consists of set positively charged amino acid residues that engage the phosphorylated headgroup of $PI(4,5)P_2$.[20, 71, 72] Mutations in residues important for binding the signaling lipid are associated with Bartter and Andersen syndromes, and another diseases.[48, 59, 134] The specific lipid binding site within Kir channels has garnered the attention of computational studies to identify and predict lipid-binding sites on ion channels.[135-138]

Kir channels have varied specificity and variable degrees of channel activation to the different phosphoinositides. All Kir channels are maximally activated by $PI(4,5)P_2$ and, in some cases, $PI(4,5)P_2$ is the only phosphoinositide (PIP) that stimulates activity.[57, 63, 65] In contrast, Kir6.x appears to be promiscuously activated by $PI(3,4)P_2$, $PI(4,5)P_2$ and $PI(3,4,5)P_2$.[63, 65] The acyl chain composition has also been shown to be a contributing factor to the level of stimulation, such as Kir3.1/Kir3.4 channels display preference for $PI(4,5)P_2$ with 18:0-20:4 (SA) acyl chain whereas Kir2.1 shows no preference towards acyl chains.[70] The concentration dependence of $PI(4,5)P_2$ activation of Kir3.2 in a lipid bilayer exhibits positive cooperativity.[36] Similar findings were found using a soluble fluorescent lipid binding assay wherein the binding of a fluorophore modified $PI(4,5)P_2$ to Kir3.2 fused to a fluorescent protein is monitored by Förster resonance energy transfer.[121]

Historically it has been difficult to dissect and interrogate lipid binding events to membrane proteins, which is necessary to fully characterize binding thermodynamics. However, native mass spectrometry (MS) has emerged as an indispensable biophysical

technique for characterizing membrane proteins and their interactions with lipids and other molecules, such as regulatory proteins.[117] In contrast to other biophysical techniques that report on the ensemble, native MS can not only capture a snapshot of solution equilibria but also resolve individual ligand-bound states of membrane protein complexes.[75] Over the past decade, native MS has discovered the role of specific lipids in stabilizing membrane protein complexes,[75, 120, 139] allosteric modulation of membrane protein interactions with protein,[76, 77] lipids,[78] and drugs,[80, 140-142] and those important for function,[75, 79, 80, 141-143] such as $PI(4,5)P_2$ in G-protein-coupled receptor activation and G-protein selectivity.[77] Lipid and toxin binding to Kir3.2 has been interrogated using native MS that has provided insight into the binding preferences for PIPs.[122] Native MS combined with mutational studies has shed light on the contribution of amino acids in the PIP binding site of Kir3.2 and how they impact binding preferences for PIPs.[121] Despite progress in understanding Kir-lipid interactions, the thermodynamics for the association of lipids with Kir3.2 has been enigmatic.

Method and Materials

Plasmid construction and protein expression

The human Kir3.2 cDNA (KCNJ6, Uniprot P48051) was purchased from Horizon with a catalog number of MHS6278-202857476. Kir3.2 (residues 49-378), was cloned into a modified pACEBac1 insect cell expression vector (Geneva Biotech) with a C-terminal StrepTag II affinity tag by following the manufacturer's protocol. The expression plasmid has been deposited at Addgene plasmid #177263. The expression

vector was transformed into *Ecoli* EmBacY (Geneva Biotech) cells and integrates of the expression cassette into the baculoviral genome were identified using blue/white colony screening following the manufacturer's protocol. A single white colony was inoculated overnight and recombinant baculoviral DNA was purified using HiPure Plasmid Midiprep kit (Invitrogen). The purified baculoviral genome DNA (30 μg) was mixed with 2ml PBS (NaCl 137 mM, KCl 2.7 mM, Na_2HPO_4 10 mM, KH_2PO_4 1.8 mM, pH 7.4) and PEI Max (Polysciences) transfection reagent (60 μl, 1 mg/ml in PBS).[124] After 20-min incubation, the mixture was added to *Spodoptera frugiperda* (Sf9) cells (30 ml, 0.8 x 10^6 cell/ml) in suspension and grown at 27 ^oC for a week to produce baculovirus. The clarified P1 was used to infect *Trichoplusia ni* (Tni) cells for protein expression and incubated at 27 ^oC for 2-3 days before harvesting. All insect cell lines and media are from Expression Systems LLC.

Protein purification

The post-infected Tni cells were harvested by centrifugation (4,000 g, 10 min, 4 ^oC). The cell pellets were resuspended in lysis buffer (300 mM KCl and 50 mM Tris pH7.4 at RT). The resuspended cell pellets were passed through a microfluidizer (M-110PS, Microfluidics Inc.) operating at 25,000 psi. The cell lysate was then clarified by centrifugation (25,000 g, 20 min, 4 ^oC) and the supernatant was subjected to ultracentrifugation (100,000g, 2hr, 4 ^oC) to harvest membranes. The membrane was resuspended in lysis buffer and homogenized using a glass tissue blender (Wheaton). DDM (n-Dodecyl-β-D-Maltopyranoside, Glycon Biochemicals) was added to a final concentration of 2% to extract membrane proteins at 4 ^oC for 2 hours. The membrane

protein extract was clarified by centrifugation (25,000 g, 20 min, 4 ^{o}C) before loading onto a drip column packed with streptactin Sepharose (IBA Biosciences) equilibrated with SPKHA buffer (150 mM KCl, 50 mM Tris, 10% glycerol, 0.025% DDM, pH 7.4 at RT). After loading the sample on the StrepTrap, 10 column volumes (CV) of SPKHA were used to wash the column, followed by a 10 CV wash of SPKHB (SPKHA with 0.025% DDM replaced by 6 mM DHPC [1,2-dihepanoyl-sn-glycero-3-phosphocholine]) and 10 CV wash of SPKHC (SPKHA with 0.025% DDM replaced by 0.065% $C_{10}E_5$ [Pentaethylene Glycol Monodecyl Ether]). The protein was then eluted with SPKHD buffer (SPKHC with 3mM D-desthiobiotin). The eluted sample was buffer exchanged into SPKHC using a desalting column. Protein concentration was measured using a DC protein assay (Bio-Rad). The purified protein was used immediately or stored at -80 ^{o}C.

Preparation and titration of phospholipids

1,2-dioleoyl-phosphatidylinositol (DOPI), 1,2-dioleoyl-phosphatidylinositol-4'-phosphate (DOPI(4)P), 1,2-dioleoyl-phosphatidylinositol-4',5'-bisphosphate (DOPI(4,5)P_2), 1,2-dioleoyl-sn-glycero-3-phospho-1'-myo-inositol-3',4',5'-trisphosphate (DOPI(3,4,5)P_3), and 1-stearoyl-2-arachidonoyl- phosphatidylinositol-4',5'-bisphosphate (SAPI(4,5)P_2) were purchased from Avanti Polar Lipids. Lipids were first dissolved in water followed by dilution into 200 mM ammonium acetate containing 0.065% $C_{10}E_5$.

Native mass spectrometry (MS)

Protein samples were exchanged into 200mM ammonium acetate (pH adjusted to 7.4 with ammonium hydroxide) containing 0.065% $C_{10}E_5$ using a centrifugal buffer exchange column (Micro Bio-Spin 6, Bio-Rad). The protein sample mixed with lipid

was loaded into a gold-coated nanoelectrospray ionization (nESI) emitter prepared as previously described.[34] The temperature of the nESI emitter mounted on the instrument was controlled using variable temperature apparatus.[144] After the set temperature was reached the sample was incubated for several minutes before data acquisition on an Exactive Plus EMR Orbitrap Mass Spectrometer (Thermo Scientific). The instrument settings are as follows: Capillary Voltage 1.60 kV; Capillary Temperature 200 ^{o}C; Collision-Induced Dissociation (CID) 100 V; Collision Energy (CE) 10 V; Trapping gas pressure setting 3.0; Source DC offset 60V; Injection Flatpole DC 4 V; Inter Flatpole lens -20 V; Bent Flatpole DC 10 V; Transfer Multipole DC 6.

Native MS data analysis

Be sure that all figures and tables fit within the document's regular margins. The native MS data collected were deconvoluted using UniDec.[145] A in-house, custom software and scripts written in Python were used to assign and determine the mole fraction of apo and lipid bound states, and determining the equilibrium binding constants (discussed below). Equilibrium binding constants and thermodynamics were determined as previously described with modification.[146] In detail, the deconvoluted mass spectra text files written by UniDec from the titration series were used to determine the intensities of Kir3.2 (P) and Kir3.2-lipid (PL) species and converted to mole fraction. The apparent equilibrium association constant (K_A) for protein binding one lipid:

$$\mathbf{P + L} \overset{K_A}{\leftrightarrow} \mathbf{PL}$$

$$\mathbf{K_A} = \frac{\mathbf{[PL]}}{\mathbf{[P][L]}} \quad \mathbf{(1)}$$

Or binding to multiple ligands:

$$\mathbf{PL_{n-1}} + \mathbf{L} \overset{\mathbf{K_{An}}}{\Longleftrightarrow} \mathbf{PL_n}$$

$$\mathbf{K_{An}} = \frac{[\mathbf{PL_n}]}{[\mathbf{PL_{n-1}}][\mathbf{L}]} \quad \textbf{(2)}$$

where K_{An} is the equilibrium association constant for the n_{th} ligand binding to the protein and n is the number of bound ligands. The total protein concentration ($[P]_{total}$):

$$[\mathbf{P}]_{\mathbf{total}} = [\mathbf{P}] + \sum_{i=1}^{n} [\mathbf{P}][\mathbf{L}]^i \prod_{j=1}^{i} \mathbf{K_{Aj}} \quad \textbf{(3)}$$

Equation (2) can be rearranged to calculate the mole fraction (F_n) of PL_n:

$$\mathbf{F_n} = \frac{[\mathbf{L}]^n \prod_{j=1}^{n} \mathbf{K_{Aj}}}{1+\sum_{i=1}^{n} [\mathbf{L}]^i \prod_{j=1}^{i} \mathbf{K_{Aj}}} = \frac{[\mathbf{PL_n}]}{[\mathbf{P}]_{\mathbf{total}}} \quad \textbf{(4)}$$

where [L] is the free ligand concentration at equilibrium. If the concentration of protein is known, the free ligand can be calculated as follows:

$$[\mathbf{L}] = [\mathbf{L}]_{\mathbf{total}} - [\mathbf{P}]_{\mathbf{total}} \cdot \sum_{i=1}^{n} i\mathbf{F}_i \quad \textbf{(5)}$$

This sequential lipid binding model was globally fit to mole fraction data collected at a given temperature to obtain K_{An} through minimization of the pseudo-χ^2 function:[147]

$$\chi^2 = \sum_{i=0}^{n} \sum_{j=1}^{d} \left(F_{i,j,exp} - F_{i,j,calc}\right)^2 \quad \textbf{(6)}$$

where d is the number of the experimental mole fraction data points and n is the number of bound ligands.

A more complex binding model (**Figure 35**) was used in cases where the sequential lipid binding model resulted in poor fits (**Figure 34**). As Kir3.2 is known to populate two states wherein the cytoplasmic domain is in a docked and extended configuration,[148, 149] we incorporated into the binding model that lipid can bind to a fraction of Kir3.2 in either the docked or extended state. For a given lipid bound state the fractional abundance can be computed:

$$F_{PL_n} = (\propto) F_{PL_n,docked} + (1-\propto) F_{PL_n,extended} \quad \textbf{(7)}$$

where $\propto$ represents the fractional abundance of the docked state and n is the number of lipids bound. One value $\propto$ is related to an equilibrium association constant for the transition from the extended to docked state:

$$K_{ED} = \frac{\propto}{(1-\propto)} \quad \textbf{(8)}$$

Incorporating this more complex lipid binding model with one $\propto$ introduces three additional fitting parameters and divides the apo and up to two lipid bounds a fraction of

two components where each component represents binding to a docked or extended state. In comparison to the sequential binding model, the more complex lipid binding model resulted in better fits (Figure S11) and was statistically justified (F-test, $p <$ 0.001). Therefore, this model was applied to determine K_{An} for each lipid-binding event. More sophisticated models were also considered, such as extending to all lipid binding events and different ∝s for each lipid bound state, however, they did not improve the fits and were often not statistically justified.

van't Hoff analysis[150] was used to determine the enthalpy change (ΔH), entropy change (-TΔS) and the Gibbs free energy of the binding (ΔG) based on the equation:

$$\mathbf{lnK_A = -\frac{\Delta H}{R} \cdot \frac{1}{T} + \frac{\Delta S}{R}} \quad \textbf{(9)}$$

Results and Discussion

Be sure that all figures and tables fit within the document's regular margins. To determine the thermodynamic basis for Kir3.2-lipid interactions, we used native MS coupled with a variable-temperature nanoelectrospray ionization (nESI) apparatus to determine through van't Hoff analysis the change in enthalpy (ΔH) and entropy (−TΔS), components of the change in Gibbs free energy (ΔG).[146, 151] The first set of lipids we investigated were dioleoyl (18:1-18:1) phosphatidylinositol (DOPI) and phosphatidylinositol 4-phosphate with DO tails (DOPI(4)P). Here, we focus our initial discussion on DOPI(4)P as up to three bound Kir3.2 whereas only one DOPI bound the channel (Figure 24, 25). More specifically, Kir3.2 solubilized in $C_{10}E_5$, a detergent that in the nESI process results in charge reduced ions that aids preservation of non-covalent interactions and native-like structure in the mass spectrometer,[75, 152] at a concentration of 0.25 μM was titrated with DOPI(4)P up to a concentration of 2.5 μM. These samples were then incubated online using a variable temperature nESI

apparatus[153] for several minutes to reach equilibrium followed by acquiring their native mass spectra (Figure 21A and 26, 27). The mass spectra from this titration series at a given temperature were deconvoluted using UniDec[154] and the abundance of Kir3.2•DOPI(4)P_{0-3} was used to compute the mole fraction for the different lipid-bound states (Figure 21B). A sequential ligand binding model was fit to the mole fraction data to determine the equilibrium binding constants at a given temperature (Figure 21B). Thermodynamics for the individual DOPI(4)P binding events to Kir3.2 was deduced through van't Hoff analysis[151] (Figure 21C). Interestingly, the binding of one to three DOPI(4)P molecules to Kir3.2 is driven by entropy and the enthalpic term near zero (Figure 21D). This result is in complete contrast to our previous study of the bacterial ammonia channel (AmtB) binding phospholipids where the binding was driven by enthalpy and, in most cases, entropy was unfavorable.[146] The thermodynamic parameters for each DOPI(4)P binding event are statistically indistinguishable. Thermodynamics for the binding of one DOPI to Kir3.2 was determined in a similar fashion as done for DOPI(4)P. The binding of this lipid is also largely driven by entropy with a marginal favorable contribution from entropy (Figure 34, 37).

We next focused on other phosphorylated forms of phosphatidylinositol known to activate Kir3.2 and other channels to better understand the molecular forces that underlie their molecular recognition. These lipids include 4,5-bisphosphate PI with DO (DOPI(4,5)P_2) and 1-stearoyl-2-arachidonoyl (SAPI(4,5)P_2) tails and 3,4,5-trisphosphate PI with DO (DOPI(3,4,5)P_3). In a similar fashion as described above, we first titrated Kir3.2 with DOPI(4,5)P_2 and recorded their native mass spectra at different temperatures

(Figure 28, 29). Regardless of the temperature, the application of a sequential lipid binding model resulted in poor fits, especially for the first and second lipid bound states of Kir3.2 (Figure 35). Specifically, the trend in the mole fraction data for the first and second binding event does not follow the smooth curve but is rather suggestive of two underlying binding distributions. Although first described for Kir2.2,[20] recent structures of Kir3.2 have shown it also populates two distinct conformations where the CTD is docked, forming contacts with the cytoplasmic face of the TMD, or in an extended state, CTD displaced from the transmembrane domain (Figure 22A).[148, 149] Modification of lipid binding model such that the first and second lipid binding events binds to either a docked or extended states (see Methods) resulted in substantially improved fits (Figure 22B and 35). Here, the binding of the third lipid to Kir3.2 could represent a transition point wherein the three bounds lipid drive the channel from an extended to the docked state. This is consistent with recent cryoEM studies showing a population shift in the abundance of the docked state with increasing concentrations of $PI(4,5)P_2$.[148, 149]

Application of lipid binding model to different states of Kir3.2 was used to determine the K_D for each lipid binding event at a given temperature followed by van't Hoff analysis(Figure 22C and 37). The K_Ds for one to four $DOPI(4,5)P_2$ binding to the docked state of Kir3.2 display positive cooperativity (Table 7). Surprisingly, the thermodynamics for $DOPI(4,5)P_2$ associating with Kir3.2 reveal that the molecular driving force is solely entropic, outweighing an enthalpic penalty, regardless of binding to the docked or extended state (Figure 22C). In the case of binding to the docked state,

which we presume has a higher affinity for the lipid based on structures,[71, 72] unfavorable enthalpy was largest for the first binding event and subsequent binding events the thermodynamic parameters were similar. In contrast, the enthalpy for the binding event to the extended state increased. The additional 3-phosphate on DOPI(3,4,5)P_3 resulted in distinct thermodynamic signatures in comparison to DOPI(4,5)P_2. Excluding the first binding event to the docked structure where it is driven by entropy and enthalpically unfavorable, all the other binding events showed enthalpy-entropy compensation whereby favorable entropy and unfavorable entropy steadily for each binding event (Figure 22C). Altering acyl chain chemistry of PI(4,5)P_2 to contain SA tails, resulting in a new subset of thermodynamic values with the majority of binding events driven by enthalpy. For binding to the docked state, favorable enthalpy was greatest for binding the first lipid whereas for second and third were similar but to a larger extent compared to the fourth. The fourth SAPI(4,5)P_2 binding event is unique among the PIPs investigated in that both entropic and enthalpy are favorable. Remarkably, these results demonstrate that specific phosphorylated forms of PI selectively engage the different states of Kir3.2.

It is striking when comparing the stepwise progression from DOPI to DOPI(3,4,5)P_3 and different acyl chains on binding thermodynamics (Figure 23). The addition of a 4-phosphate to DOPI pushes the reaction to be driven by entropy. Going from DOPI(4)P to DOPI(4,5)P_2 results in ~60 kJ/mol contributing to both enthalpy and entropy but in opposing directions for the first lipid binding. This is consistent for the other binding events but to half the extent. DOPI(3,4,5)P_3 with three phosphates displays

a strong enthalpy-entropy dependence. A remarkably 175 kJ/mol alteration in thermodynamic parameters but the opposing direction is observed for the first binding event of DOPI(3,4,5)P_3 to the docked state. Compared to DOI(4,5)P_2, the binding of two or more DOPI(3,4,5)P_3 to Kir3.2 are accompanied by compensatory gains in favorable entropy and unfavorable enthalpy spanning 50 kJ/mol. The replacement of DOPI(4,5)P_2 with SA tails displayed marked gains in favorable enthalpy and unfavorable entropy and the first SAPI(4,5)P_2 binding event with a remarkable change of nearly 200 kJ/mol. These results illustrate the difference in the chemistry of the lipid can have a marked impact on binding thermodynamics.

The thermodynamics of Kir3.2-lipid interactions provide rich chemical insight into the molecular forces driving underlying specific Kir3.2-lipid interactions. The majority of phosphorylated forms of DOPI binding events are driven by entropy and, in most cases, there is an unfavorable change in enthalpy. It is important to note these lipids possess DO tails and therefore the entropic contribution from desolvation of the acyl chains plays a minor role in the large entropies observed here. While solvent reorganization of the phosphorylated headgroup and/or PIP binding can contribute in a positive way to entropy,[155, 156] the largely favorable entropy accompanied by unfavorable enthalpy observed here is reminiscent of protein-ligand interactions that are driven by large conformational entropy originating in enhanced protein motions.[157-160] The first binding events of DOPI(4,5)P_2, DOPI(3,4,5)P_3, and SAPI(4,5)P_2 indicate significant structural changes upon binding. The thermodynamics for DOPI(4,5)P_2 suggests the lipid results in a significant enhancement in protein dynamics whereas for

the two other lipids there is significant structuring of Kir3.2. We have previously observed enthalpy-entropy compensation for AmtB-lipid interactions.[146] However, the enthalpy-entropy compensation is more pronounced for Kir3.2-DOPI(3,4,5)P_3 in comparison to that observed for AmtB-lipid interactions and likely due to significant structuring of the channel at the cost of a reduction in disorder. The enthalpically driven binding of SAPI(4,5)P_2 to Kir3.2 suggests the SA tails interact more favorably with Kir3.2 in comparison to the lipid with DO tails.

Conclusion

In summary, the thermodynamics of lipids associating with Kir3.2 reveal different thermodynamic strategies and, in some cases, in unpredictable ways. It is remarkably the changes in binding thermodynamics observed upon phosphorylation(s) of the inositol headgroup or altering the acyl chains. Recently, the dynamics of lipids have been suggested to promote their interaction with membrane proteins.[161] Conformational entropy has recently been observed for monomeric proteins and is independent of the membrane mimetic.[162] Here, we show that the association of Kir3.2 with specific PIPs can be driven by a large change in entropy deriving likely from enhanced protein dynamics. Conformational entropy is established for soluble proteins and here we provide evidence that entropy can greatly influence membrane protein-lipid interactions.

CHAPTER V

SUMMARY AND CONCLUSION

The regulation of lipids has been widely recognized in the field of membrane protein study. This thesis focused on the study of the interaction between inwardly rectifying potassium channels with phospholipids, especially with phosphorylated phosphotidylinositdes (PIPs) under the guidance of native mass spectrometry (MS). We first combined the native MS and fluorescent-lipid binding assays to gain insight into the contribution of specific Kir3.2 residues binding to phospholipids. We have demonstrated the importance of membrane protein samples devoid of co-purified contaminants for protein-lipid binding studies and show that $PI(4,5)P_2$ cooperatively binds Kir3.2 with a Hill coefficient of 2.7. We also find lipid binding profiles determined from native MS and solution binding assays are in direct agreement. Point mutations of Kir3.2 residues that interact with PIPs distinctly alter selective lipid binding. The K64Q mutation results in altered binding profiles with the highest binding affinity to lipids with specific acyl chains. Mutation of R92 to Pro, a residue found in Kir6.2, results in promiscuous binding of PIP isoforms. Kir3.2 with the K194A mutation results in a distinct binding preference for $PI(3,4,5)P_3$ over other PIP isoforms. Taken together, our results underscore the utmost importance of protein quality for protein-lipid binding studies and a single mutation in Kir3.2 can alter the selectivity toward PIPs.

The G-protein gated inwardly rectifying potassium channel 4 (Kir3.4) subunit forms homomeric or heterometric tetramers. Previous studies have established that $PI(4,5)P_2$ is required for Kir3.4 function. However, the binding preferences of Kir3.4 for

the head group and acyl chains of phosphorylated phosphatidylinositides (PIPs) and other lipids is not well understood. Here, the interactions between full-length, human Kir3.4 and lipids are characterized using native mass spectrometry (MS) in conjuction with a soluble fluorescent lipid binding assay. Kir3.4 displays binding preferences for PIPs and, in some cases, the degree of binding is influenced by the type of acyl chains. The interactions between Kir3.4 and PIPs are weaker in comparison to full-length, human Kir3.2. The binding of $PI(4,5)P_2$ modified with a fluorophore to Kir3.2 can be enhanced by other lipids, such as phosphatidylcholine. Introduction of S143T, a mutation that enhances Kir3.4 sensitivity to $G_{\beta\gamma}$, results in an overall reduction in the channel binding PIPs. In contrast, the D223N mutant of Kir3.4 that mimics the sodium bound state exhibited stronger binding for $PI(4,5)P_2$, particularly for those with 18:0–20:4 acyl chains. Taken together, these results provide additional insight into the interaction between Kir3.4 and lipids that are important for channel function.

All inward rectifier potassium (Kir) channels are regulated by phosphorylated phosphotidylinositdes (PIPs). Understanding the molecular driving forces that underlie Kir-PIP interactions requires the characterization of their binding thermodynamics. Here, we employ native mass spectrometry in conjunction with a variable temperature apparatus to determine the thermodynamics of individual lipid binding events to Kir3.2, a G-protein-gated Kir channel. We found that Kir3.2 displays distinct thermodynamic strategies to engage phosphatidylinositol (PI) and phosphorylated forms thereof. More specifically, the addition of a 4'-phosphate to PI with 18:1-18:1 (DO) tails results in an increase in favorable entropy along with an enthalpic penalty. The binding of PI with

two or more phosphates is more complex where lipids bind to Kir3.2 with the cytoplasmic domain in either a docked or extended configuration. The interaction of 4,5-bisphosphate DOPI (DOPI(4,5)P_2) with Kir3.2 is driven by a large, favorable entropy change that outcompetes an unfavorable change in enthalpy. Installment of a third 3'-phosphate to DOPI(4,5)P_2 results in an alternative thermodynamic strategy for the first binding event whereas each successive binding event shows strong enthalpy-entropy compensation. PI(4,5)P_2 with 18:0-20:4 tails results in an inversion of thermodynamic parameters where the change in enthalpy now dominates. Collectively, the data show the interaction between Kir3.2 and specific PIPs can be driven by large entropy providing evidence that entropy can indeed play important roles in regulating membrane protein-lipid interactions.

In this thesis, the inwardly rectifying potassium channels have been used as example to show the great potential of native MS in membrane protein studies. With further development and application of native MS, we will be able to decipher more detailed information of membrane protein in terms of biochemical, biophysical, and structural characteristics.

REFERENCES

1. Nicolson, G.L., *The Fluid-Mosaic Model of Membrane Structure: still relevant to understanding the structure, function and dynamics of biological membranes after more than 40 years.* Biochimica et biophysica acta, 2014. **1838**(6): p. 1451-1466.
2. Ghirlanda, G. and A. Senes, *Membrane Proteins*. Methods in Molecular Biology. 2013: Humana Press, Totowa, NJ. x, 246.
3. Campbell, N.A., et al., *Campbell Biology*. 2016: Pearson: Boston, Mass.
4. Li, Y. and D. Zhao, *Basics of Molecular Biology*, in *Molecular Imaging: Fundamentals and Applications*, J. Tian, Editor. 2013, Springer Berlin Heidelberg: Berlin, Heidelberg. p. 541-601.
5. Seddon, A.M., P. Curnow, and P.J. Booth, *Membrane proteins, lipids and detergents: not just a soap opera.* Biochim Biophys Acta, 2004. **1666**(1-2): p. 105-17.
6. Whitelegge, J.P., *Integral membrane proteins and bilayer proteomics.* Analytical chemistry, 2013. **85**(5): p. 2558-2568.
7. Dufrisne, M.B., et al., *Structural basis for catalysis at the membrane-water interface.* Biochimica et biophysica acta. Molecular and cell biology of lipids, 2017. **1862**(11): p. 1368-1385.

8. Cournia, Z., et al., *Membrane Protein Structure, Function, and Dynamics: a Perspective from Experiments and Theory.* J Membr Biol, 2015. **248**(4): p. 611-40.

9. Ng, D.P., B.E. Poulsen, and C.M. Deber, *Membrane protein misassembly in disease.* Biochimica et Biophysica Acta (BBA) - Biomembranes, 2012. **1818**(4): p. 1115-1122.

10. Gorman, P.M., et al., *Dimerization of the transmembrane domain of amyloid precursor proteins and familial Alzheimer's disease mutants.* BMC Neurosci, 2008. **9**: p. 17.

11. Cheung, J.C. and C.M. Deber, *Misfolding of the cystic fibrosis transmembrane conductance regulator and disease.* Biochemistry, 2008. **47**(6): p. 1465-73.

12. Overington, J.P., B. Al-Lazikani, and A.L. Hopkins, *How many drug targets are there?* Nat Rev Drug Discov, 2006. **5**(12): p. 993-6.

13. Phillips, R., et al., *Emerging roles for lipids in shaping membrane-protein function.* Nature, 2009. **459**(7245): p. 379-85.

14. Yèagle, P.L., *Lipid regulation of cell membrane structure and function.* The FASEB Journal, 1989. **3**(7): p. 1833-1842.

15. Stuart McLaughlin, et al., *PIP2 and Proteins: Interactions, Organization, and Information Flow.* Annual Review of Biophysics and Biomolecular Structure, 2002. **31**(1): p. 151-175.

16. Bechara, C., et al., *A subset of annular lipids is linked to the flippase activity of an ABC transporter.* Nature Chemistry, 2015. **7**(3): p. 255-262.

17. Gupta, K., et al., *The role of interfacial lipids in stabilizing membrane protein oligomers.* Nature, 2017. **541**(7637): p. 421-424.

18. Laganowsky, A., et al., *Membrane proteins bind lipids selectively to modulate their structure and function.* Nature, 2014. **510**(7503): p. 172-175.

19. Contreras, F.X., et al., *Specificity of intramembrane protein-lipid interactions.* Cold Spring Harb Perspect Biol, 2011. **3**(6).

20. Hansen, S.B., X. Tao, and R. MacKinnon, *Structural basis of PIP2 activation of the classical inward rectifier K+ channel Kir2.2.* Nature, 2011. **477**(7365): p. 495-8.

21. Dowhan, W. and M. Bogdanov, *Lipid-protein interactions as determinants of membrane protein structure and function.* Biochemical Society transactions, 2011. **39**(3): p. 767-774.

22. Suh, B.C. and B. Hille, *PIP2 is a necessary cofactor for ion channel function: how and why?* Annu Rev Biophys, 2008. **37**: p. 175-95.

23. Tucker, S.J. and T. Baukrowitz, *How highly charged anionic lipids bind and regulate ion channels.* The Journal of general physiology, 2008. **131**(5): p. 431-438.

24. Sun, Y., et al., *Phosphatidylinositol 4,5-bisphosphate: targeted production and signaling.* BioEssays : news and reviews in molecular, cellular and developmental biology, 2013. **35**(6): p. 513-522.

25. Hilgemann, D.W., et al., *Lipid signaling to membrane proteins: From second messengers to membrane domains and adapter-free endocytosis.* Journal of General Physiology, 2018. **150**(2): p. 211-224.

26. Harraz, O.F., D. Hill-Eubanks, and M.T. Nelson, *PIP2: A critical regulator of vascular ion channels hiding in plain sight.* Proceedings of the National Academy of Sciences, 2020. **117**(34): p. 20378-20389.

27. le Maire, M., P. Champeil, and J.V. Møller, *Interaction of membrane proteins and lipids with solubilizing detergents.* Biochimica et Biophysica Acta (BBA) - Biomembranes, 2000. **1508**(1): p. 86-111.

28. Valiyaveetil, F.I., Y. Zhou, and R. MacKinnon, *Lipids in the structure, folding, and function of the KcsA K+ channel.* Biochemistry, 2002. **41**(35): p. 10771-7.

29. Ilgü, H., et al., *Variation of the detergent-binding capacity and phospholipid content of membrane proteins when purified in different detergents.* Biophysical journal, 2014. **106**(8): p. 1660-1670.

30. Teo, A.C.K., et al., *Analysis of SMALP co-extracted phospholipids shows distinct membrane environments for three classes of bacterial membrane protein.* Scientific Reports, 2019. **9**(1): p. 1813.

31. Bogdanov, M., E. Mileykovskaya, and W. Dowhan, *Lipids in the assembly of membrane proteins and organization of protein supercomplexes: implications for lipid-linked disorders.* Sub-cellular biochemistry, 2008. **49**: p. 197-239.

32. Barrera, N.P., M. Zhou, and C.V. Robinson, *The role of lipids in defining membrane protein interactions: insights from mass spectrometry.* Trends Cell Biol, 2013. **23**(1): p. 1-8.

33. Calabrese, A.N. and S.E. Radford, *Mass spectrometry-enabled structural biology of membrane proteins.* Methods, 2018. **147**: p. 187-205.

34. Laganowsky, A., et al., *Mass spectrometry of intact membrane protein complexes.* Nature Protocols, 2013. **8**(4): p. 639-651.

35. Cabanos, C., et al., *A Soluble Fluorescent Binding Assay Reveals PIP2 Antagonism of TREK-1 Channels.* Cell Rep, 2017. **20**(6): p. 1287-1294.

36. Wang, W., M.R. Whorton, and R. MacKinnon, *Quantitative analysis of mammalian GIRK2 channel regulation by G proteins, the signaling lipid PIP2 and Na+ in a reconstituted system.* eLife, 2014. **3**: p. e03671-e03671.

37. Lee, S.J., et al., *Structural basis of control of inward rectifier Kir2 channel gating by bulk anionic phospholipids.* J Gen Physiol, 2016. **148**(3): p. 227-37.

38. Lacin, E., et al., *Dynamic role of the tether helix in PIP2-dependent gating of a G protein–gated potassium channel.* Journal of General Physiology, 2017. **149**(8): p. 799-811.

39. Smith, R., et al., *Proteomics, lipidomics, metabolomics: a mass spectrometry tutorial from a computer scientist's point of view.* BMC Bioinformatics, 2014. **15**(7): p. S9.

40. Leney, A.C. and A.J. Heck, *Native Mass Spectrometry: What is in the Name?* J Am Soc Mass Spectrom, 2017. **28**(1): p. 5-13.

41. Loo, J.A., *Electrospray ionization mass spectrometry: a technology for studying noncovalent macromolecular complexes.* International Journal of Mass Spectrometry, 2000. **200**(1): p. 175-186.

42. Keener, J.E., G. Zhang, and M.T. Marty, *Native Mass Spectrometry of Membrane Proteins.* Analytical Chemistry, 2021. **93**(1): p. 583-597.

43. Cong, X., et al., *Allosteric modulation of protein-protein interactions by individual lipid binding events.* Nature Communications, 2017. **8**(1): p. 2203.

44. Cong, X., et al., *Determining Membrane Protein–Lipid Binding Thermodynamics Using Native Mass Spectrometry.* Journal of the American Chemical Society, 2016. **138**(13): p. 4346-4349.

45. Liu, Y., et al., *Selective binding of a toxin and phosphatidylinositides to a mammalian potassium channel.* Nature Communications, 2019. **10**(1): p. 1352.

46. Le Franc, Y., *Inward Rectifier Potassium Channels*, in *Encyclopedia of Computational Neuroscience*, D. Jaeger and R. Jung, Editors. 2013, Springer New York: New York, NY. p. 1-4.

47. Hibino, H., et al., *Inwardly rectifying potassium channels: their structure, function, and physiological roles.* Physiol Rev, 2010. **90**(1): p. 291-366.

48. Pattnaik, B.R., et al., *Genetic defects in the hotspot of inwardly rectifying K(+) (Kir) channels and their metabolic consequences: a review.* Mol Genet Metab, 2012. **105**(1): p. 64-72.

49. Inagaki, N., et al., *Cloning and functional characterization of a novel ATP-sensitive potassium channel ubiquitously expressed in rat tissues, including*

pancreatic islets, pituitary, skeletal muscle, and heart. J Biol Chem, 1995. **270**(11): p. 5691-4.

50. Ashcroft, F.M., *ATP-sensitive potassium channelopathies: focus on insulin secretion.* J Clin Invest, 2005. **115**(8): p. 2047-58.

51. Simon, D.B., et al., *Genetic heterogeneity of Bartter's syndrome revealed by mutations in the K+ channel, ROMK.* Nat Genet, 1996. **14**(2): p. 152-6.

52. Donaldson, M.R., et al., *Andersen-Tawil syndrome: a model of clinical variability, pleiotropy, and genetic heterogeneity.* Ann Med, 2004. **36 Suppl 1**: p. 92-7.

53. Reichold, M., et al., *KCNJ10 gene mutations causing EAST syndrome (epilepsy, ataxia, sensorineural deafness, and tubulopathy) disrupt channel function.* Proc Natl Acad Sci U S A, 2010. **107**(32): p. 14490-5.

54. Jiao, X., et al., *Genetic Linkage of Snowflake Vitreoretinal Degeneration to Chromosome 2q36.* Investigative Ophthalmology & Visual Science, 2004. **45**(12): p. 4498-4503.

55. McLaughlin, S. and D. Murray, *Plasma membrane phosphoinositide organization by protein electrostatics.* Nature, 2005. **438**(7068): p. 605-11.

56. Huang, C.L., S. Feng, and D.W. Hilgemann, *Direct activation of inward rectifier potassium channels by PIP2 and its stabilization by Gbetagamma.* Nature, 1998. **391**(6669): p. 803-6.

57. Rohacs, T., et al., *Specificity of activation by phosphoinositides determines lipid regulation of Kir channels.* Proc Natl Acad Sci U S A, 2003. **100**(2): p. 745-50.

58. Fujiwara, Y. and Y. Kubo, *Regulation of the desensitization and ion selectivity of ATP-gated P2X2 channels by phosphoinositides.* J Physiol, 2006. **576**(Pt 1): p. 135-49.

59. Lopes, C.M., et al., *Alterations in conserved Kir channel-PIP2 interactions underlie channelopathies.* Neuron, 2002. **34**(6): p. 933-44.

60. Aryal, P., et al., *A discrete alcohol pocket involved in GIRK channel activation.* Nat Neurosci, 2009. **12**(8): p. 988-95.

61. Ruppersberg, J.P., *Intracellular regulation of inward rectifier K+ channels.* Pflugers Arch, 2000. **441**(1): p. 1-11.

62. Monica, S.-R. and G.N. Colin, *Inward Rectifying Potassium Channels*, in *Handbook of Ion Channels*. 2015, CRC Press. p. 241-260.

63. Rohacs, T., et al., *Distinct specificities of inwardly rectifying K(+) channels for phosphoinositides.* J Biol Chem, 1999. **274**(51): p. 36065-72.

64. Cheng, W.W.L., et al., *Dual-mode phospholipid regulation of human inward rectifying potassium channels.* Biophys J, 2011. **100**(3): p. 620-628.

65. D'Avanzo, N., et al., *Direct and specific activation of human inward rectifier K+ channels by membrane phosphatidylinositol 4,5-bisphosphate.* J Biol Chem, 2010. **285**(48): p. 37129-32.

66. Li, J., M.L. Blankenship, and M.L. Baccei, *Inward-Rectifying Potassium (K_{ir}) Channels Regulate Pacemaker Activity in Spinal Nociceptive Circuits during Early Life.* The Journal of Neuroscience, 2013. **33**(8): p. 3352-3362.

67. Wenk, M.R., et al., *Phosphoinositide profiling in complex lipid mixtures using electrospray ionization mass spectrometry.* Nat Biotechnol, 2003. **21**(7): p. 813-7.

68. Milne, S.B., et al., *A targeted mass spectrometric analysis of phosphatidylinositol phosphate species.* J Lipid Res, 2005. **46**(8): p. 1796-802.

69. Traynor-Kaplan, A., et al., *Fatty-acyl chain profiles of cellular phosphoinositides.* Biochimica et biophysica acta. Molecular and cell biology of lipids, 2017. **1862**(5): p. 513-522.

70. D'Avanzo, N., et al., *Energetics and location of phosphoinositide binding in human Kir2.1 channels.* The Journal of biological chemistry, 2013. **288**(23): p. 16726-16737.

71. Whorton, M.R. and R. MacKinnon, *Crystal structure of the mammalian GIRK2 K+ channel and gating regulation by G proteins, PIP2, and sodium.* Cell, 2011. **147**(1): p. 199-208.

72. Whorton, M.R. and R. MacKinnon, *X-ray structure of the mammalian GIRK2-betagamma G-protein complex.* Nature, 2013. **498**(7453): p. 190-7.

73. Zhang, H., et al., *Activation of inwardly rectifying K+ channels by distinct PtdIns(4,5)P2 interactions.* Nat Cell Biol, 1999. **1**(3): p. 183-8.

74. Zhou, W., et al., *Mechanism underlying bupivacaine inhibition of G protein-gated inwardly rectifying K⁺ channels.* Proceedings of the National Academy of Sciences, 2001. **98**(11): p. 6482-6487.

75. Laganowsky, A., et al., *Membrane proteins bind lipids selectively to modulate their structure and function.* Nature, 2014. **510**(7503): p. 172-5.

76. Cong, X., et al., *Allosteric modulation of protein-protein interactions by individual lipid binding events.* Nat Commun, 2017. **8**(1): p. 2203.

77. Yen, H.Y., et al., *PtdIns(4,5)P2 stabilizes active states of GPCRs and enhances selectivity of G-protein coupling.* Nature, 2018. **559**(7714): p. 423-427.

78. Patrick, J.W., et al., *Allostery revealed within lipid binding events to membrane proteins.* Proc Natl Acad Sci U S A, 2018. **115**(12): p. 2976-2981.

79. Bolla, J.R., et al., *Direct observation of the influence of cardiolipin and antibiotics on lipid II binding to MurJ.* Nat Chem, 2018. **10**(3): p. 363-371.

80. Marcoux, J., et al., *Mass spectrometry reveals synergistic effects of nucleotides, lipids, and drugs binding to a multidrug resistance efflux pump.* Proc Natl Acad Sci U S A, 2013. **110**(24): p. 9704-9.

81. Weis, R., *High-Throughput Screening and Selection of Pichia pastoris Strains.* Methods Mol Biol, 2019. **1923**: p. 169-185.

82. Gandhi, C.S., T.A. Walton, and D.C. Rees, *OCAM: A new tool for studying the oligomeric diversity of MscL channels.* Protein Science, 2011. **20**(2): p. 313-326.

83. Marty, M.T., et al., *Bayesian Deconvolution of Mass and Ion Mobility Spectra: From Binary Interactions to Polydisperse Ensembles.* Analytical Chemistry, 2015. **87**(8): p. 4370-4376.

84. Hieb, A.R., et al., *Fluorescence strategies for high-throughput quantification of protein interactions.* Nucleic Acids Res, 2012. **40**(5): p. e33.

85. Madeira, F., et al., *The EMBL-EBI search and sequence analysis tools APIs in 2019.* Nucleic acids research, 2019. **47**(W1): p. W636-W641.

86. Shaner, N.C., et al., *Improved monomeric red, orange and yellow fluorescent proteins derived from Discosoma sp. red fluorescent protein.* Nat Biotechnol, 2004. **22**(12): p. 1567-72.

87. Mehmood, S., et al., *Charge reduction stabilizes intact membrane protein complexes for mass spectrometry.* J Am Chem Soc, 2014. **136**(49): p. 17010-2.

88. Tong, A., et al., *Direct binding of phosphatidylglycerol at specific sites modulates desensitization of a ligand-gated ion channel.* eLife, 2019. **8**: p. e50766.

89. Laganowsky, A., et al., *Mass spectrometry of intact membrane protein complexes.* Nat Protoc, 2013. **8**(4): p. 639-51.

90. Laemmli, U.K., *Cleavage of structural proteins during the assembly of the head of bacteriophage T4.* Nature, 1970. **227**(5259): p. 680-5.

91. Whitelegge, J.P., C.B. Gundersen, and K.F. Faull, *Electrospray-ionization mass spectrometry of intact intrinsic membrane proteins.* Protein Sci, 1998. **7**(6): p. 1423-30.

92. Laganowsky, A., et al., *Hydroponics on a chip: analysis of the Fe deficient Arabidopsis thylakoid membrane proteome.* J Proteomics, 2009. **72**(3): p. 397-415.

93. Wang, W., M.R. Whorton, and R. MacKinnon, *Quantitative analysis of mammalian GIRK2 channel regulation by G proteins, the signaling lipid PIP2 and Na+ in a reconstituted system.* Elife, 2014. **3**: p. e03671.

94. Yohannan, S., et al., *The evolution of transmembrane helix kinks and the structural diversity of G protein-coupled receptors.* Proc Natl Acad Sci U S A, 2004. **101**(4): p. 959-63.

95. Lacin, E., et al., *Dynamic role of the tether helix in PIP*. J Gen Physiol, 2017. **149**(8): p. 799-811.

96. Takahashi, T., *Inward rectification in neonatal rat spinal motoneurones.* J Physiol, 1990. **423**: p. 47-62.

97. Kurachi, Y., *Voltage-dependent activation of the inward-rectifier potassium channel in the ventricular cell membrane of guinea-pig heart.* J Physiol, 1985. **366**: p. 365-85.

98. Lewis, D.L., et al., *Expression of an inwardly rectifying K+ channel from rat basophilic leukemia cell mRNA in Xenopus oocytes.* FEBS Lett, 1991. **290**(1-2): p. 17-21.

99. Silver, M.R. and T.E. DeCoursey, *Intrinsic gating of inward rectifier in bovine pulmonary artery endothelial cells in the presence or absence of internal Mg2+*. J Gen Physiol, 1990. **96**(1): p. 109-33.

100. Chen, R. and D.R. Swale, *Inwardly Rectifying Potassium (Kir) Channels Represent a Critical Ion Conductance Pathway in the Nervous Systems of Insects.* Scientific Reports, 2018. **8**(1): p. 1617.

101. Baronas, V.A. and H.T. Kurata, *Inward rectifiers and their regulation by endogenous polyamines.* Frontiers in Physiology, 2014. **5**(325): p. 325.

102. Touhara, K.K., W. Wang, and R. MacKinnon, *The GIRK1 subunit potentiates G protein activation of cardiac GIRK1/4 hetero-tetramers.* eLife, 2016. **5**: p. e15750.

103. Koster, J.C., M.A. Permutt, and C.G. Nichols, *Diabetes and insulin secretion: the ATP-sensitive K+ channel (K ATP) connection.* Diabetes, 2005. **54**(11): p. 3065-72.

104. Lyford, L.K. and R.L. Rosenberg, *Chapter 13 - Reconstitution in planar lipid bilayers of ion channels synthesized in ovo and in vitro*, in *Membrane Science and Technology*, H.T. Tien and A. Ottova-Leitmannova, Editors. 2003, Elsevier. p. 391-412.

105. Tristani-Firouzi, M., *94 - Andersen-Tawil Syndrome*, in *Cardiac Electrophysiology: From Cell to Bedside (Seventh Edition)*, D.P. Zipes, J. Jalife, and W.G. Stevenson, Editors. 2018, Elsevier. p. 905-909.

106. Issa, Z.F., J.M. Miller, and D.P. Zipes, *2 - Cardiac Ion Channels*, in *Clinical Arrhythmology and Electrophysiology (Third Edition)*, Z.F. Issa, J.M. Miller, and D.P. Zipes, Editors. 2019, Elsevier: Philadelphia. p. 15-50.

107. Fujiwara, Y. and Y. Kubo, *Regulation of the desensitization and ion selectivity of ATP-gated P2X2 channels by phosphoinositides.* The Journal of physiology, 2006. **576**(Pt 1): p. 135-149.

108. McLaughlin, S. and D. Murray, *Plasma membrane phosphoinositide organization by protein electrostatics.* Nature, 2005. **438**(7068): p. 605-611.

109. Ruppersberg, J.P., *Intracellular regulation of inward rectifier K+ channels.* Pflügers Archiv, 2000. **441**(1): p. 1-11.

110. Sala-Rabanal, M., G.N. Colin, and M.N. Crina, *Inward rectifying potassium channels*, in *Handbook of Ion Channels*. 2015, CRC Press.

111. Ho, I.H. and R.D. Murrell-Lagnado, *Molecular determinants for sodium-dependent activation of G protein-gated K+ channels.* J Biol Chem, 1999. **274**(13): p. 8639-48.

112. Ho, I.H. and R.D. Murrell-Lagnado, *Molecular mechanism for sodium-dependent activation of G protein-gated K+ channels.* J Physiol, 1999. **520 Pt 3**: p. 645-51.

113. Furst, O., B. Mondou, and N. D'Avanzo, *Phosphoinositide regulation of inward rectifier potassium (Kir) channels.* Front Physiol, 2014. **4**: p. 404.

114. Cheng, W.W.L., et al., *Dual-Mode Phospholipid Regulation of Human Inward Rectifying Potassium Channels.* Biophysical Journal, 2011. **100**(3): p. 620-628.

115. Heck, A.J.R., *Native mass spectrometry: a bridge between interactomics and structural biology.* Nature Methods, 2008. **5**(11): p. 927-933.

116. Liko, I., et al., *Mass spectrometry guided structural biology.* Curr Opin Struct Biol, 2016. **40**: p. 136-144.

117. Agasid, M.T. and C.V. Robinson, *Probing membrane protein-lipid interactions.* Curr Opin Struct Biol, 2021. **69**: p. 78-85.

118. Tamara, S., M.A. den Boer, and A.J.R. Heck, *High-Resolution Native Mass Spectrometry.* Chem Rev, 2021.

119. Allison, T.M., et al., *Quantifying the stabilizing effects of protein–ligand interactions in the gas phase.* Nature Communications, 2015. **6**: p. 8551.

120. Fantin, S.M., et al., *Collision Induced Unfolding Classifies Ligands Bound to the Integral Membrane Translocator Protein.* Anal Chem, 2019. **91**(24): p. 15469-15476.

121. Qiao, P., et al., *Insight into the selectivity of Kir3.2 toward phosphatidylinositides.* Biochemistry, 2020. **59**(22): p. 2089-2099.

122. Liu, Y., et al., *Selective binding of a toxin and phosphatidylinositides to a mammalian potassium channel.* Nat Commun, 2019. **10**(1): p. 1352.

123. Vivaudou, M., et al., *Probing the G-protein regulation of GIRK1 and GIRK4, the two subunits of the KACh channel, using functional homomeric mutants.* J Biol Chem, 1997. **272**(50): p. 31553-60.

124. Scholz, J. and S. Suppmann, *A new single-step protocol for rapid baculovirus-driven protein production in insect cells.* BMC Biotechnol, 2017. **17**(1): p. 83.

125. Chan, K.W., et al., *Control of channel activity through a unique amino acid residue of a G protein-gated inwardly rectifying K⁺ channel subunit.* Proceedings of the National Academy of Sciences, 1996. **93**(24): p. 14193-14198.

126. Lesage, F., et al., *Molecular properties of neuronal G-protein-activated inwardly rectifying K+ channels.* J Biol Chem, 1995. **270**(48): p. 28660-7.

127. Sui, J.L., K.W. Chan, and D.E. Logothetis, *Na+ activation of the muscarinic K+ channel by a G-protein-independent mechanism.* J Gen Physiol, 1996. **108**(5): p. 381-91.

128. Sui, J.L., J. Petit-Jacques, and D.E. Logothetis, *Activation of the atrial KACh channel by the betagamma subunits of G proteins or intracellular Na+ ions depends on the presence of phosphatidylinositol phosphates.* Proc Natl Acad Sci U S A, 1998. **95**(3): p. 1307-12.

129. Lüscher, C. and P.A. Slesinger, *Emerging roles for G protein-gated inwardly rectifying potassium (GIRK) channels in health and disease.* Nat Rev Neurosci, 2010. **11**(5): p. 301-15.

130. Neusch, C., J.H. Weishaupt, and M. Bahr, *Kir channels in the CNS: emerging new roles and implications for neurological diseases.* Cell Tissue Res, 2003. **311**(2): p. 131-8.

131. Abraham, M.R., et al., *Channelopathies of inwardly rectifying potassium channels.* FASEB J, 1999. **13**(14): p. 1901-10.

132. Shieh, C.C., et al., *Potassium channels: molecular defects, diseases, and therapeutic opportunities.* Pharmacol Rev, 2000. **52**(4): p. 557-94.

133. Tao, X., et al., *Crystal structure of the eukaryotic strong inward-rectifier K+ channel Kir2.2 at 3.1 A resolution.* Science, 2009. **326**(5960): p. 1668-74.

134. Zangerl-Plessl, E.M., et al., *Disease Associated Mutations in K(IR) Proteins Linked to Aberrant Inward Rectifier Channel Trafficking.* Biomolecules, 2019. **9**(11).

135. Hedger, G. and M.S.P. Sansom, *Lipid interaction sites on channels, transporters and receptors: Recent insights from molecular dynamics simulations.* Biochim Biophys Acta, 2016. **1858**(10): p. 2390-2400.

136. Corey, R.A., et al., *Insights into Membrane Protein–Lipid Interactions from Free Energy Calculations.* Journal of Chemical Theory and Computation, 2019. **15**(10): p. 5727-5736.

137. Pipatpolkai, T., et al., *Evaluating inositol phospholipid interactions with inward rectifier potassium channels and characterising their role in disease.* Communications Chemistry, 2020. **3**(1): p. 147.

138. Corradi, V., et al., *Lipid-Protein Interactions Are Unique Fingerprints for Membrane Proteins.* ACS Cent Sci, 2018. **4**(6): p. 709-717.

139. Allison, T.M., et al., *Quantifying the stabilizing effects of protein-ligand interactions in the gas phase.* Nat Commun, 2015: p. in press.

140. Barrera, N.P., et al., *Micelles protect membrane complexes from solution to vacuum.* Science, 2008. **321**(5886): p. 243-6.

141. Gault, J., et al., *High-resolution mass spectrometry of small molecules bound to membrane proteins.* Nat Methods, 2016. **13**(4): p. 333-6.

142. Yen, H.Y., et al., *Ligand binding to a G protein-coupled receptor captured in a mass spectrometer.* Sci Adv, 2017. **3**(6): p. e1701016.

143. Marcoux, J. and C.V. Robinson, *Twenty years of gas phase structural biology.* Structure, 2013. **21**(9): p. 1541-50.

144. McCabe, J.W., et al., *Variable-Temperature Electrospray Ionization for Temperature-Dependent Folding/Refolding Reactions of Proteins and Ligand Binding.* Analytical Chemistry, 2021. **93**(18): p. 6924-6931.

145. Marty, M., et al., *Bayesian Deconvolution of Mass and Ion Mobility Spectra: From Binary Interactions to Polydisperse Ensembles.* Anal. Chem., 2015. **87**: p. 4370-4376.

146. Cong, X., et al., *Determining Membrane Protein-Lipid Binding Thermodynamics Using Native Mass Spectrometry.* J Am Chem Soc, 2016. **138**(13): p. 4346-9.

147. Stengel, F., et al., *Dissecting heterogeneous molecular chaperone complexes using a mass spectrum deconvolution approach.* Chem Biol, 2012. **19**(5): p. 599-607.

148. Niu, Y., et al., *Cryo-EM analysis of PIP2 regulation in mammalian GIRK channels.* eLife, 2020. **9**: p. e60552.

149. Mathiharan, Y.K., et al., *Structural insights into GIRK2 channel modulation by cholesterol and PIP2.* Cell Reports, 2021. **36**(8): p. 109619.

150. van't Hoff, M.J.H., *Etudes de dynamique chimique.* Recl. Trav. Chim. Pays-Bas, 1884. **3**(10): p. 333-336.

151. van't Hoff, M.J.H., *Etudes de dynamique chimique.* Recueil des Travaux Chimiques des Pays-Bas, 1884. **3**(10): p. 333-336.

152. Reading, E., et al., *The role of the detergent micelle in preserving the structure of membrane proteins in the gas phase.* Angew Chem Int Ed Engl, 2015. **54**(15): p. 4577-81.

153. McCabe, J.W., et al., *Variable-Temperature Electrospray Ionization for Temperature-Dependent Folding/Refolding Reactions of Proteins and Ligand Binding.* Anal Chem, 2021. **93**(18): p. 6924-6931.

154. Marty, M.T., et al., *Bayesian deconvolution of mass and ion mobility spectra: from binary interactions to polydisperse ensembles.* Anal Chem, 2015. **87**(8): p. 4370-6.

155. Dill, K.A., *Dominant forces in protein folding.* Biochemistry, 1990. **29**(31): p. 7133-55.

156. Dragan, A.I., C.M. Read, and C. Crane-Robinson, *Enthalpy-entropy compensation: the role of solvation.* Eur Biophys J, 2017. **46**(4): p. 301-308.

157. Tzeng, S.R. and C.G. Kalodimos, *Dynamic activation of an allosteric regulatory protein.* Nature, 2009. **462**(7271): p. 368-72.

158. Tzeng, S.R. and C.G. Kalodimos, *Protein activity regulation by conformational entropy.* Nature, 2012. **488**(7410): p. 236-40.

159. Caro, J.A., et al., *Entropy in molecular recognition by proteins.* Proc Natl Acad Sci U S A, 2017. **114**(25): p. 6563-6568.

160. Frederick, K.K., et al., *Conformational entropy in molecular recognition by proteins.* Nature, 2007. **448**(7151): p. 325-9.

161. Bacle, A., et al., *Inverse Conformational Selection in Lipid-Protein Binding.* J Am Chem Soc, 2021. **143**(34): p. 13701-13709.

162. O'Brien, E.S., et al., *Membrane Proteins Have Distinct Fast Internal Motion and Residual Conformational Entropy.* Angewandte Chemie International Edition, 2020. **59**(27): p. 11108-11114.

APPENDIX A

FIGURES

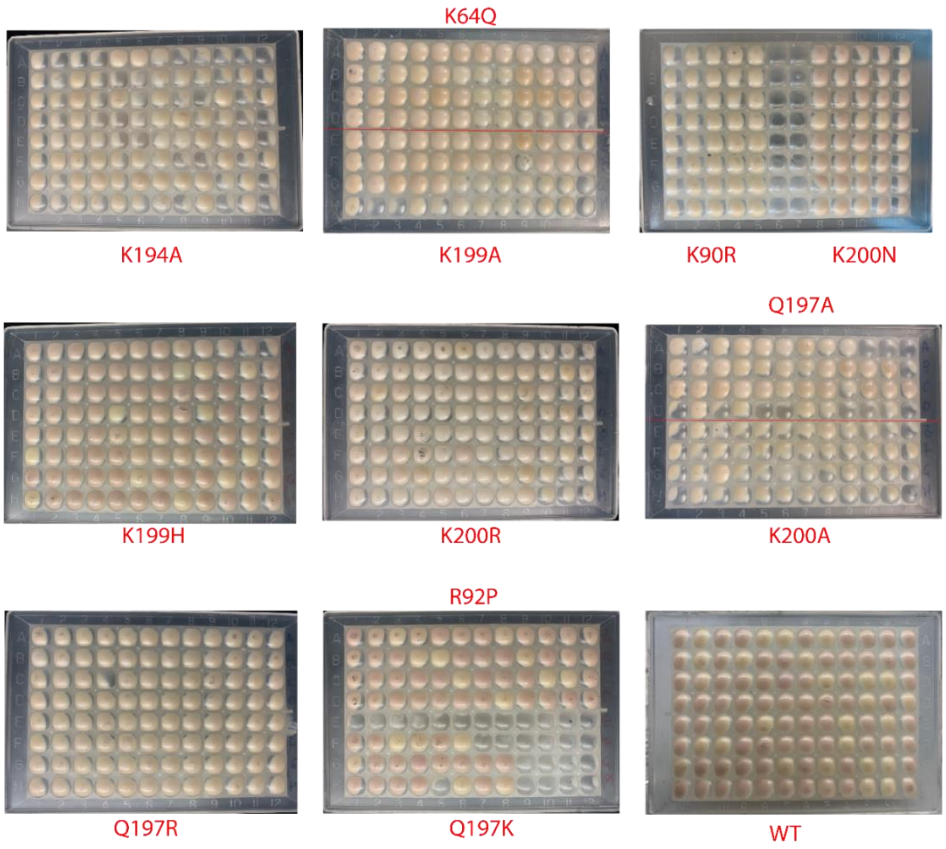

Figure 1 High-throughput expression screen of *Pichia* transformants.

Shown are photographs of pelleted cells in 96 deep well blocks after expression for two days. The mCherry fusion protein results in cell pellets red in color. The variation in protein expression observed here is commonly observed and previously reported.

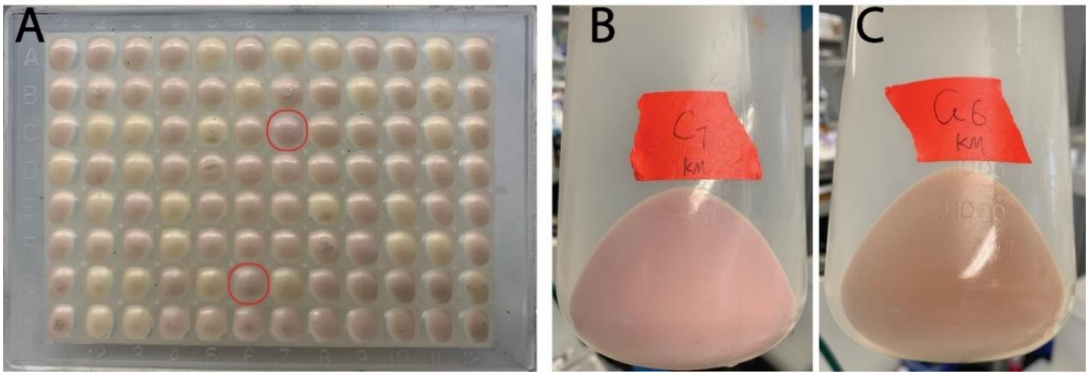

Figure 2 Identification and scale-up of well expressing Pichia transformants.

A) Photograph of screening block for Kir3.2 showing variations in protein expression. Red circles denote two candidates (C7 and G6) selected for scale up expression. B-C) Photograph of cell pellets from large-scale expression (4 L) of C7 and G6.

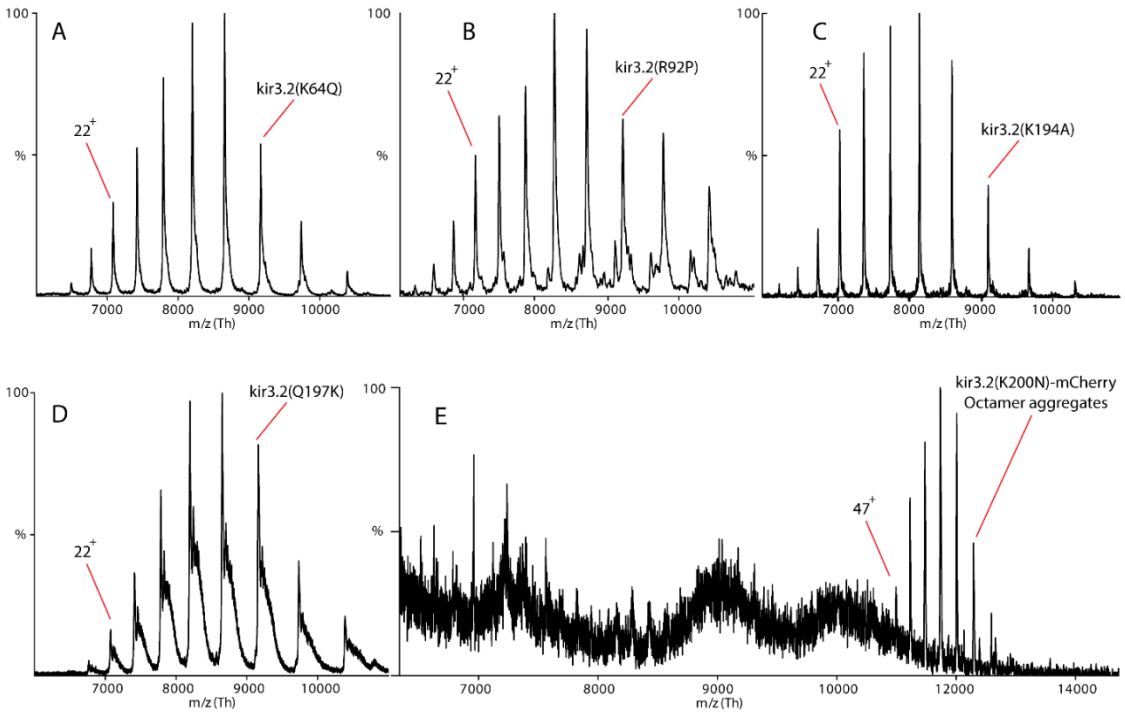

Figure 3 Native mass spectra of purified Kir3.2 mutants after delipidation with DHPC. The Kir3.2 mutant is labeled within each spectrum along with assignment of charge state. The mutant Kir3.2(K200N) has a resolved charge state distribution for an octameric assemble, which we suspect is an aggregate.

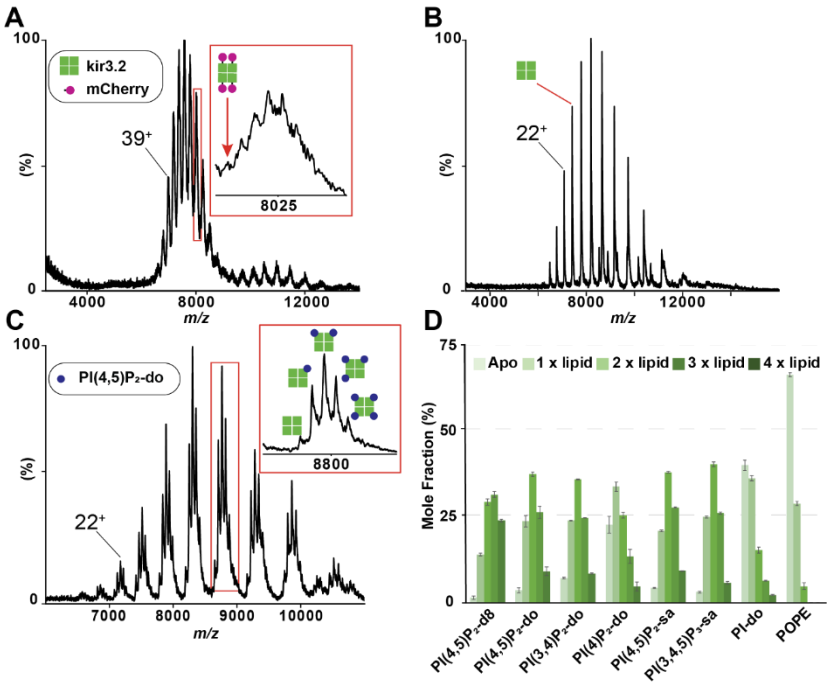

Figure 4 Biophysical characterization of mouse Kir3.2-lipid interactions using native mass spectrometry (MS).

A) Representative native mass spectrum of the Kir3.2-mCherry fusion protein purified only in DDM. Mass spectral peak broadness indicates an impure, heterogenous sample stemming from co-purified contaminants. In the inset, the red arrow denotes the peak corresponding to the apo tetramer. B) Native mass spectrum of Kir3.2 devoid of contaminants solubilized in 2x critical micelle concentration (CMC) of $C_{10}E_5$ detergent . C) Mass spectrum of Kir3.2 (500 nM final concentration) mixed with 3.3 molar equivalents of PI(4,5)P_2-sa in $C_{10}E_5$ detergent. Inset is a zoom of the 18^+ charge state and individual lipid binding events are labeled. D) Plot of mole fraction data obtained from deconvoluting mass spectra of Kir3.2 in the presence of different lipids at a molar ratio of 3.3:1, respectively. Reported are the average and s.e.m. (n = 3).

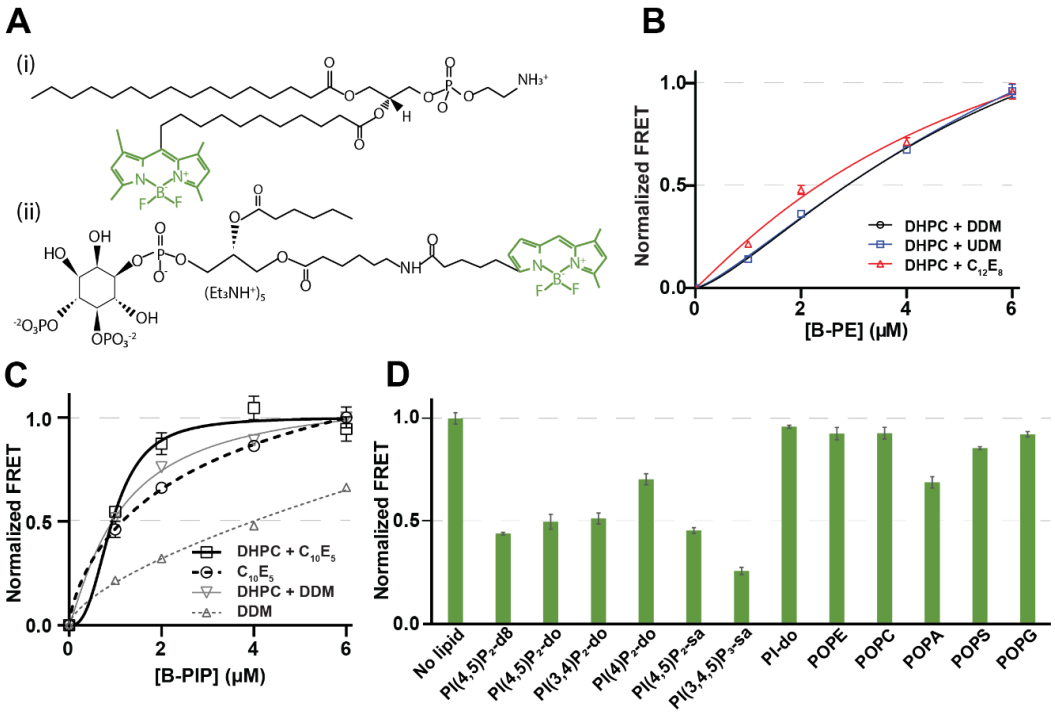

Figure 5 Kir3.2-lipid interactions characterized by solution FRET-based lipid binding assays.

A) Structures of green colored donor lipids: (i) BODIY-PE (B-PE) and (ii) BODIPY-PI(4,5)P_2 (B-PI(4,5)P_2). B) Plot of normalized FRET signals for B-PE binding Kir3.2-mCherry samples (500 nM) devoid of contaminants in different detergents. The Hill equation (solid lines) was fit to the experimental data (dots). C) Plot of normalized FRET signals for B-PI(4,5)P_2 binding Kir3.2-mCherry (500 nM) before and after removal of contaminant with 1,2-dihepanoyl-sn-glycero-3-phosphocholine (DHPC) in either $C_{10}E_5$ or DDM. The altered binding curves for contaminated Kir3.2-mCherry samples underscore the importance of pure samples. D) Competition of pure Kir3.2-mCherry samples binding to B-PI(4,5)P_2 (4 μM) in the presence of two equivalents of lipid.

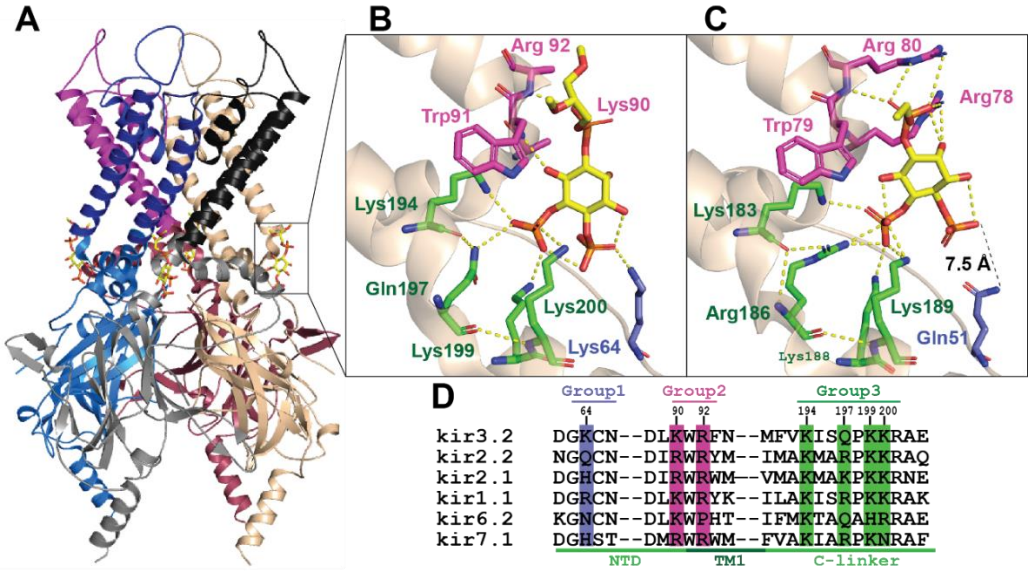

Figure 6 Details of the molecular interaction of PI(4,5)P2-d8 with Kir2.2 and Kir3.2.

A) Cartoon representation of tetrameric mouse Kir3.2 (PDB 3SYA). PI(4,5)P_2-d8 is shown in stick representation. B-C) Details of the atomic interaction between mouse Kir3.2 (panel B) or chicken Kir2.2 (panel C, PDB 5KUM) bound to PI(4,5)P_2-d8. Residues that interact with the lipid are colored by group in panel D. D) Multiple sequence alignment for a subset of Kir subfamily members. Color scheme of groups correspond with that of panels B and C.

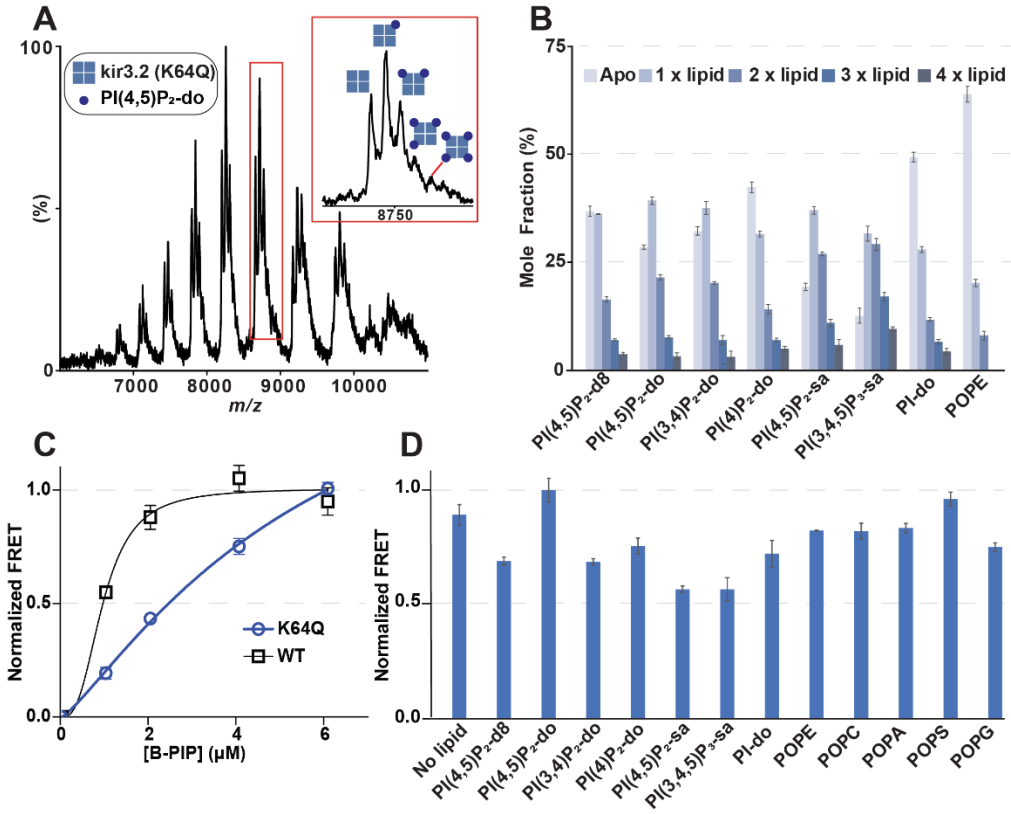

Figure 7 Kir3.2^{K64Q} characterized by native MS and FRET-based lipid binding assays uncover a preference toward acyl chains.

A) Representative mass spectrum of Kir3.2^{K64Q} in the presence of PI(4,5)P_2-do at a 10:3 molar ratio, respectively. B) Plot of mole fraction data obtained from deconvoluting mass spectra for various lipids mixed with Kir3.2^{K64Q}. C) Binding curve for B-PI(4,5)P_2 interacting with Kir3.2^{K64Q} in the $C_{10}E_5$ detergent (blue). For reference, data for Kir3.2 binding B-PI(4,5)P_2 is shown (black). D) Competition of bound B-PI(4,5)P_2 (4 μM) to Kir3.2^{K64Q} by the addition of phospholipids (8 μM).

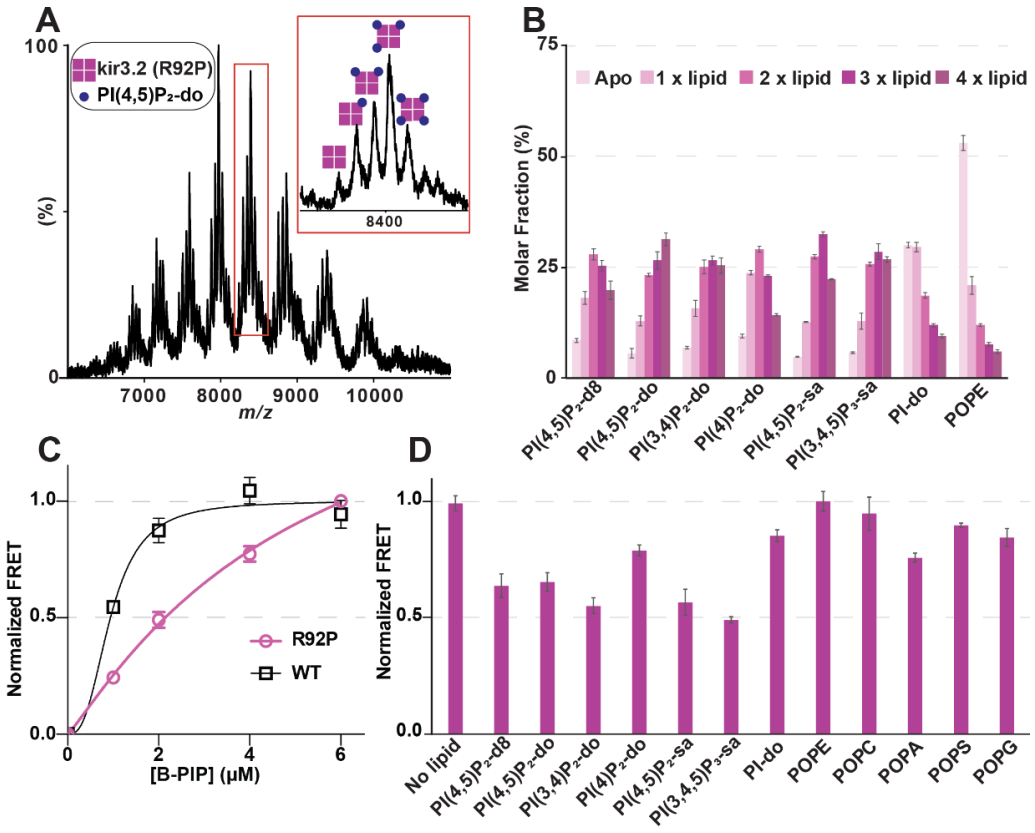

Figure 8 Native MS and FRET assay reveal Kir3.2^{R92P} non-selective binding to PIPs.

A) Representative mass spectrum of Kir3.2^{R92P} in the presence of PI(4,5)P_2-do at a 10:3 molar ratio, respectively. B) Plot of mole fraction data obtained from deconvoluting mass spectra for Kir3.2^{R92P} in the presence of different lipids. C) Binding curve for B-PI(4,5)P_2 interacting with Kir3.2^{R92P} in the $C_{10}E_5$ detergent (purple). Binding for B-PI(4,5)P_2 to Kir3.2 is shown as described in Figure 4. D) Competition of bound B-PI(4,5)P_2 to Kir3.2^{R92P} by the addition of two equivalents of phospholipids.

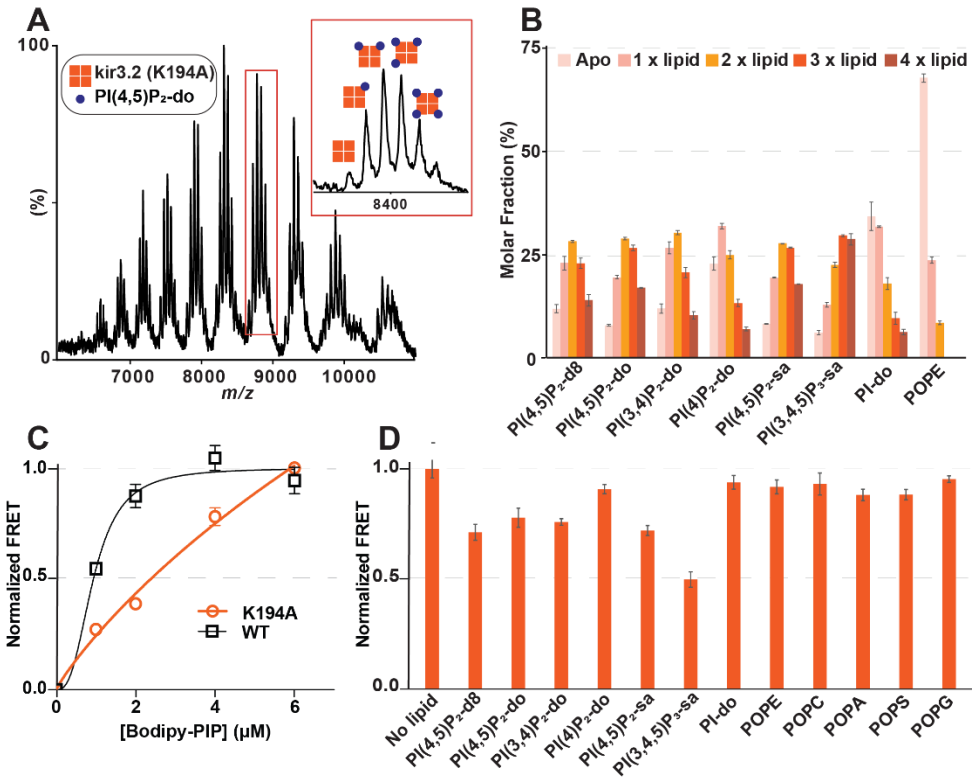

Figure 9 Native MS and FRET-based lipid binding assays of Kir3.2^{K194A}-lipid interactions. A) Representative mass spectrum of Kir3.2^{K194A} in the presence of PI(4,5)P_2-do at a 10:3 molar ratio, respectively. B) Plot of mole fraction data obtained from deconvoluting mass spectra for Kir3.2^{K194A} in the presence of different lipids. C) Binding curve for B-PI(4,5)P_2 interacting with Kir3.2^{K194A} in the $C_{10}E_5$ detergent (orange). Binding for B-PI(4,5)P_2 to Kir3.2 is shown as described in Figure 4. D) Competition of bound B-PI(4,5)P_2 to Kir3.2^{K194A} by the addition of two equivalents of phospholipids.

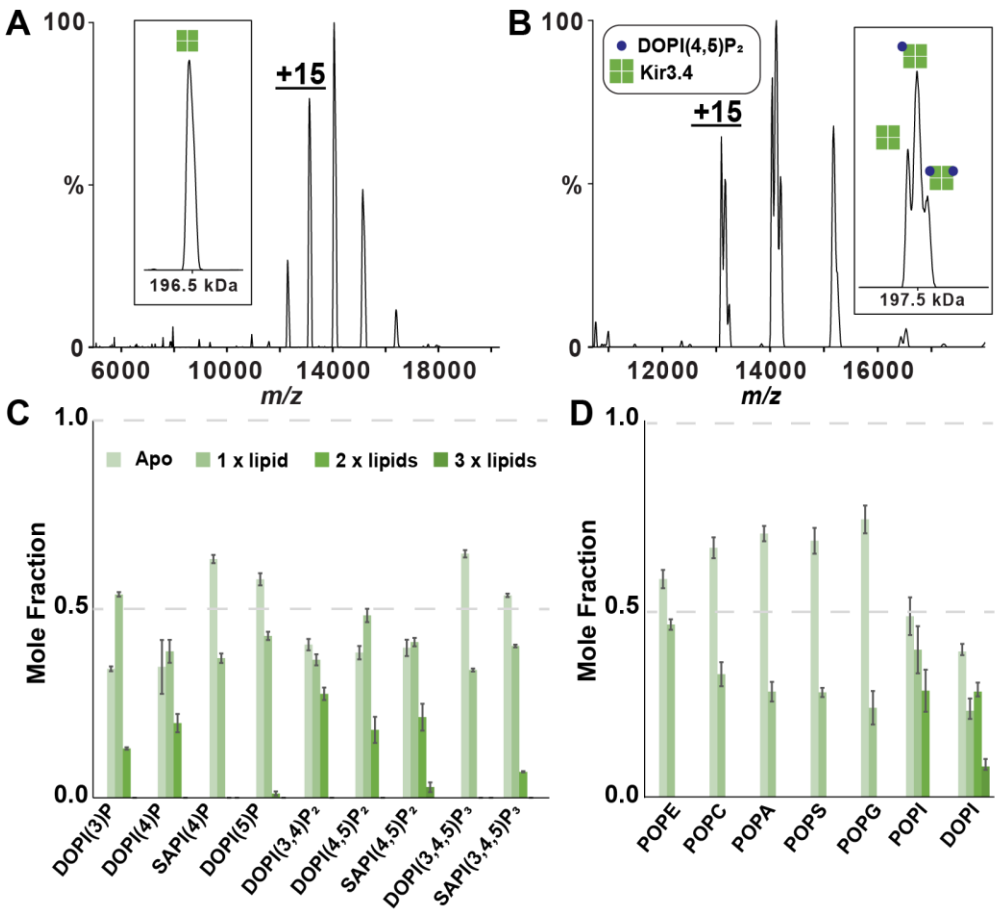

Figure 10 Biophysical characterization of Kir3.4-lipid interactions.

A) Representative native mass spectrum of optimized Kir3.4 samples solubilized in the $C_{10}E_5$ detergent. The deconvoluted mass spectrum is shown in the inset. B) Mass spectrum of 0.5 μM Kir3.4 mixed with 5 μM DOPI(4,5)P_2. Deconvolution of the mass spectrum is shown in the inset. C-D) Plot of mole fraction for individual binding events from deconvoluted native mass spectra of Kir3.4 in the presence of 10-fold molar excess of (C) PIPs and (D) phospholipids. Reported are the average and s.e.m. (n=3).

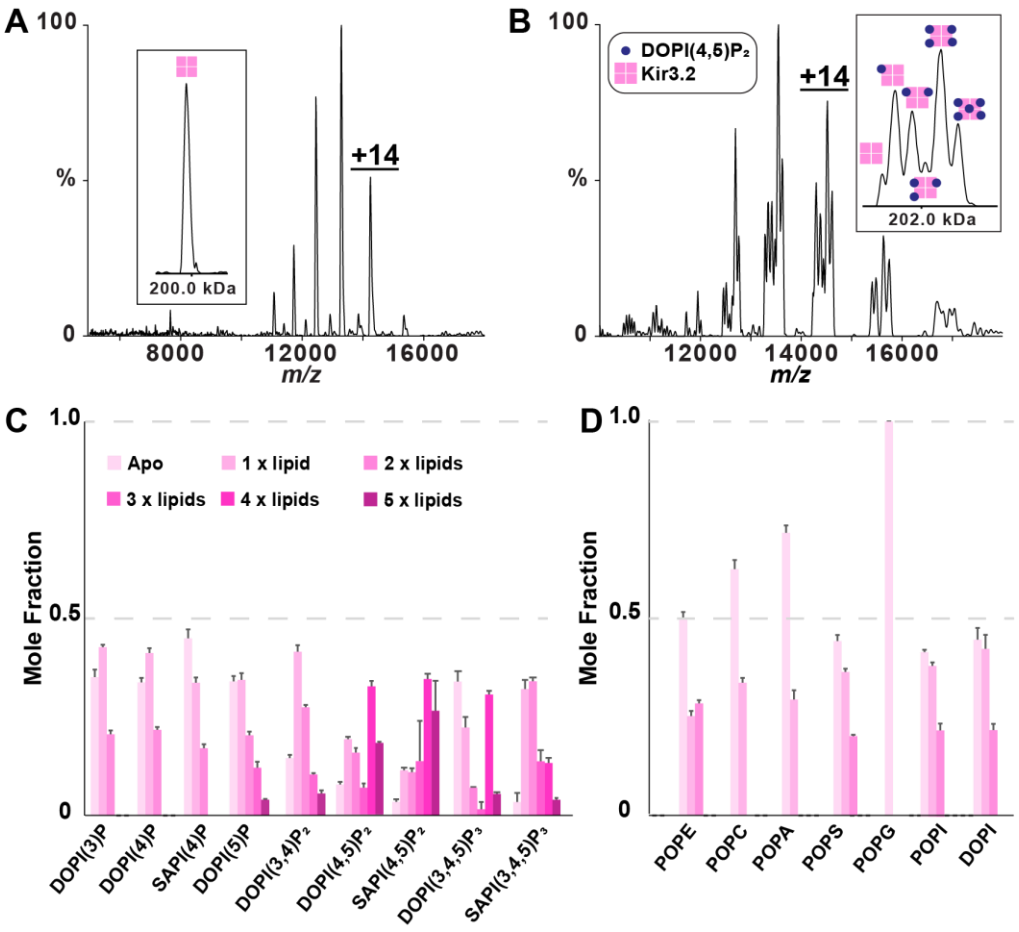

Figure 11 Native MS of human Kir3.2 in complex with phospholipids.

A) Representative native mass spectrum of Kir3.2 samples optimized for native MS. Shown as described in Figure 1. B) Mass spectrum of a mixture containing 0.5 μM Kir3.2 and 5 μM DOPI(4,5)P_2. The deconvoluted mass spectrum is shown in the inset. C-D) Plot of mole fraction for individual binding events from deconvoluted native mass spectra of Kir3.2 in the presence of 10-fold molar excess of (C) PIPs and (D) phospholipids. Reported are the average and s.e.m. (*n*=3).

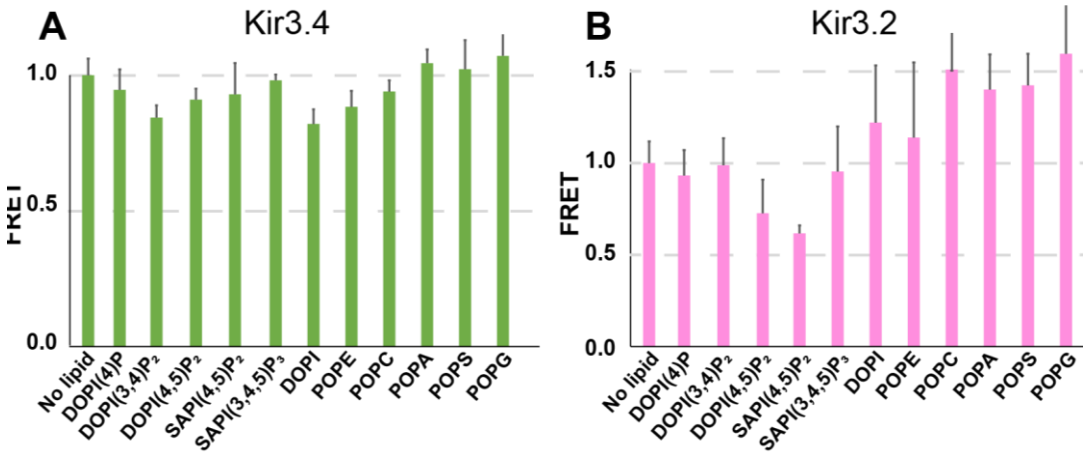

Figure 12 Kir3.4 and Kir3.2 fluorescent lipid binding and competition assays. Competition of 0.5 μM (A) Kir3.4-mCherry and (B) Kir3.2-mCherry binding to B-PIP (4 μM) in the presence of 8 μM phospholipid. Lipid abbreviations are provided in Table 5. Reported are the average and s.e.m. (*n*=3).

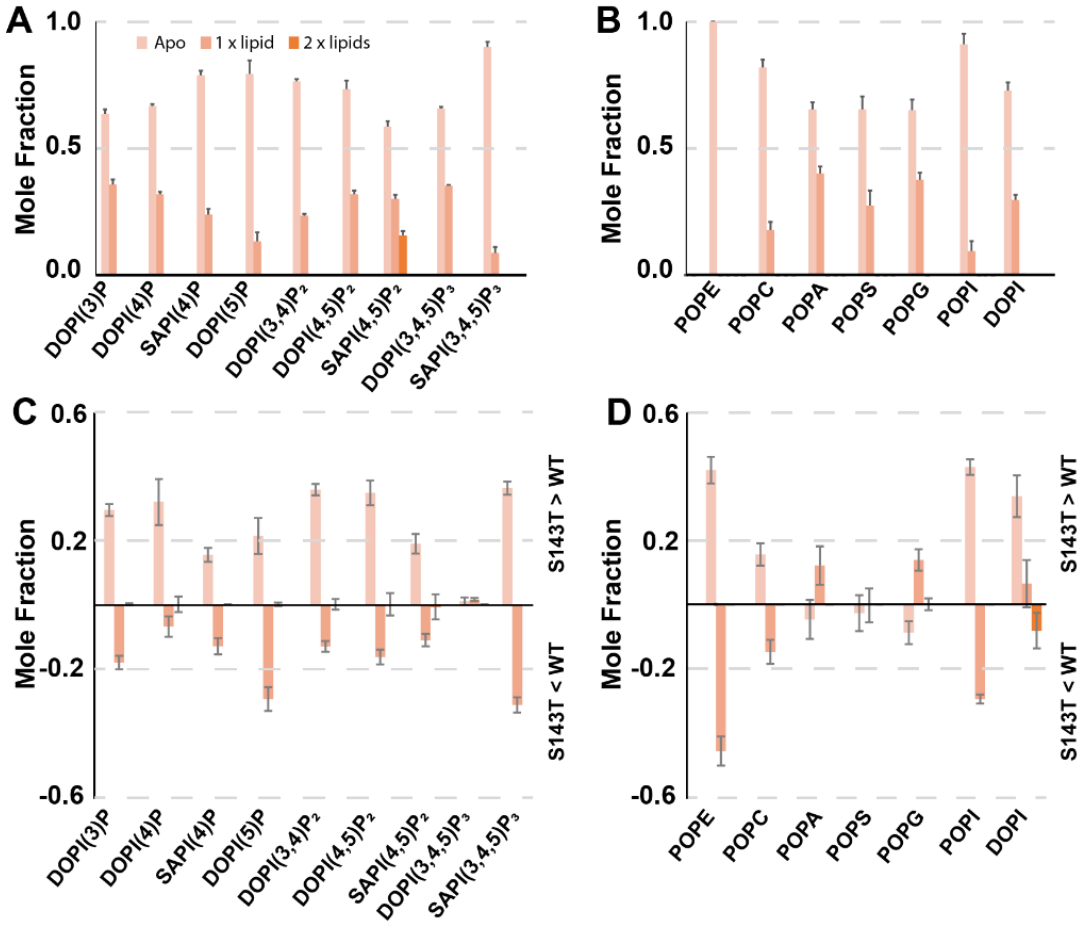

Figure 13 Kir3.4^{S143T} lipid interactions characterized by native MS.

A-B) Plot of mole fraction for of apo and lipid bound states of Kir3.4^{S143T} determined from the deconvoluted native mass spectra. Kir3.4^{S143T} was mixed with a 10-fold molar excess of (A) PIPs and (B) lipids. C-D) Plot of the difference in mole fraction of (C) PIPs and (D) lipids bound to Kir3.4^{S143T} from Kir3.4. Positive values indicate a higher mole fraction of the particular state for Kir3.4^{S143T}. Reported are the average and s.e.m. (*n*=3).

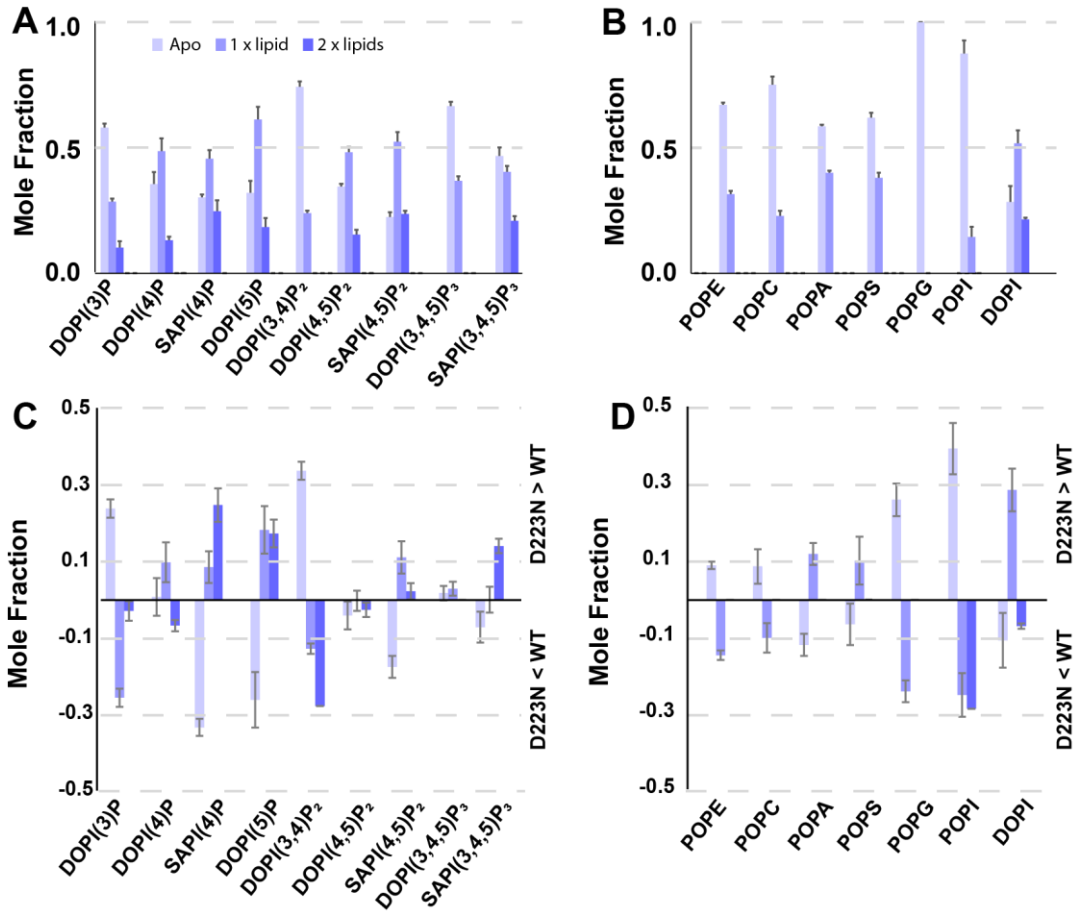

Figure 14 Native MS reveals Kir3.4^{D223N} enhanced binding to PIPs.

A-B) Plot of mole fraction for of apo and lipid-bound states of Kir3.4^{D223N} determined from the deconvoluted native mass spectra. Kir3.4^{D223N} was mixed with a 10-fold molar excess of (A) PIPs and (B) lipids. C-D) Plot of the difference in mole fraction of (C) PIPs and (D) lipids bound to Kir3.4^{D223N} from Kir3.4. Negative values indicate a higher mole fraction of the particular state for Kir3.4^{WT}. Reported are the average and s.e.m. (n=3).

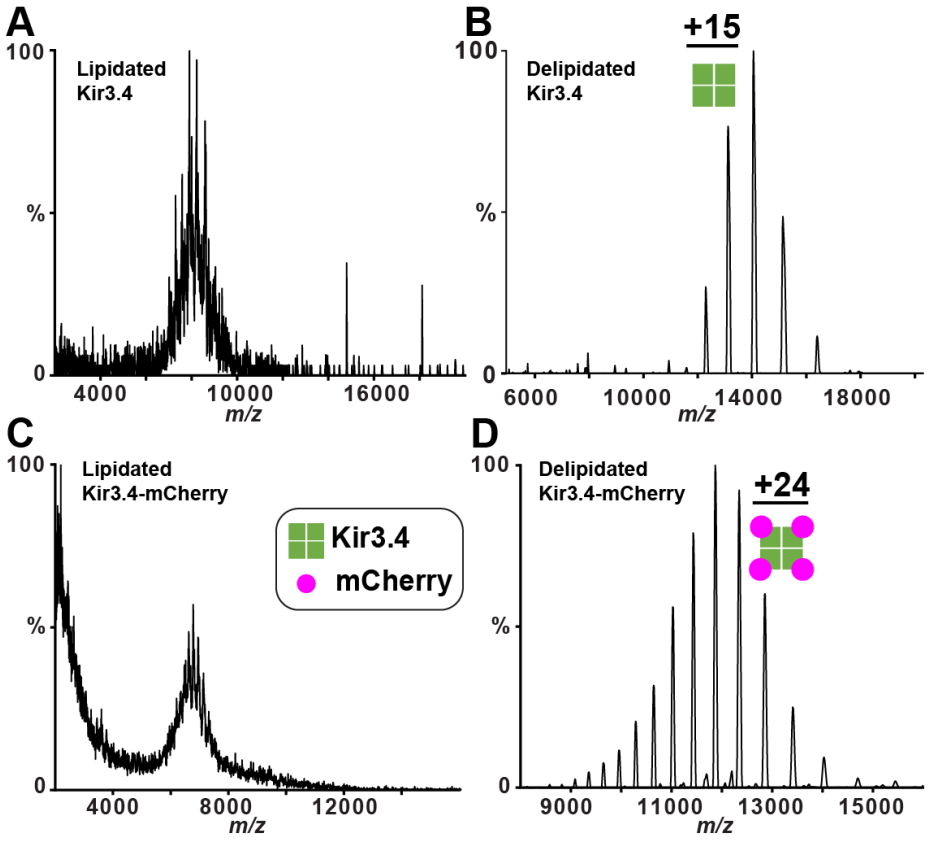

Figure 15 Biophysical characterization of full-length human Kir3.4 channels before and after delipidation.

A) Representative native mass spectrum of Kir3.4 before delipidation. B) Representative native mass spectrum of Kir3.4 after delipidation. C) Representative native mass spectrum of Kir3.4-mCherry fusion protein before delipidation. D) Representative native mass spectrum of Kir3.4-mCherry fusion protein after delipidation.

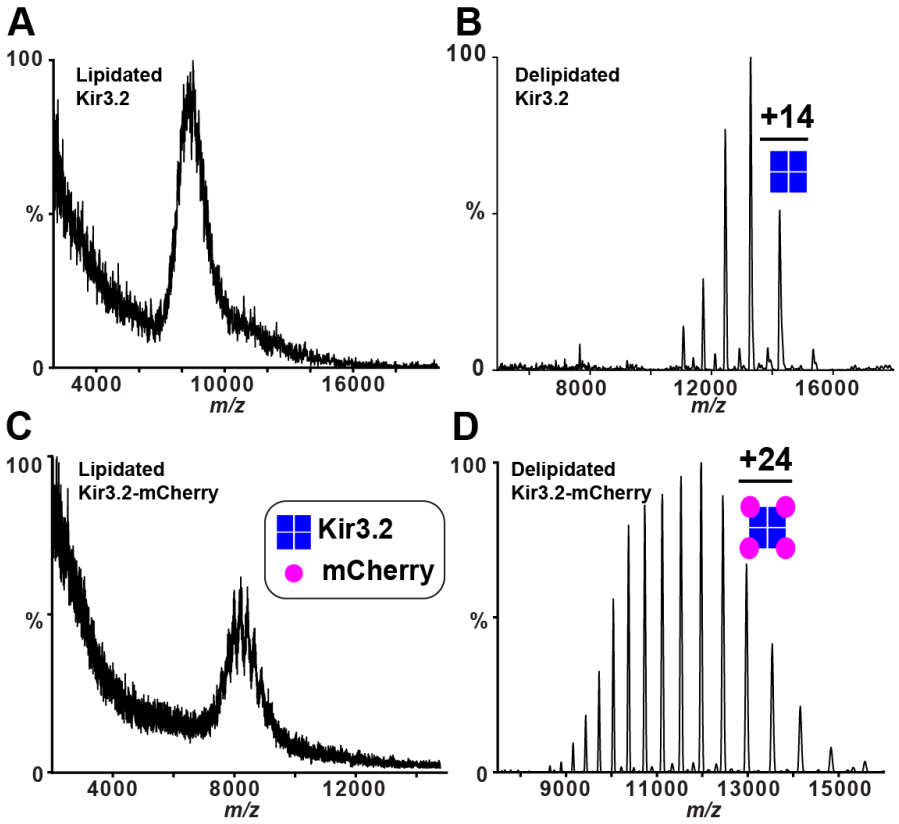

Figure 16 Biophysical characterization of full-length human Kir3.2 channels before and after delipidation.

A) Representative native mass spectrum of Kir3.2 before delipidation. B) Representative native mass spectrum of Kir3.2 after delipidation. C) Representative native mass spectrum of Kir3.2-mCherry fusion protein before delipidation. D) Representative native mass spectrum of Kir3.2-mCherry fusion protein after delipidation.

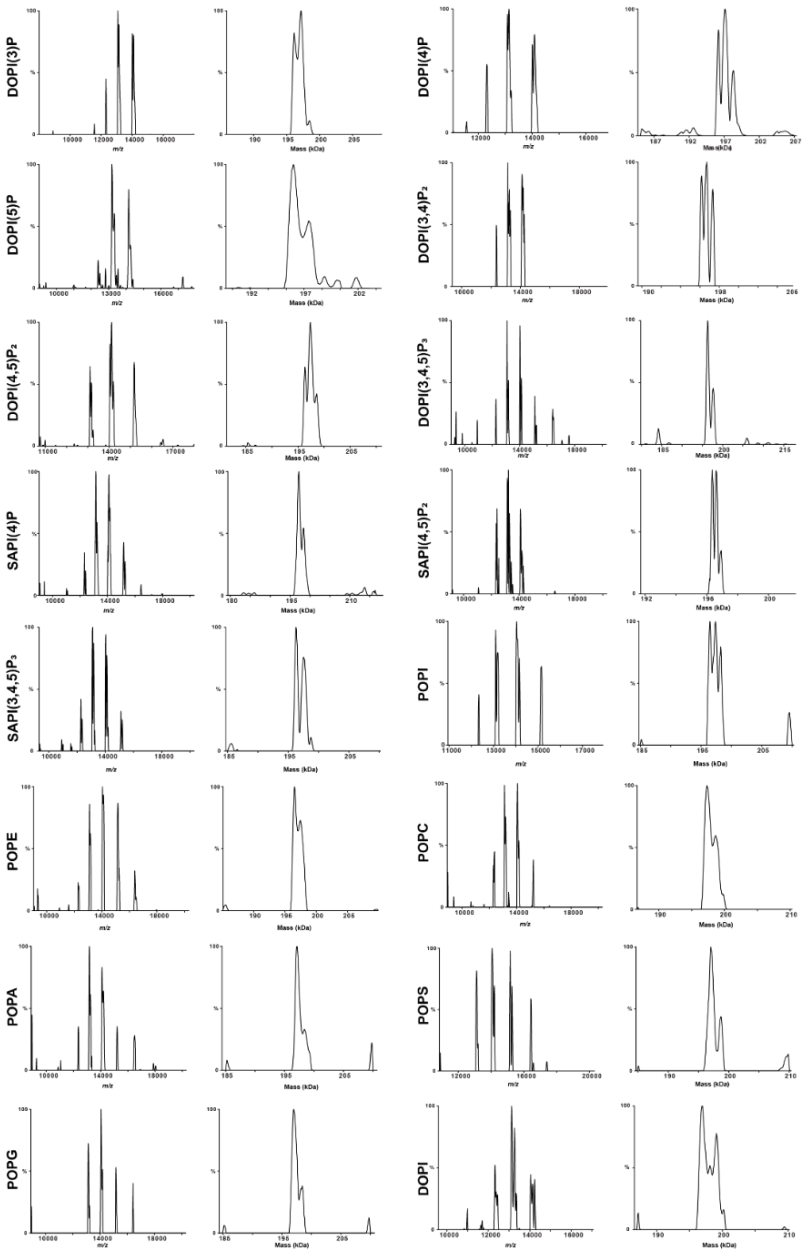

Figure 17 Native mass spectra for Kir3.4 with lipids.

Shown are representative native mass spectra for Kir3.4^{WT} in the presence of lipids (molar ratio 1:10). The native mass spectra are shown in the left panel with deconvolution shown in the right panel.

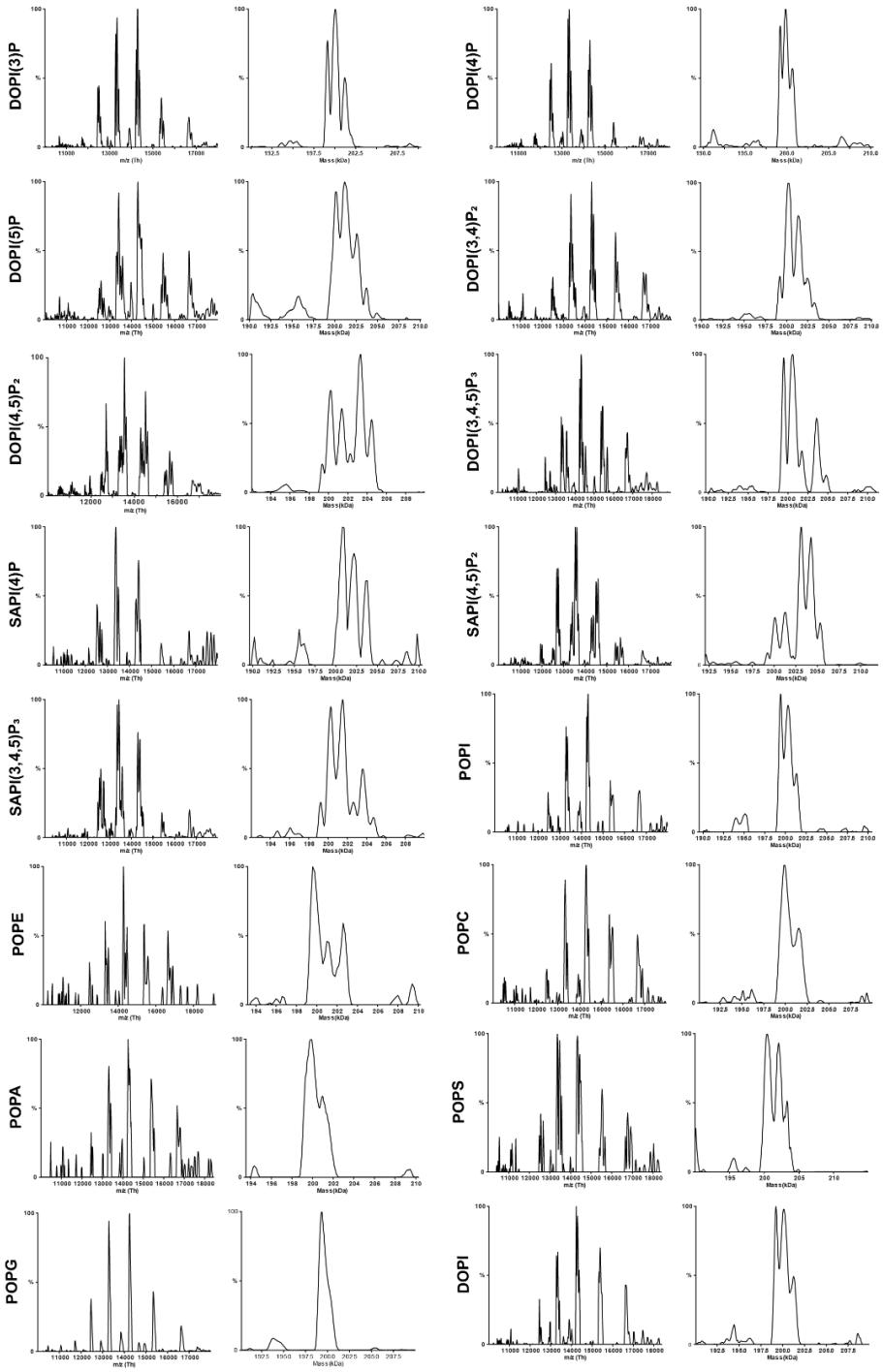

Figure 18 Native mass spectra for Kir3.2 with lipids.

Shown as described in Figure 17.

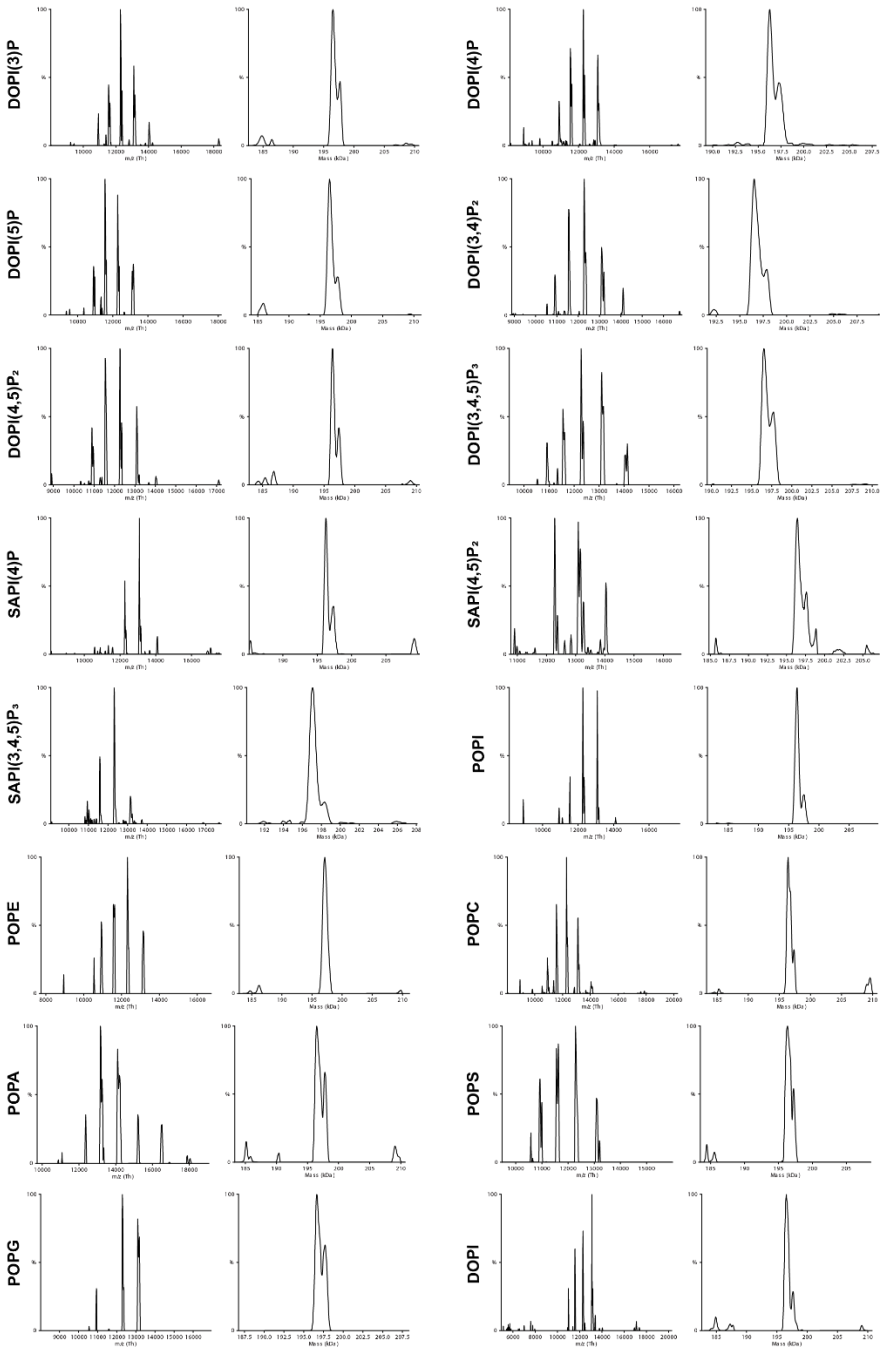

Figure 19 Native mass spectra for Kir3.4^{S143T} with lipids.

Shown as described in Figure 17.

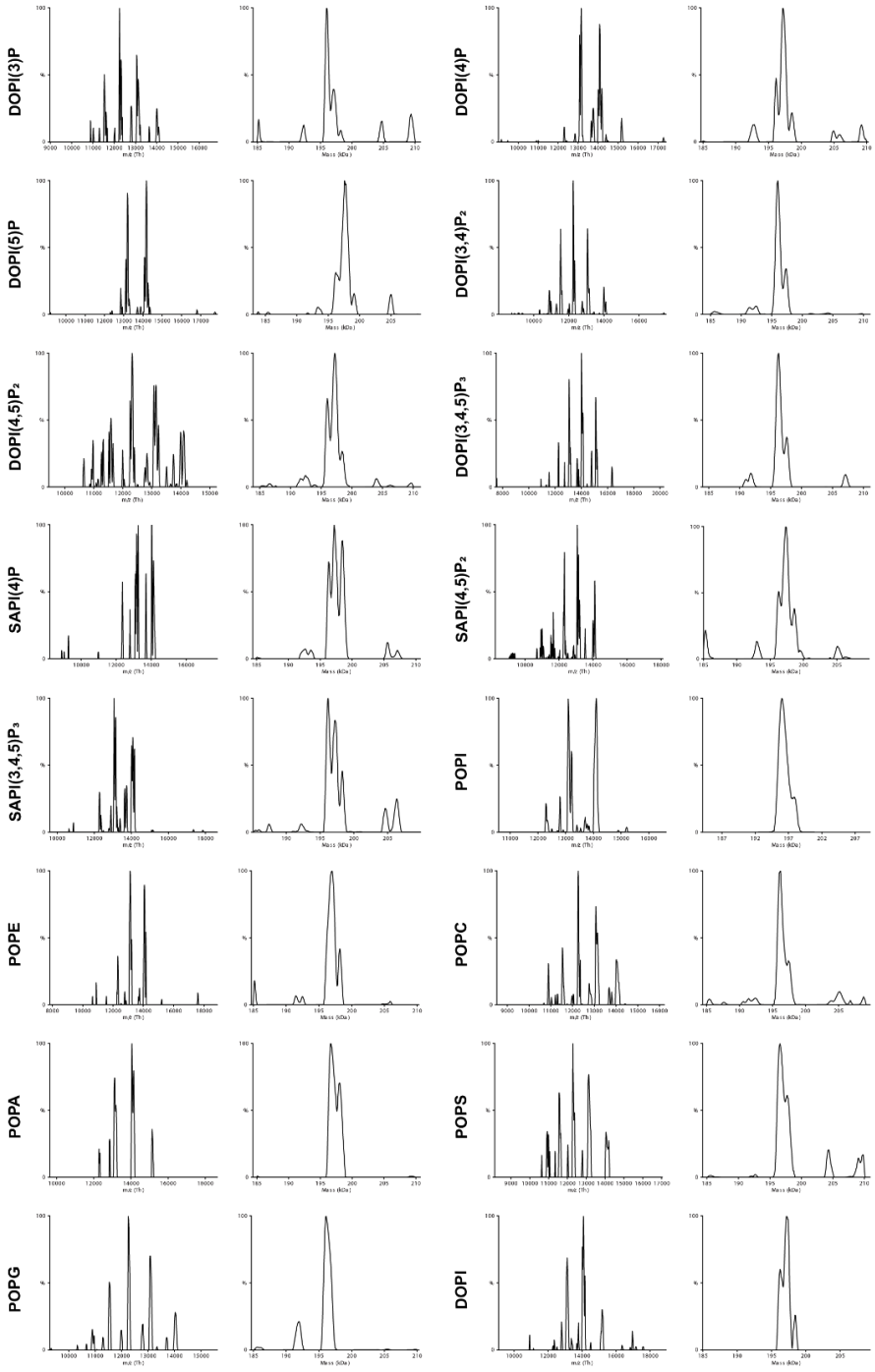

Figure 20 Native mass spectra for Kir3.4^{D223N} with lipids.

Shown as described in Figure 17.

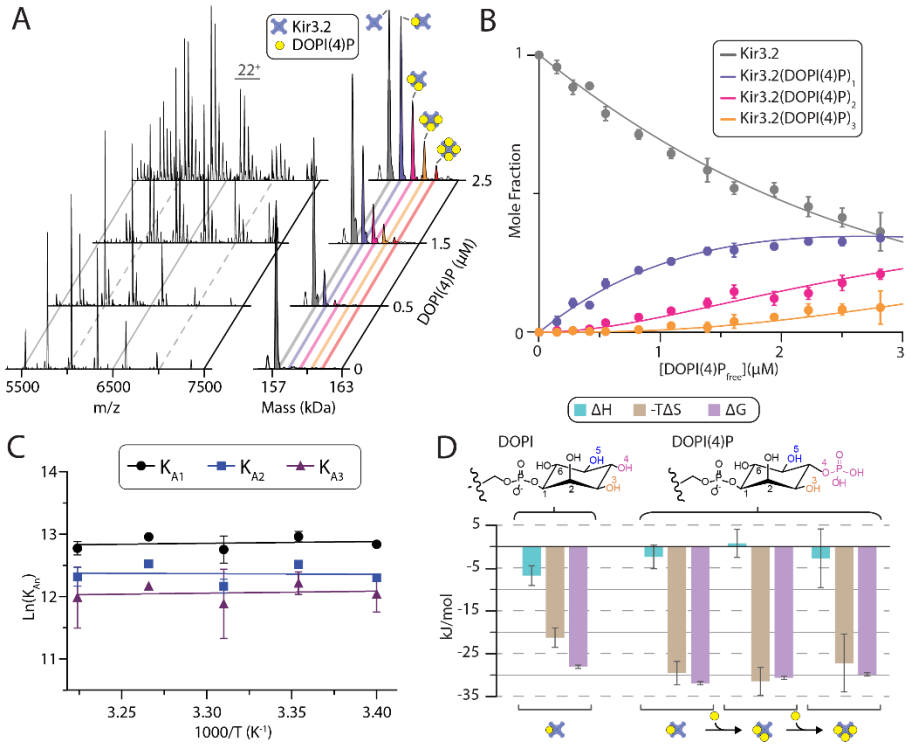

Figure 21 Determination of binding thermodynamics for Kir3.2-lipid interactions.

A) Representative native mass spectra and their deconvoluted from a titration series of Kir3.2 with DOPI(4)P recorded at 298 K. B) Plot of the mole fraction for Kir3.2 and Kir3.2•DOPI(4)$P_{1\text{-}3}$ bound states of Kir3.2 determined from a titration series and resulting fit (R^2 = 0.99) of a sequential lipid binding model (lines). C) van't Hoff plot for Kir3.2 binding Kir3.2•DOPI(4)$P_{1\text{-}3}$ (dots) and regression of linear equations (solid lines) to deduce thermodynamics for each lipid binding event. D) Thermodynamics of DOPI(4)P and DOPI binding Kir3.2 at 298 K. The first, second, and third lipid (labeled as 1x−3x) is shown for DOPI(4)P. Reported are the average and s.e.m. from repeated measurements (n = 3).

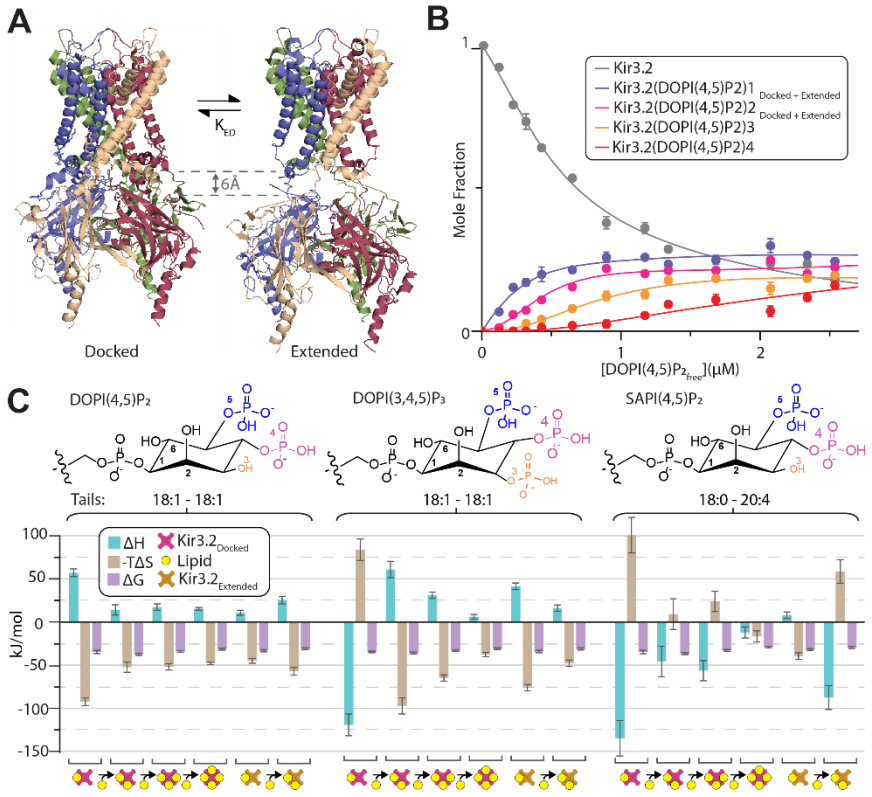

Figure 22 Thermodynamic signatures of specific phosphoinositides binding to different states of Kir3.2.

A) Structures of Kir2.2 in the docked (PDB 3SPI) and extended states (PDB 3JYC) shown in cartoon representation. B) Plot of the mole fraction of Kir3.2 and the channel bound to PI(4,5)P_2 with DO tails (DOPI(4,5)P_2). Resulting fit (solid lines, R^2 = 0.99) of lipid binding model where the lipid can bind to either the docked or extended states of Kir3.2. C) Binding thermodynamics for DOPI(4,5)P_2, DOPI(3,4,5)P_3, and SAPI(4,5)P_2 to Kir3.2 determined through van't Hoff analysis for binding to the docked and extended states at 298 K. Reported are the average and s.e.m. from repeated measurements (n = 3).

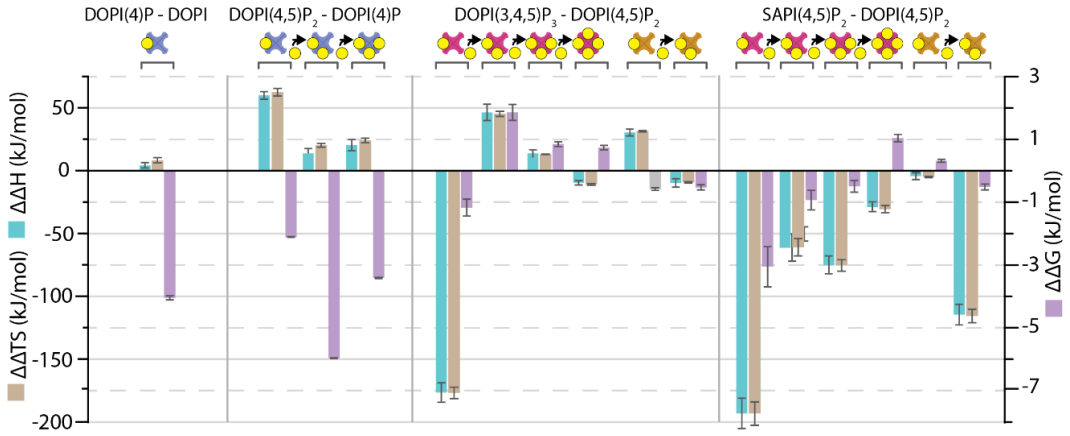

Figure 23 Alterations in thermodynamic signatures for a stepwise transition from DOPI to DOPI(3,4,5)P_3 and acyl chain chemistry of PI(4,5)P_2.

The delta values were calculated for example as DOI(4)P – DOPI, and a temperature of 298K was used. Reported are the average and s.e.m. (n=3).

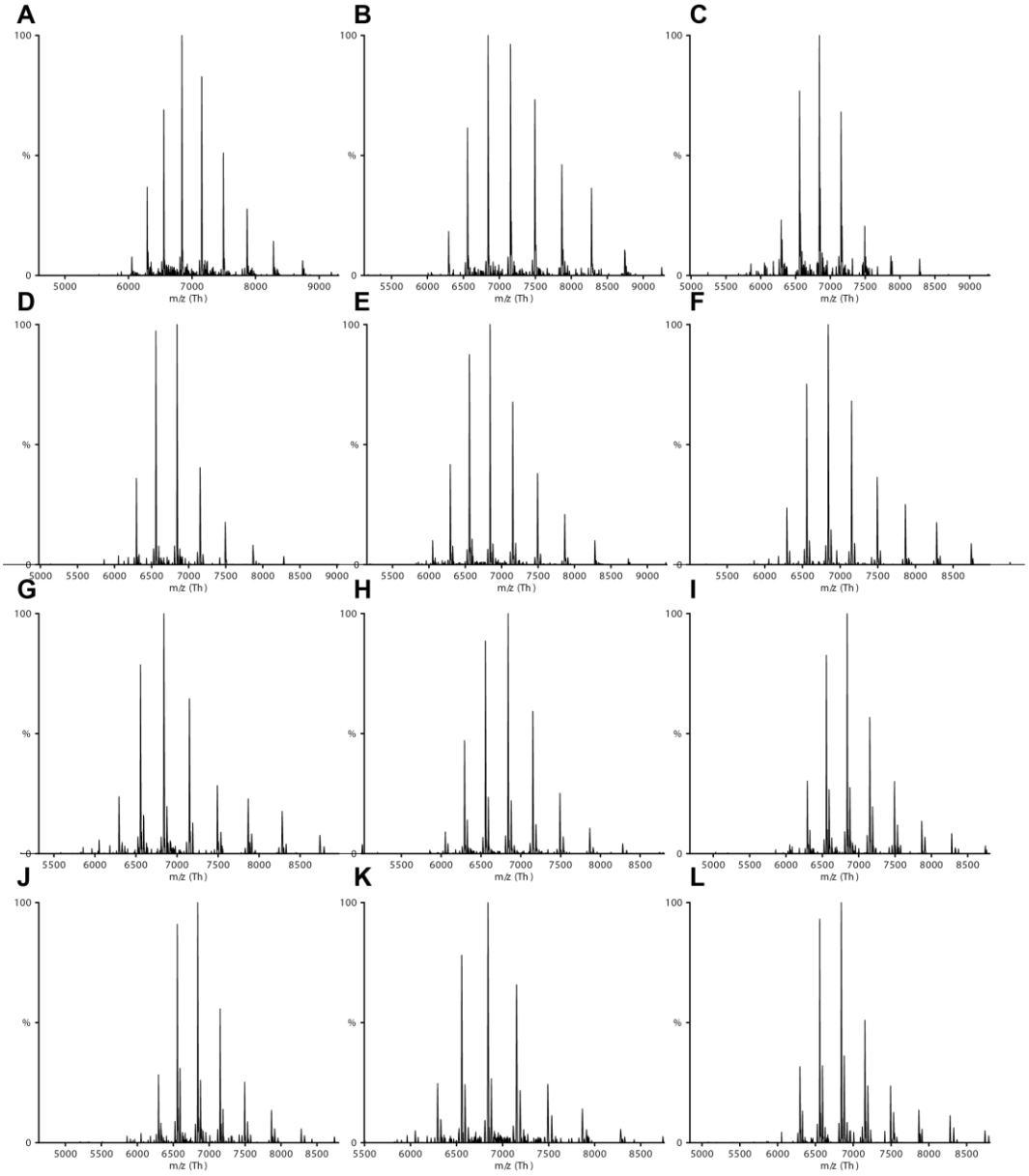

Figure 24 Native mass spectra of Kir3.2 with DOPI from one of the titration series. Kir3.2 (0.25 μM) was mixed with DOPI at a concentration of A) 0.125 μM, B) 0.25 μM, C) 0.375 μM, D) 0.5 μM, E) 0.75 μM, F) 1 μM, G) 1.25 μM, H) 1.5 μM, I) 1.75 μM, J) 2 μM, K) 2.25 μM, and L) 2.5 uM.

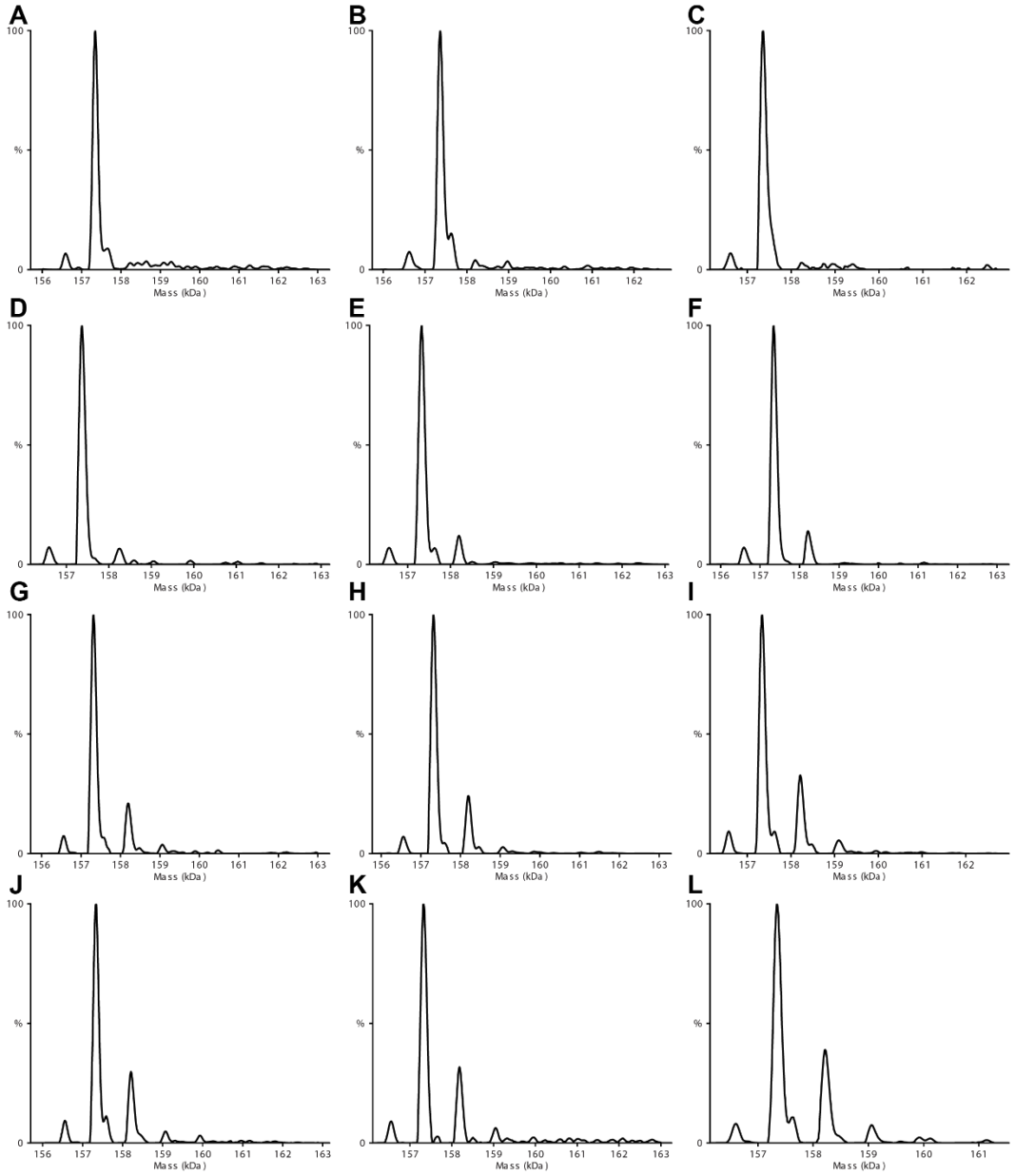

Figure 25 Deconvoluted native mass spectra of Kir3.2 with DOPI.

The panels match the concentrations reported in figure 24.

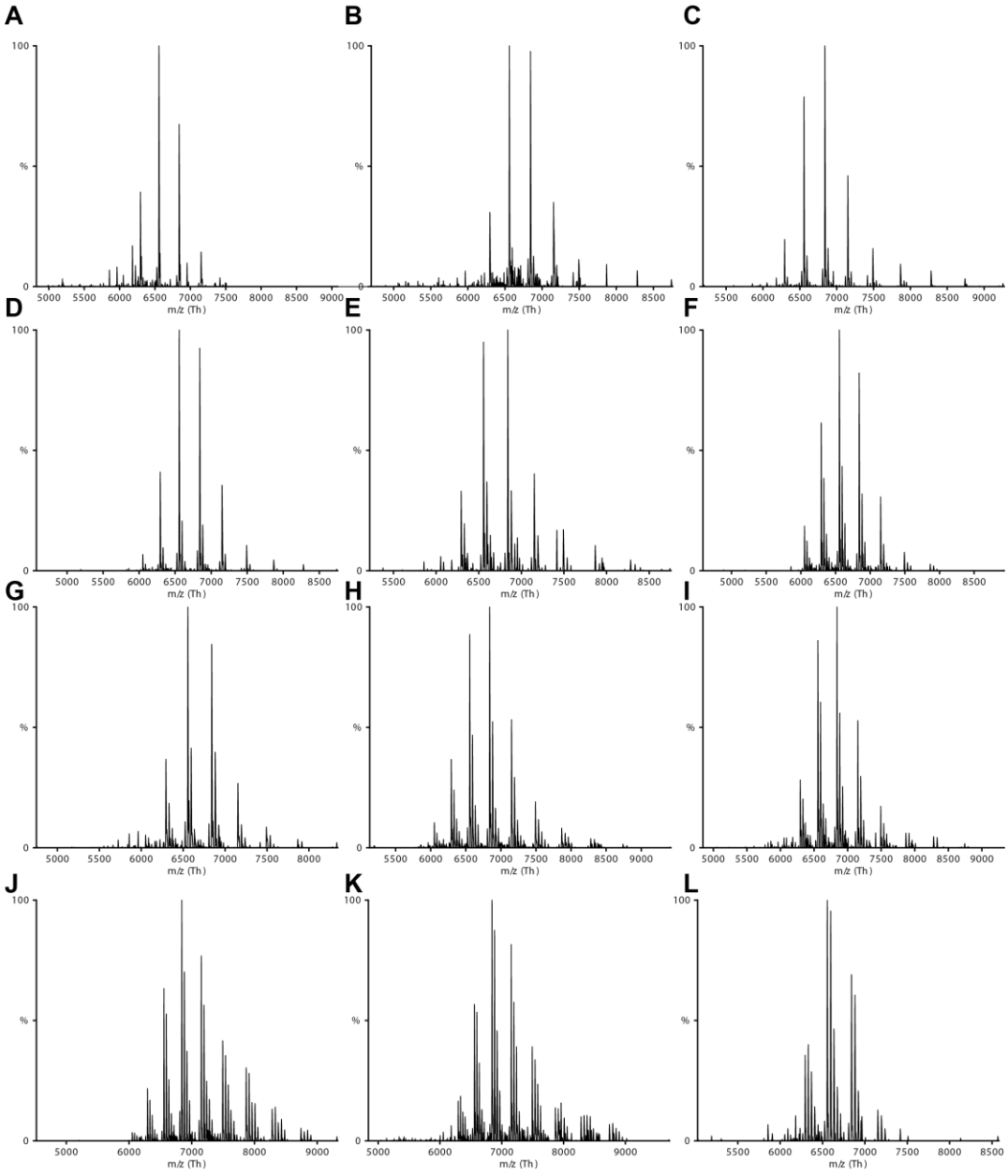

Figure 26 Representative native mass spectra of Kir3.2 with DOPI(4)P.

Kir3.2 was titrated by DOPI(4)P under the same conditions as described for DOPI in figure 24.

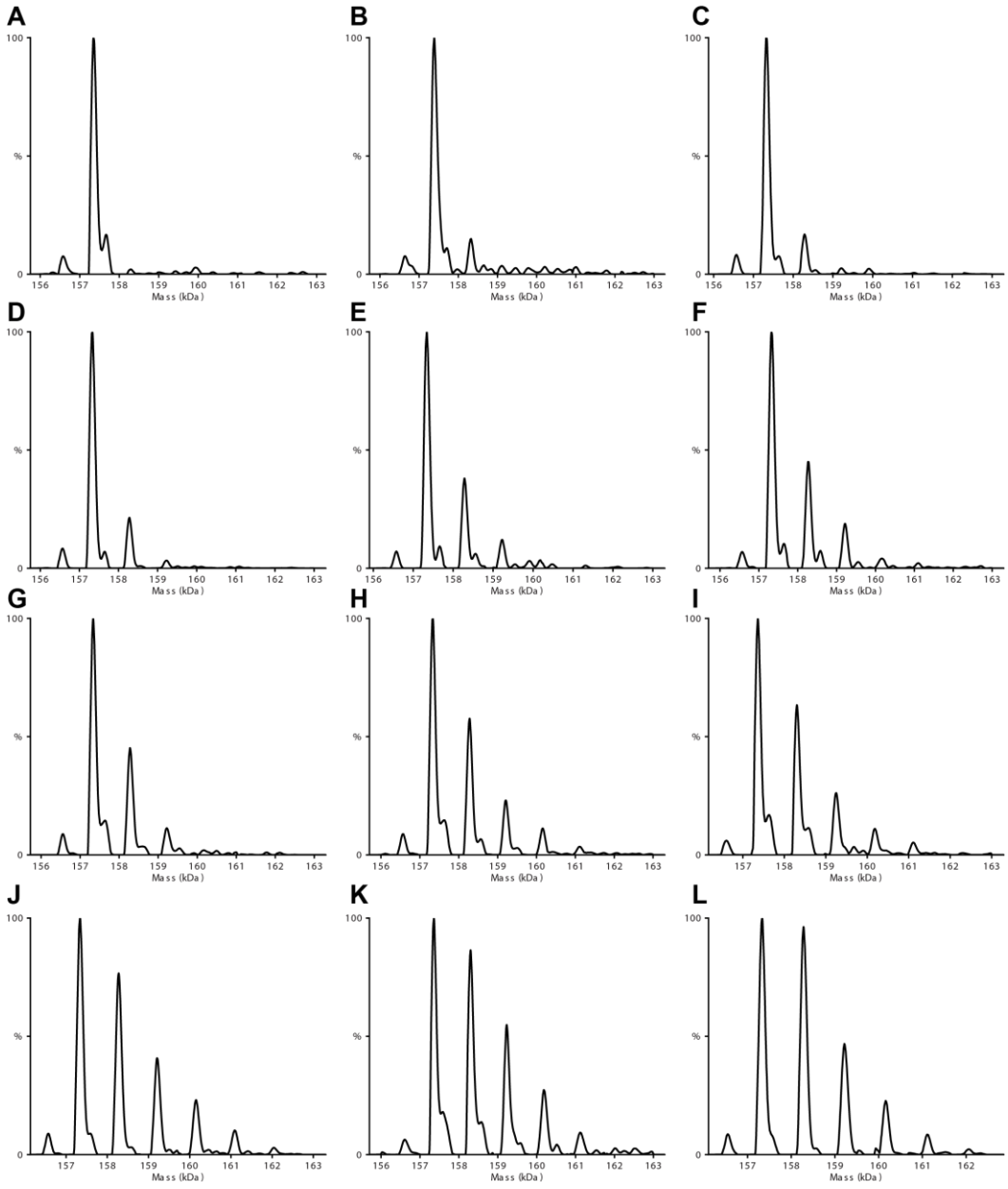

Figure 27 Deconvoluted native mass spectra of Kir3.2 with DOPI(4)P.

The panels match the concentrations reported in figure 24.

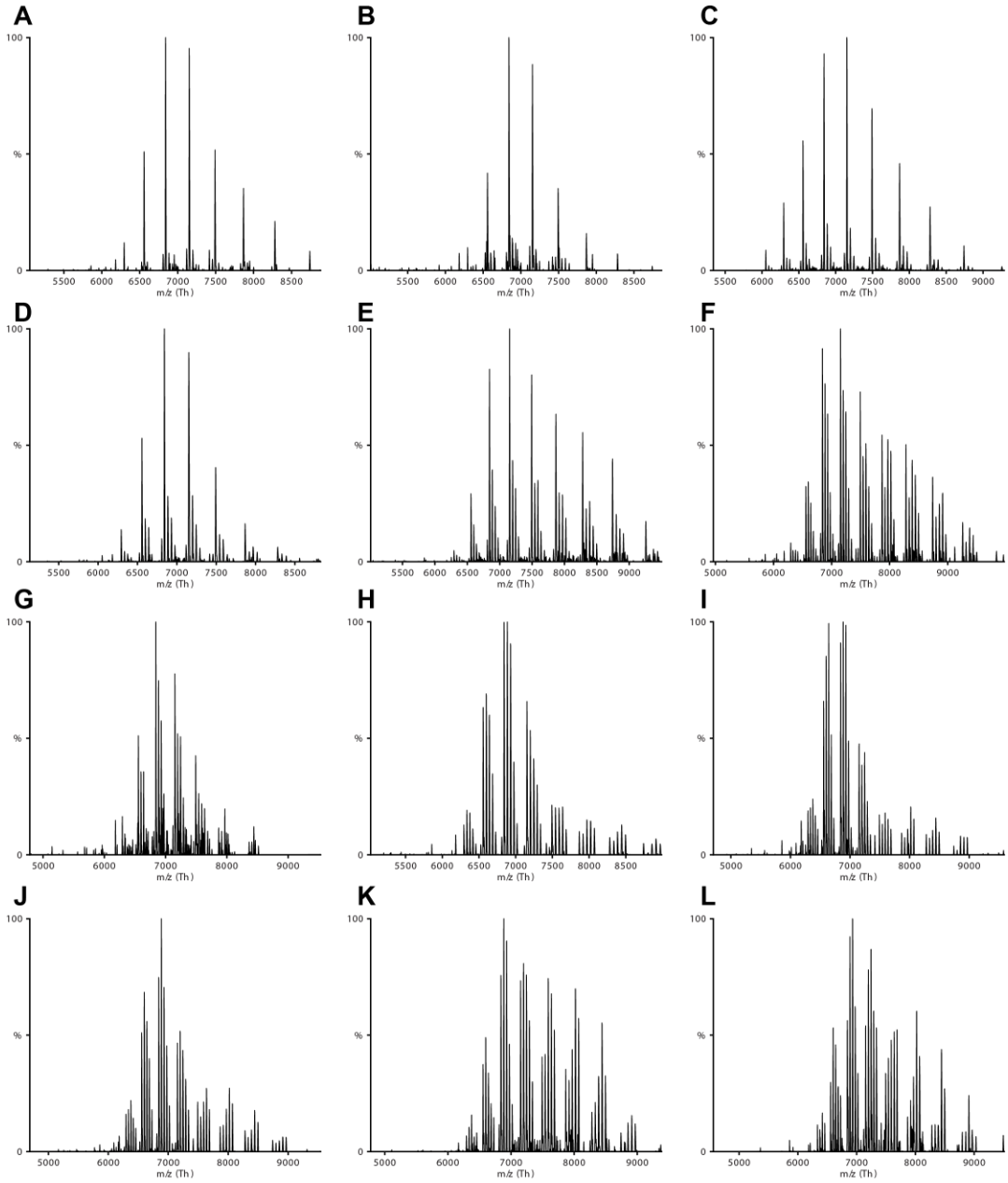

Figure 28 Representative native mass spectra of Kir3.2 with DOPI(4,5)P_2.

Kir3.2 was titrated by DOPI(4,5)P_2 under the same conditions as described for DOPI in figure 24.

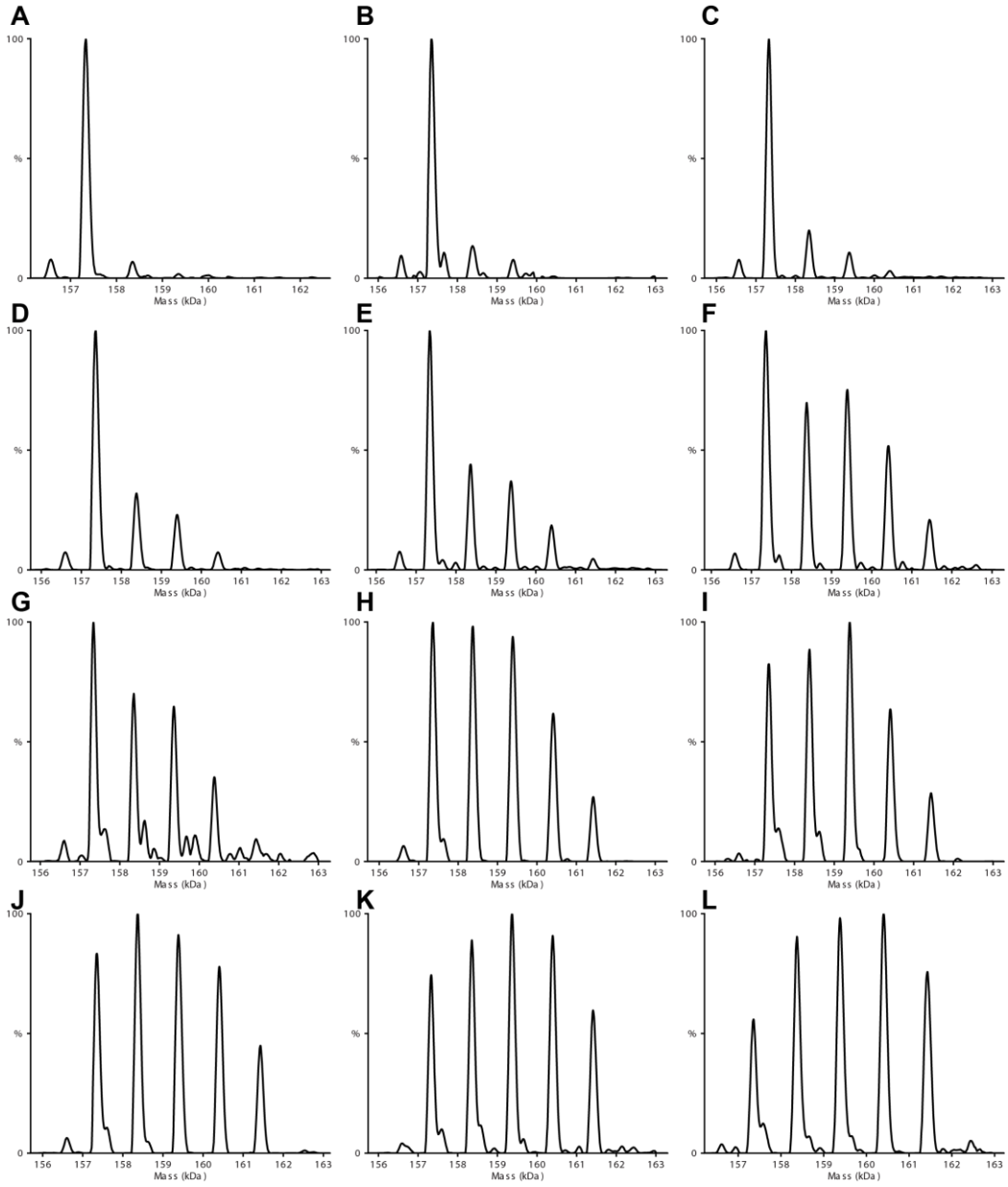

Figure 29 Deconvoluted native mass spectra of Kir3.2 with DOPI(4,5)P_2.

The panels match the concentrations reported in figure 24.

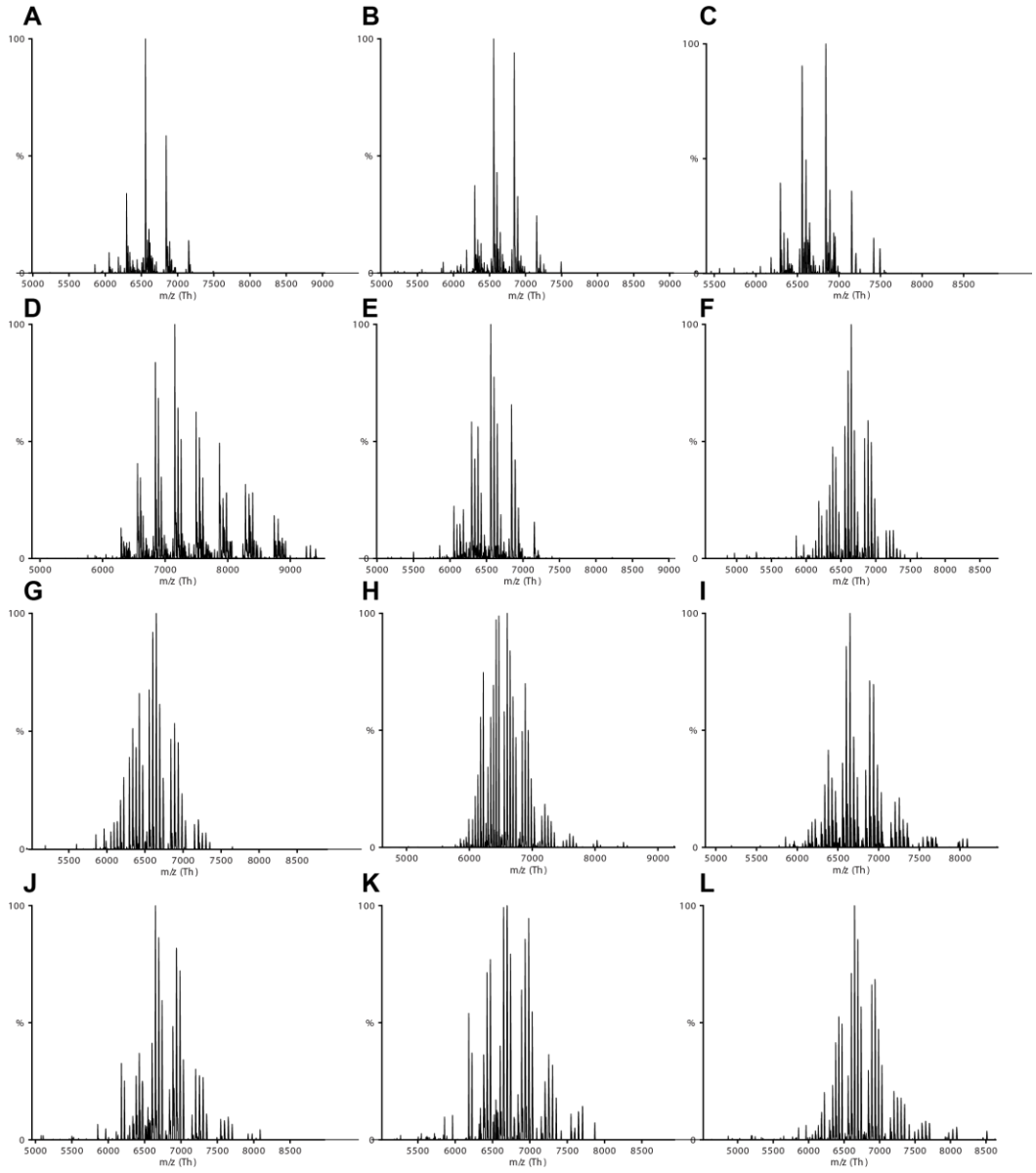

Figure 30 Representative native mass spectra of Kir3.2 with DOPI(3,4,5)P_3.

Kir3.2 was titrated by DOPI(3,4,5)P_3 under the same conditions as described for DOPI in figure 24.

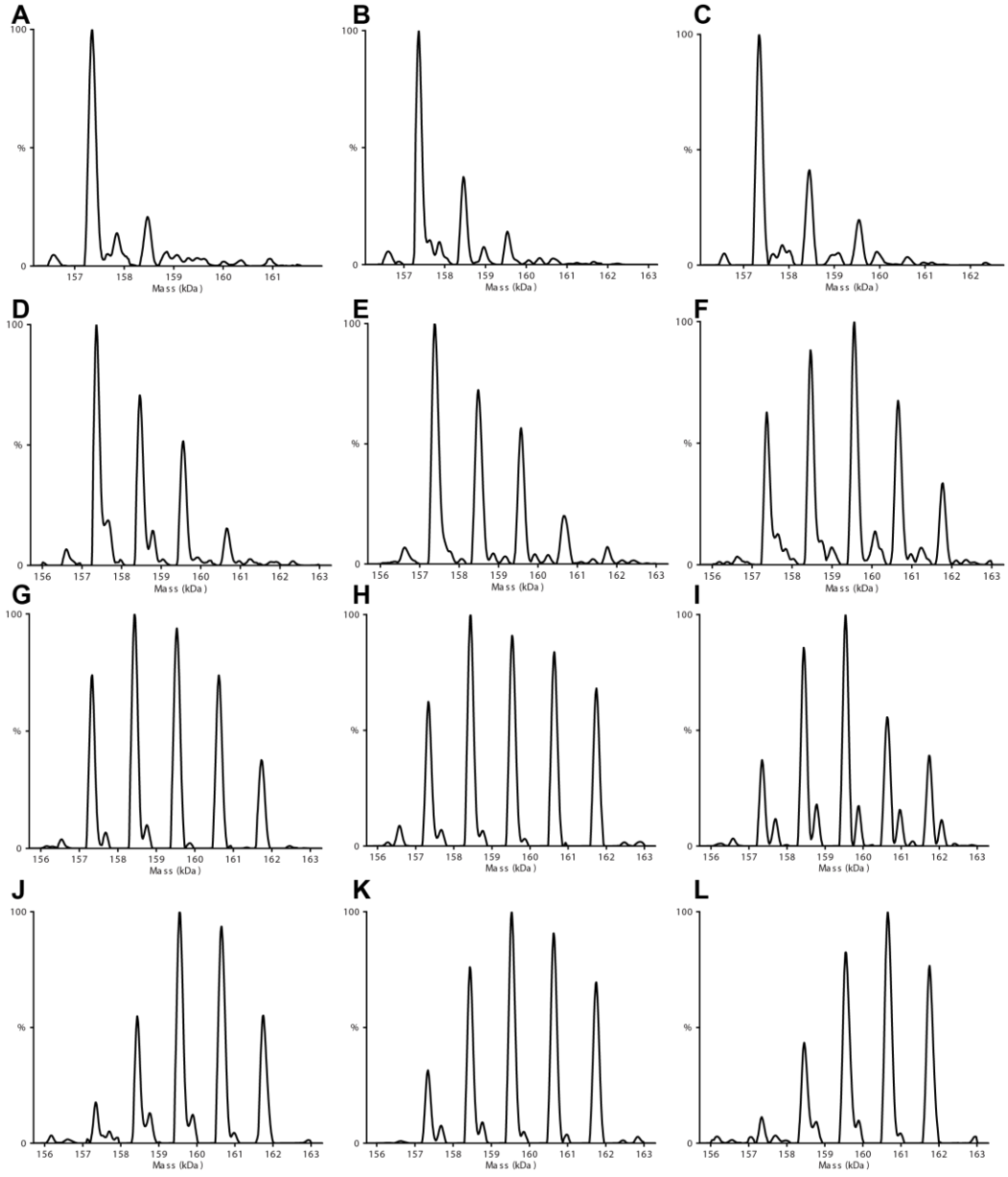

Figure 31 Deconvoluted native mass spectra of Kir3.2 with DOPI(3,4,5)P_3.

The panels match the concentrations reported in figure 24.

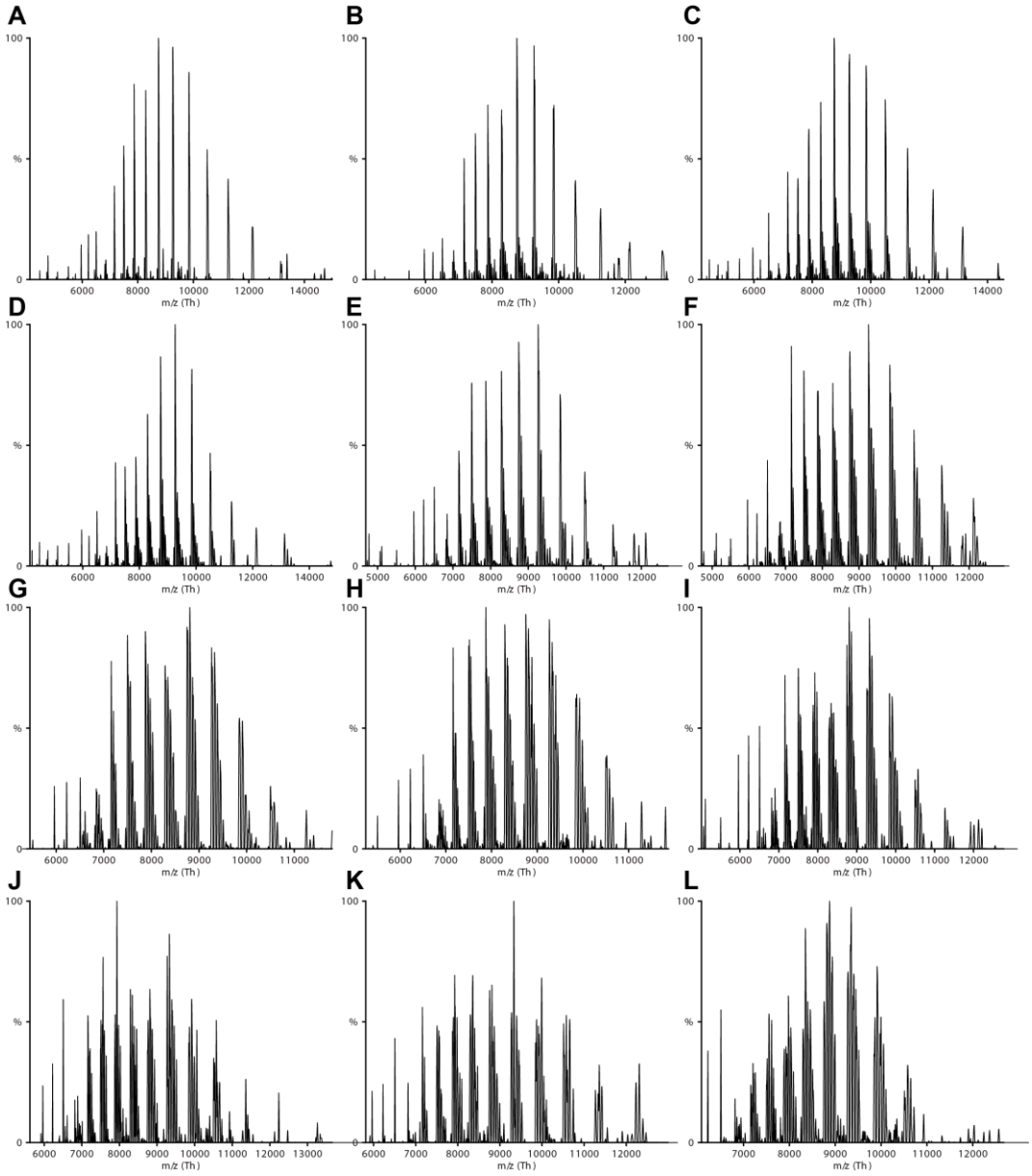

Figure 32 Representative native mass spectra of Kir3.2 with SAPI(4,5)P_2.

Kir3.2 was titrated by SAPI(4,5)P_2 under the same conditions as described for DOPI in figure 24.

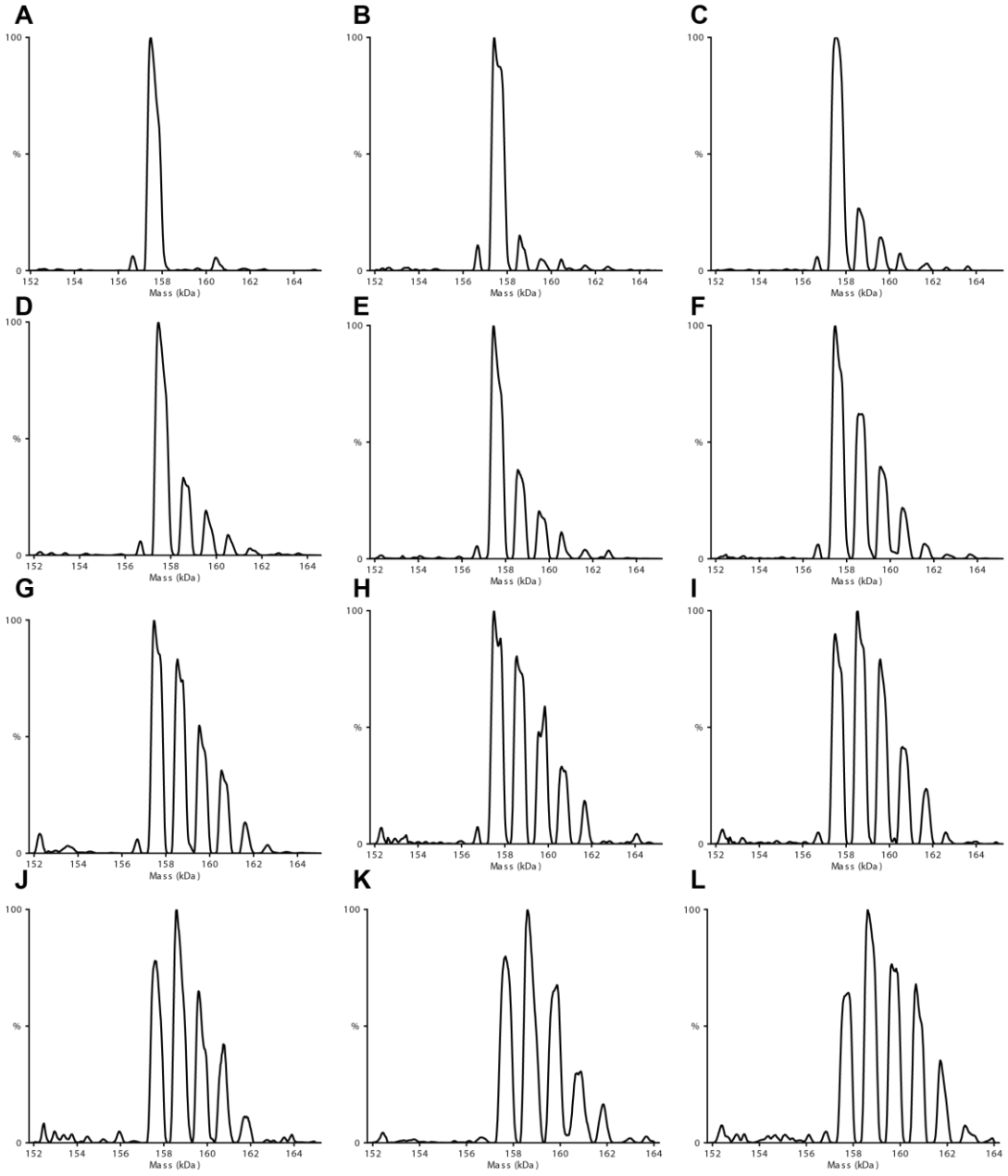

Figure 33 Deconvoluted native mass spectra of Kir3.2 with SAPI(4,5)P_2. The panels match the concentrations reported in figure 24.

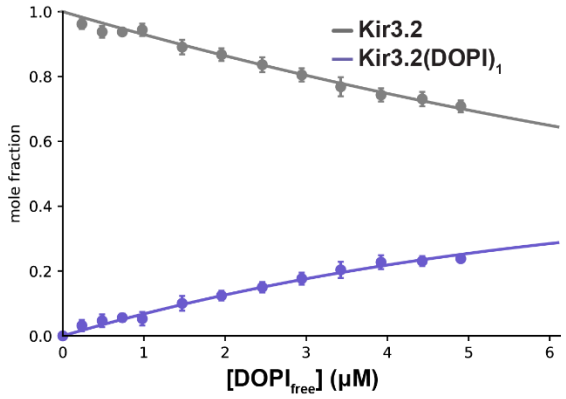

Figure 34 The plot of the mole fraction of Kir3.2 and Kir3.2•$DOPI_1$ as a function of free DOPI concentration.

The resulting fit (R^2 = 0.99) of a sequential lipid binding model (lines). The average and standard deviation are shown for the mole fraction data (dots).

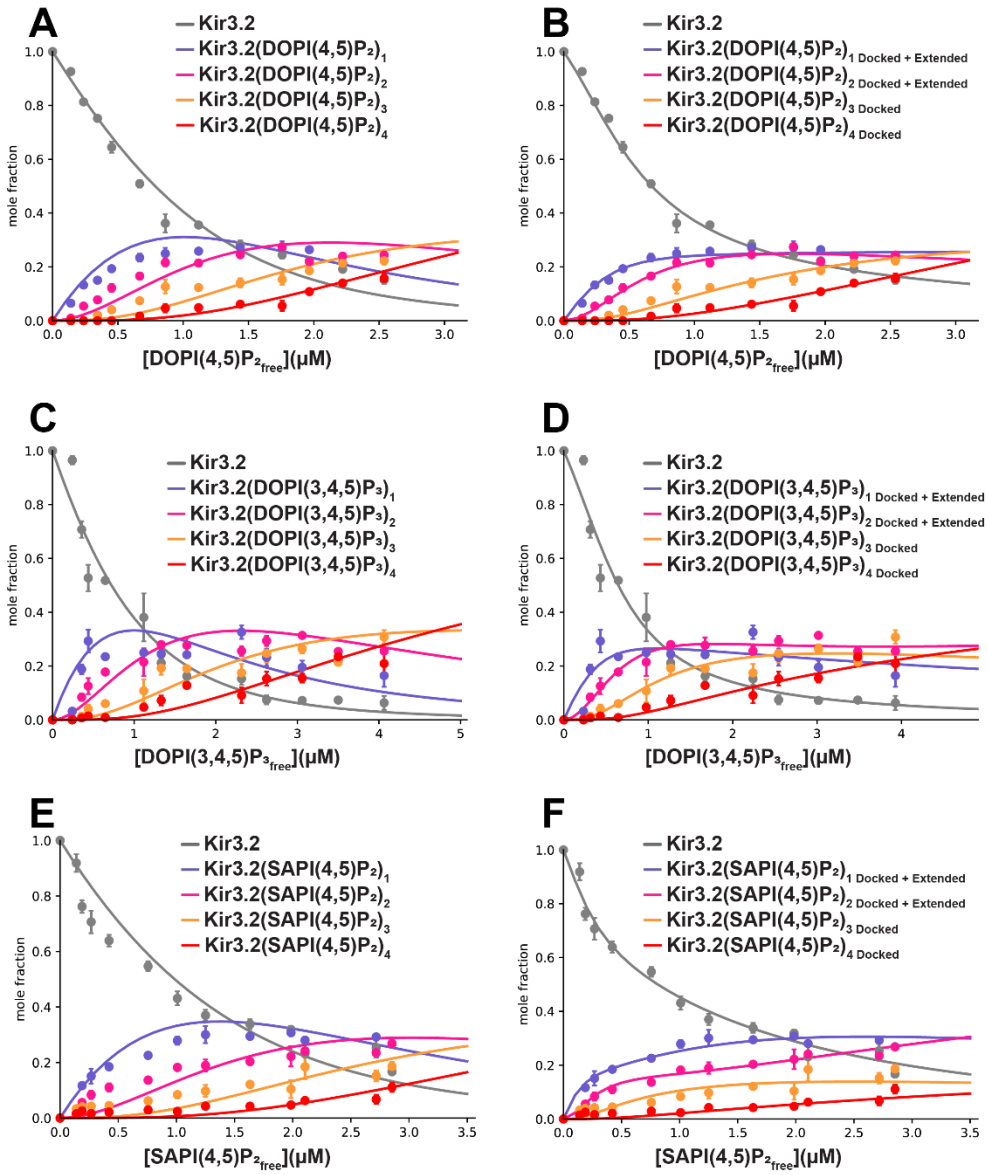

Figure 35 Plots of the mole fraction of apo and lipid-bound protein as a function of free lipid concentration.

The resulting fit of a sequential lipid or more complex binding models (lines) are shown in the left and right panels, respectively. The average and standard deviation are shown for the mole fraction data (dots) at 298 K.

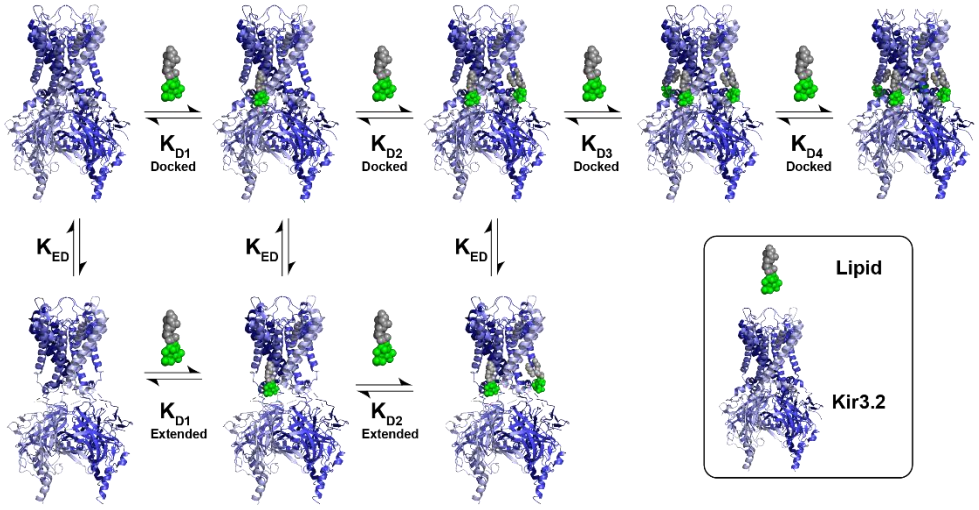

Figure 36 Equilibrium-coupled-binding model for the docked and extended states of Kir3.2 binding lipids.

The 3-4x lipid binding to the extended state is not included in this model.

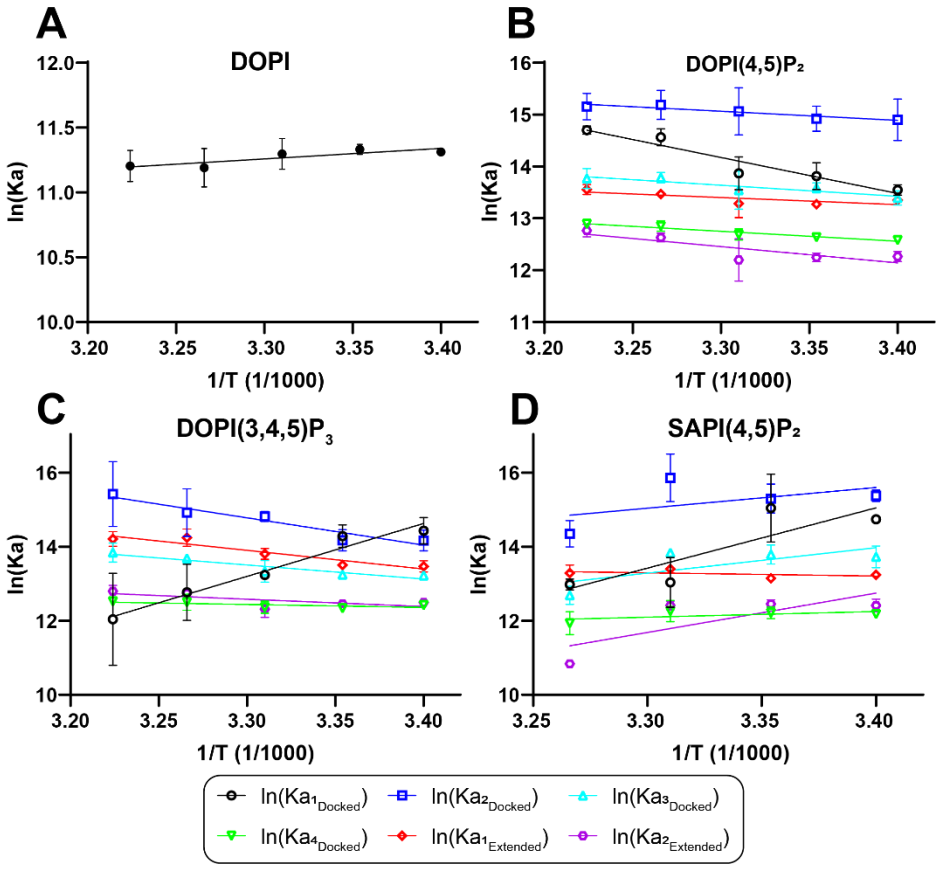

Figure 37 van't Hoff plots for Kir3.2-lipid interactions.

Kir3.2 binding A) DOPI, B) DOPI(4,5)P_2, C) DOPI(3,4,5)P_3, D) SAPI(4,5)P_2 (dots) and regression of a linear equation (solid lines). Reported are the average and s.e.m. (n=3).

APPENDIX B

TABLES

Table 1 Full name and abbreviations for synthetic and BODIPY-modified lipids used in Chapter 2.

Lipid	Abbreviation	Tails (sn1-sn2)
1,2-dioctanoyl-phosphatidylinositol-4',5'-bisphosphate	PI(4,5)P_2-d8	08:0-08:0
1,2-dioleoyl-phosphatidylinositol-4',5'-bisphosphate	PI(4,5)P_2-do	18:1-18:1
1,2-dioleoyl-phosphatidylinositol-3',4'-bisphosphate	PI(3,4)P_2-do	18:1-18:1
1,2-dioleoyl-phosphatidylinositol-4'-phosphate	PI(4)P_2-do	18:1-18:1
1-stearoyl-2-arachidonoyl- phosphatidylinositol-4',5'-bisphosphate	PI(4,5)P_2-sa	18:0-20:4
1-stearoyl-2-arachidonoyl- phosphatidylinositol-3',4',5'-bisphosphate	PI(3,4,5)P_3-sa	18:0-20:4
1,2-dioleoyl-phosphatidylinositol	PI-do	18:1-18:1
1-palmitoyl-2-oleoyl-phosphatidylethanolamine	POPE	16:0-18:1
1-palmitoyl-2-oleoyl-phosphatidylcholine	POPC	16:0-18:1
1-palmitoyl-2-oleoyl-phosphatidic acid	POPA	16:0-18:1
1-palmitoyl-2-oleoyl-phosphatidylserine	POPS	16:0-18:1
1-palmitoyl-2-oleoyl-phosphatidylglycerol	POPG	16:0-18:1
1-palmitoyl-2-(dipyrrometheneboron difluoride) undecanoyl-sn-glycero-3-phosphoethanolamine	B-PE	16:0-BODIPY
BODIPY FL Phosphatidylinositol 4,5-bisphosphate	B-PI(4,5)P_2	BODIPY-6:0

Table 2 Apparent binding parameters determined for WT and mutant Kir channels binding BODIPY-modified lipids in Chapter 2.

Protein	Detergent	Lipid	K_D	Hill coefficient
Kir3.2	DDM	B-PE	6.7 ± 2.3	1.4 ± 0.1
Kir3.2†	UDM	B-PE	5.6 ± 0.7	1.3 ± 0.2
Kir3.2†	$C_{12}E_8$	B-PE	7.5 ± 2.7	1.1 ± 0.1
Kir3.2	DDM	B-PI(4,5)P_2	*	*
Kir3.2†	DDM	B-PI(4,5)P_2	1.1 ± 0.1	1.2 ± 0.1
Kir3.2	$C_{10}E_5$	B-PI(4,5)P_2	2.6 ± 0.9	0.8 ± 0.3
Kir3.2†	$C_{10}E_5$	B-PI(4,5)P_2	0.9 ± 0.1	2.7 ± 0.7
$Kir3.2^{K64Q}$†	$C_{10}E_5$	B-PI(4,5)P_2	3.8 ± 0.3	1.3 ± 0.3
$Kir3.2^{R92P}$†	$C_{10}E_5$	B-PI(4,5)P_2	8.7 ± 6.8	1.1 ± 0.2
$Kir3.2^{K194A}$†	$C_{10}E_5$	B-PI(4,5)P_2	12.9 ± 2.7	0.9 ± 0.1

†The fusion protein was treated with DHPC to remove contaminants.

*Regression of Hill model results in ambiguous values.

Reported is the average and standard deviation (n = 3).

Table 3. Summary of expression and purification of mutant Kir3.2 channels in Chapter 2.

Group	Mutant Name	His In Block	Scale-up Expressed	Successfully Purified	Decipherable On MS	Lipid Binding
1	K64Q	Y	Y	Y	Y	Y
2	K90R	N	N	N	N	N
2	R92P	Y	Y	Y	Y	Y
3	K194A	Y	Y	Y	Y	Y
3	Q197A	Y	N	N	N	N
3	Q197K	Y	Y	Y	N	N
3	Q197R	N	N	N	N	N
3	K199A	Y	Y	N	N	N
3	K199H	Y	N	N	N	N
3	K200A	N	N	N	N	N
3	K200N	Y	Y	Y	N	N
3	K200R	N	N	N	N	N

Y: Positive results

N: Negative results

Table 4 Representative average number of lipids bound to WT and mutant Kir3.2 channels in Chapter2.

Lipid	Kir3.2	Kir3.2^{K64Q}	Kir3.2^{R92P}	Kir3.2^{K194A}
PI(4,5)P_2-d8	2.6	1.1	2.3	2.0
PI(4,5)P_2-do	2.1	1.2	2.7	2.3
PI(3,4)P_2-do	2.0	1.1	2.5	1.9
PI(4)P_2-do	1.4	1.0	2.1	1.5
PI(4,5)P_2-sa	2.2	1.5	2.6	2.3
PI(3,4,5)P_3-sa	2.1	1.79	2.6	2.6
PI-do	1.0	0.9	1.4	1.2
POPE	0.4	0.4	0.9	0.4

Table 5 Phospholipids and their abbreviations used in Chapter 3.

Lipid Name	Abbreviation	Tails (sn1-sn2)	MW (Da)
1,2-dioleoyl-phosphatidylinositol-3'-phosphate	DOPI(3)P	18:1-18:1	977
1,2-dioleoyl-phosphatidylinositol-4'-phosphate	DOPI(4)P	18:1-18:1	977
1,2-dioleoyl-phosphatidylinositol-5'-phosphate	DOPI(5)P	18:1-18:1	977
1,2-dioleoyl-phosphatidylinositol-3',4'-bisphosphate	DOPI(3,4)P_2	18:1-18:1	1074
1,2-dioleoyl-phosphatidylinositol-4',5'-bisphosphate	DOPI(4,5)P_2	18:1-18:1	1074
1,2-dioleoyl-sn-glycero-3-phospho-1'-myo-inositol-3',4',5'-trisphosphate	DOPI(3,4,5)P_3	18:1-18:1	1171
1-stearoyl-2-arachidonoyl-phosphatidylinositol-4'-bisphosphate	SAPI(4)P	18:0-20:4	1001
1-stearoyl-2-arachidonoyl-phosphatidylinositol-4',5'-bisphosphate	SAPI(4,5)P_2	18:0-20:4	1098
1-stearoyl-2-arachidonoyl-phosphatidylinositol-3',4',5'-bisphosphate	SAPI(3,4,5)P_3	18:0-20:4	1195
1,2-dioleoyl-phosphatidylinositol	DOPI	18:1-18:1	880
1-palmitoyl-2-oleoyl-sn-glycero-3-phosphoinositol	POPI	16:0-18:1	854
1-palmitoyl-2-oleoyl-phosphatidylethanolamine	POPE	16:0-18:1	718
1-palmitoyl-2-oleoyl-phosphatidylcholine	POPC	16:0-18:1	760
1-palmitoyl-2-oleoyl-phosphatidic acid	POPA	16:0-18:1	697
1-palmitoyl-2-oleoyl-phosphatidylserine	POPS	16:0-18:1	784
1-palmitoyl-2-oleoyl-phosphatidylglycerol	POPG	16:0-18:1	771
BODIPY FL Phosphatidylinositol 4,5-bisphosphate	B-PIP	BODIPY-6:0	1514

Table 6 Theoretical and measured mass of protein complexes in Chapter 3.

Protein Name	Theoretical (kDa)	Measured (kDa)
Kir3.4(WT)	195.9	196.0 ± 0.3
Kir3.2(WT)	199.1	199.2 ± 0.4
Kir3.4(S143T)	196.0	196.4 ± 0.6
Kir3.4(D223N)	195.9	196.1 ± 0.6
Kir3.4-mCherry	308.1	308.7 ± 0.7
Kir3.2-mCherry	311.2	311.3 ± 0.7

Table 7 Equilibrium binding constants for Kir3.2-lipid interactions in chapter 4.

Lipid	T (K)	Docked State (μM)				Extended State (μM)			
		K_{D1}	K_{D2}	K_{D3}	K_{D4}	K_{D1}	K_{D2}	R^2	χ^2
DOPI	310	13.7 ± 1.7						1.00	0.01
	306	13.9 ± 1.6						1.00	0.01
	302	12.5 ± 1.2						0.99	0.03
	298	11.9 ± 0.4						0.99	0.02
	294	12.2 ± 0.1						1.00	0.02
DOPI(4)P	310	2.8 ± 0.3	4.5 ± 0.6	6.8 ± 2.9				0.99	0.02
	306	2.4 ± 0.1	3.6 ± 0.1	5.2 ± 0.1				0.99	0.03
	302	2.9 ± 0.5	5.2 ± 0.5	7.6 ± 3.3				0.99	0.02
	298	2.4 ± 0.2	3.7 ± 0.1	5.0 ±0.7				0.99	0.04
	294	2.7 ± 0.1	4.5 ± 0.1	6.1 ± 1.5				0.99	0.06
$DOPI(4,5)P_2$	310	0.4 ± 0.1	0.3 ± 0.1	1.1 ± 0.2	2.5 ± 0.1	1.3 ± 0.1	2.9 ± 0.3	0.98	0.07
	306	0.5 ± 0.1	0.3 ± 0.1	1.0 ± 0.1	2.6 ± 0.2	1.4 ± 0.1	3.3 ± 0.2	0.99	0.04
	302	1.0 ± 0.3	0.3 ± 0.1	1.4 ± 0.4	3.1 ± 0.3	1.7 ± 0.4	5.3 ± 1.5	0.98	0.05
	298	1.0 ± 0.2	0.3 ± 0.1	1.3 ± 0.1	3.3 ± 0.2	1.7 ± 0.1	4.8 ± 0.3	0.99	0.02
	294	1.3 ± 0.1	0.4 ± 0.1	1.5 ± 0.2	3.4 ± 0.1	1.6 ± 0.1	4.7 ± 0.4	0.99	0.03
$DOPI(3,4,5)P_3$	310	8.6 ± 5.4	0.3 ± 0.2	1.0 ± 0.2	3.7 ± 0.3	0.7 ± 0.1	2.8 ± 0.4	0.98	0.09
	306	3.8 ± 2.2	0.4 ± 0.2	1.1 ± 0.1	3.8 ± 0.7	0.7 ± 0.1	2.9 ± 0.1	0.97	0.09
	302	1.8 ± 0.1	0.4 ± 0.1	1.7 ± 0.4	4.3 ± 0.6	1.0 ± 0.1	4.6 ± 0.9	0.96	0.13
	298	0.6 ± 0.1	0.7 ± 0.2	1.8 ± 0.1	4.4 ± 0.3	1.4 ± 0.1	3.9 ± 0.3	0.98	0.06
	294	0.6 ± 0.2	0.7 ± 0.2	1.8 ± 0.1	4.0 ± 0.1	1.4 ± 0.2	3.8 ± 0.3	0.98	0.07
$SAPI(4,5)P_2$	306	2.3 ± 0.3	0.6 ± 0.2	3.2 ± 0.6	6.8 ± 1.6	1.7 ± 0.3	19.7 ± 0.1	0.96	0.14
	302	2.5 ± 1.0	0.2 ± 0.1	1.0 ± 0.1	4.9 ± 1.1	1.5 ± 0.1	4.1 ± 0.4	0.99	0.03
	298	0.4 ± 0.2	0.2 ± 0.1	1.0 ± 0.2	5.0 ± 0.6	2.0 ± 0.1	3.9 ± 0.3	0.98	0.06
	294	0.4 ± 0.1	0.2± 0.1	1.1 ± 0.5	5.2 ± 0.3	1.8 ± 0.1	4.1 ± 0.6	0.98	0.05

Reported are the average and s.e.m. (n = 3).

Table 8 Thermodynamic parameters for Kir3.2-lipid binding in chapter 4.

lipid		ΔH (kJ/mol)	-TΔS (298k) (kJ/mol)	ΔG (298K) (kJ/mol)
DOPI	K_{A1}	-6.8 ± 2.3	-21.2 ± 2.3	-28.1±0.04
DOPI(4)P	K_{A1}	-2.4 ± 2.8	-29.5 ± 2.7	-32.1±0.1
	K_{A2}	0.8 ± 3.3	-31.4 ± 3.2	-31.0±0.03
	K_{A3}	-2.7 ± 6.8	-27.2 ± 6.8	-30.3±0.2
DOPI(4,5)P_2	$K_{A1\ Docked}$	57.7 ± 4.5	-91.9 ± 4.5	-34.2±0.3
	$K_{A2\ Docked}$	14.6 ± 6.0	-51.7 ± 5.9	-37.0±0.3
	$K_{A3\ Docked}$	17.8 ± 3.8	-51.3 ± 3.8	-33.7±0.1
	$K_{A4\ Docked}$	15.9 ± 1.6	-47.3 ± 1.5	-31.3±0.1
	$K_{A1\ Extended}$	11.4 ± 2.8	-44.4 ± 2.8	-32.9±0.1
	$K_{A2\ Extended}$	26.1 ± 4.4	-56.5 ± 4.4	-30.4±0.1
DOPI(3,4,5)P_3	$K_{A1\ Docked}$	-118.8 ± 12.6	84.2 ± 12.4	-35.4±0.4
	$K_{A2\ Docked}$	61.2 ± 9.5	-96.9 ± 9.4	-35.1±0.3
	$K_{A3\ Docked}$	31.5 ± 3.6	-64.4 ± 3.6	-32.8±0.1
	$K_{A4\ Docked}$	6.6 ± 2.6	-37.3 ± 2.6	-30.6±0.1
	$K_{A1\ Extended}$	41.9 ± 3.7	-75.7 ± 3.7	-33.5±0.01
	$K_{A2\ Extended}$	16.5 ± 3.7	-47.4 ± 3.7	-30.9±0.1
SAPI(4,5)P_2	$K_{A1\ Docked}$	-135.4 ± 20.7	99.9 ± 20.6	-37.3±1.1
	$K_{A2\ Docked}$	-46.5 ± 17.8	8.4 ± 17.7	-37.9±0.5
	$K_{A3\ Docked}$	-57.1 ± 11.8	23.2 ± 11.7	-34.2±0.3
	$K_{A4\ Docked}$	-12.7 ± 6.5	-17.5 ± 6.5	-30.3±0.2
	$K_{A1\ Extended}$	7.3 ± 3.8	-40.1 ± 3.8	-32.6±0.1
	$K_{A2\ Extended}$	-88.3 ± 13.7	57.9 ± 13.6	-30.9±0.1

The reported ΔG was computed using equilibrium binding constants. Reported are the average and s.e.m. (*n*=3).

Table 9 Differences in thermodynamic parameters for Kir3.2-lipid interactions in chapter 4.

lipid		ΔΔH (kJ/mol)	ΔΔS (J/mol/K)	ΔΔG (kJ/mol)
DOPI(4)P - DOPI	K_{A1}	4.38±2.08	27.85±6.87	-4.04±0.06
DOPI(4,5)P_2 - DOPI(4)P	K_{A1}	60.06±3.06	209.40±10.17	-2.11±0.01
	K_{A2}	13.82±3.92	68.12±5.23	-5.97±0.01
	K_{A3}	20.53±4.53	80.87±-5.81	-3.41±0.02
DOPI(3,4,5)P_3 - DOPI(4,5)P_2	$K_{A1\ Docked}$	-176.48±7.71	-590.94±15.31	-1.17±0.27
	$K_{A2\ Docked}$	46.62±6.50	151.68±6.78	1.86±0.25
	$K_{A3\ Docked}$	13.66±3.04	43.96±-0.39	0.85±0.08
	$K_{A4\ Docked}$	-9.36±1.74	-33.56±2.13	0.74±0.07
	$K_{A1\ Extended}$	30.52±2.71	105.03±1.74	-0.57±0.04
	$K_{A2\ Extended}$	-9.62±3.34	-30.54±-1.36	-0.53±0.08
SA(4,5)P_2 - DOPI(3,4,5)P_3	$K_{A1\ Docked}$	-16.56±13.98	-52.68±15.89	-1.88±0.65
	$K_{A2\ Docked}$	-107.70±11.65	-353.36±16.08	-2.79±0.33
	$K_{A3\ Docked}$	-88.52±7.11	-293.96±15.69	-1.35±0.18
	$K_{A4\ Docked}$	-19.30±4.04	-66.44±7.56	0.30±0.12
	$K_{A1\ Extended}$	-34.65±3.07	-119.46±0.19	0.89±0.04
	$K_{A2\ Extended}$	-104.76±8.20	-353.36±19.18	0.01±0.10
SA(4,5)P_2 - DOPI(4,5)P_2	$K_{A1\ Docked}$	-193.04±12.23	-643.62±31.19	-3.05±0.64
	$K_{A2\ Docked}$	-61.08±10.82	-201.68±22.86	-0.93±0.31
	$K_{A3\ Docked}$	-74.86±7.14	-250.00±15.31	-0.50±0.19
	$K_{A4\ Docked}$	-28.67±3.86	-100.00±9.69	1.04±0.12
	$K_{A1\ Extended}$	-4.13±2.73	-14.43±1.94	0.32±0.05
	$K_{A2\ Extended}$	-114.38±8.32	-383.89±17.82	-0.52±0.10

Reported are the average and s.e.m. (n=3).